: official publication of the Orthopaedic Research Society, 2005. **23**(1): p. 164-174.

32. Kretlow, J.D., et al., *Donor age and cell passage affects differentiation potential of murine bone marrow-derived stem cells.* BMC cell biology, 2008. **9**: p. 60-72.

33. Hairfield-Stein, M., et al., *Development of self-assembled, tissue-engineered ligament from bone marrow stromal cells.* Tissue engineering, 2007. **13**(4): p. 703-10.

34. Maniatopoulos, C., J. Sodek, and A.H. Melcher, *Bone formation in vitro by stromal cells obtained from bone marrow of young adult rats.* Cell and tissue research, 1988. **254**(2): p. 317-330.

35. Noff, D., S. Pitaru, and N. Savion, *Basic fibroblast growth factor enhances the capacity of bone marrow cells to form bone-like nodules in vitro.* FEBS letters, 1989. **250**(2): p. 619-621.

36. Scutt, A. and P. Bertram, *Basic fibroblast growth factor in the presence of dexamethasone stimulates colony formation, expansion, and osteoblastic differentiation by rat bone marrow stromal cells.* Calcified tissue international, 1999. **64**(1): p. 69-77.

37. Pitaru, S., et al., *Effect of basic fibroblast growth factor on the growth and differentiation of adult stromal bone marrow cells: enhanced development of mineralized bone-like tissue in culture.* Journal of bone and mineral research : the official journal of the American Society for Bone and Mineral Research, 1993. **8**(8): p. 919-929.

38. Locklin, R.M., R.O. Oreffo, and J.T. Triffitt, *Effects of TGFbeta and bFGF on the differentiation of human bone marrow stromal fibroblasts.* Cell biology international, 1999. **23**(3): p. 185-194.

39. Ronchetti, I.P., D. Quaglino, Jr., and G. Bergamini, *Ascorbic acid and connective tissue.* Sub-cellular biochemistry, 1996. **25**: p. 249-64.

40. Syed-Picard, F.N., et al., *Three-dimensional engineered bone from bone marrow stromal cells and their autogenous extracellular matrix.* Tissue engineering.Part A, 2009. **15**(1): p. 187-195.

41. Marui, T., et al., *Effect of growth factors on matrix synthesis by ligament fibroblasts.* Journal of orthopaedic research : official publication of the Orthopaedic Research Society, 1997. **15**(1): p. 18-23.

42. Martin, I., et al., *Selective differentiation of mammalian bone marrow stromal cells cultured on three-dimensional polymer foams.* Journal of biomedical materials research, 2001. **55**(2): p. 229-35.

43. Sell, S.A., et al., *Incorporating platelet-rich plasma into electrospun scaffolds for tissue engineering applications.* Tissue engineering. Part A, 2011. **17**(21-22): p. 2723-37.

44. Taylor, D.W., et al., *A systematic review of the use of platelet-rich plasma in sports medicine as a new treatment for tendon and ligament injuries.* Clinical journal of sport medicine : official journal of the Canadian Academy of Sport Medicine, 2011. **21**(4): p. 344-52.

45. Nauman, E.A., et al., *bFGF administration lowers the phosphate threshold for mineralization in bone marrow stromal cells.* Calcified tissue international, 2003. **73**(2): p. 147-152.

46. Marie, P.J., *Transcription factors controlling osteoblastogenesis.* Archives of Biochemistry and Biophysics, 2008. **473**(2): p. 98-105.

47. Woodfin, A., M.B. Voisin, and S. Nourshargh, *PECAM-1: a multi-functional molecule in inflammation and vascular biology.* Arteriosclerosis, thrombosis, and vascular biology, 2007. **27**(12): p. 2514-23.

48. Woo, S.L., et al., *Biomechanics and anterior cruciate ligament reconstruction.* Journal of orthopaedic surgery and research, 2006. **1**: p. 2-10.

49. Moffat, K.L., et al., *Characterization of the structure-function relationship at the ligament-to-bone interface.* Proceedings of the National Academy of Sciences of the United States of America, 2008. **105**(23): p. 7947-7952.

50. Scheffler, S.U., F.N. Unterhauser, and A. Weiler, *Graft remodeling and ligamentization after cruciate ligament reconstruction.* Knee Surgery, Sports Traumatology, Arthroscopy, 2008. **16**(9): p. 834-842.

51. Larkin, L.M., et al., *Functional evaluation of nerve-skeletal muscle constructs engineered in vitro.* In vitro cellular & developmental biology.Animal, 2006. **42**(3-4): p. 75-82.

52. Larkin, L.M., et al., *Structure and functional evaluation of tendon-skeletal muscle constructs engineered in vitro.* Tissue engineering, 2006. **12**(11): p. 3149-3158.

53. Ma, J., et al., *Morphological and functional characteristics of three-dimensional engineered bone-ligament-bone constructs following implantation.* Journal of Biomechanical Engineering, 2009. **131**(10): p. 101017.

54. Urbanchek, M.S., et al., *Rat walking tracks do not reflect maximal muscle force capacity.* Journal of reconstructive microsurgery, 1999. **15**(2): p. 143-9.

55. Nirmalanandhan, V.S., et al., *Combined effects of scaffold stiffening and mechanical preconditioning cycles on construct biomechanics, gene expression, and tendon repair biomechanics.* Tissue engineering.Part A, 2009. **15**(8): p. 2103-2111.

56. Lundberg, W.R., et al., *In vivo forces during remodeling of a two-segment anterior cruciate ligament graft in a goat model.* Journal of orthopaedic research : official publication of the Orthopaedic Research Society, 1997. **15**(5): p. 645-651.

57. Singhatat, W., et al., *How four weeks of implantation affect the strength and stiffness of a tendon graft in a bone tunnel: a study of two fixation devices in an extraarticular model in ovine.* The American Journal of Sports Medicine, 2002. **30**(4): p. 506-513.

58. Woo, S.L., R. Liang, and M.B. Fisher, *Future of Orthopaedic Sports Medicine and Soft Tissue Healing: The Important Role of Engineering.* Cellular and Molecular Bioengineering, 2009. **2**(3).

59. Tapper, J.E., et al., *In vivo measurement of the dynamic 3-D kinematics of the ovine stifle joint.* Journal of Biomechanical Engineering, 2004. **126**(2): p. 301-305.

60. Seitz, H., et al., *Vascular anatomy of the ovine anterior cruciate ligament. A macroscopic, histological and radiographic study.* Archives of orthopaedic and trauma surgery, 1997. **116**(1-2): p. 19-21.

61. Murray, M.M., A. Weiler, and K.P. Spindler, *Interspecies variation in the fibroblast distribution of the anterior cruciate ligament.* The American Journal of Sports Medicine, 2004. **32**(6): p. 1484-1491.

62. Radford, W.J.P., A.A. Amis, and A.C. Stead, *The Ovine Stifle as a Model for Human Cruciate Ligament Surgery.* Vet Comp Orthop Trauma, 1996. **9**: p. 134-139.

63. Dustmann, M., et al., *The extracellular remodeling of free-soft-tissue autografts and allografts for reconstruction of the anterior cruciate ligament: a comparison study in a sheep model.* Knee surgery, sports traumatology, arthroscopy : official journal of the ESSKA, 2008. **16**(4): p. 360-369.

64. Hunt, P., et al., *A model of soft-tissue graft anterior cruciate ligament reconstruction in sheep.* Archives of orthopaedic and trauma surgery, 2005. **125**(4): p. 238-248.

65. Durselen, L., et al., *Comparative animal study of three ligament prostheses for the replacement of the anterior cruciate and medial collateral ligament.* Biomaterials, 1996. **17**(10): p. 977-982.

66. Meller, R., et al., *Histologic and Biomechanical Analysis of Anterior Cruciate Ligament Graft to Bone Healing in Skeletally Immature Sheep.* Arthroscopy: The Journal of Arthroscopic & Related Surgery, 2008. **24**(11): p. 1221-1231.

67. Ma, J., et al., *Three-dimensional engineered bone-ligament-bone constructs for anterior cruciate ligament replacement.* Tissue engineering.Part A, 2012. **18**(1-2): p. 103-116.

68. Gutierrez-Adan, A., et al., *Ovine-specific Y-chromosome RAPD-SCAR marker for embryo sexing.* Animal Genetics, 1997. **28**(2): p. 135-138.

69. Jackson, D.W. and T. Simon, *Assessment of donor cell survival in fresh allografts (ligament, tendon, and meniscus) using DNA probe analysis in a goat model.* The Iowa orthopaedic journal, 1993. **13**: p. 107-14.

70. Rhee, D.K., et al., *The secreted glycoprotein lubricin protects cartilage surfaces and inhibits synovial cell overgrowth.* The Journal of clinical investigation, 2005. **115**(3): p. 622-31.

71. Elsaid, K.A., et al., *Decreased lubricin concentrations and markers of joint inflammation in the synovial fluid of patients with anterior cruciate ligament injury.* Arthritis and rheumatism, 2008. **58**(6): p. 1707-15.

72. B. Alberts, A. Johnson, J. Lewis, M. Raff, K. Roberts, and P. Walter. Molecular Biology of the Cell. Garland Science, New York, NY, 4th edition, 2002.

CHAPTER 4

Biomechanical Characterization of Native and Engineered Ligaments

A variety of mechanical experiments has been carried out with the aim of understanding and evaluating the functions and biomechanical properties of the ACL, tendon grafts, and tissue engineered grafts. Extensive human cadaver studies and animal studies have been conducted to elucidate the biomechanics of these tissues. Several types of experiments, including laxity tests, *in situ* force tests, uniaxial tension tests, and viscoelastic tests, have been conducted to study the tissues' functional properties and nonlinear viscoelastic mechanical responses. Although these tests are standard, because of the intrinsic properties of these tissues such as anisotropy, inhomogeneity, and multi-directional fiber orientation, experiments must be carefully designed and quantities such as stress and strain must be accurately computed to reveal the real biomechanical properties of the soft tissues. We have conducted mechanical tests incorporating these important factors and evaluated our tissue engineered BLB constructs from rat MCL replacement and sheep ACL replacement by comparing them with native ligaments and tendon grafts. Our experimental data demonstrated that after implantation the tissue engineered BLBs showed dramatic increases in their mechanical properties and the properties are comparable to those of the native ligaments and tendons.

4.1 Current Understanding of the Biomechanics of Soft Tissue

To characterize the function and biomechanical properties of native and engineered ligaments and tendons, several types of experiments have been conducted. These characterization methods may be classified as functional tests

--knee laxity measurements at different knee flexion angle and *in situ* force measurements at different knee flexion angles; biomechanical property tests --uniaxial load-unload tests and strain to failure tests; and viscoelastic characterization tests --uniaxial tests at various strain rates, stress relaxation, and creep tests. Human cadaver studies are often limited by specimen size and specimen availability which affect the accuracy and comprehensiveness of the measurements of a tissue's biomechanical properties. Therefore, many studies using various animal models have been conducted with the goal of better characterizing the biomechanical properties of the ACL and its grafts.

Clinically, the function of the ACL has been evaluated by measuring knee laxity from anterior tibial translation tests (ATT) at different knee flexion angles. This is because the major function of the ACL is to restrict the knee motion in an anteriortibial translation [[1-3]. Cadaver studies have found that the maximum laxity occurs at a knee flexion angle of 30 degrees with a measured laxity of 6 - 8 mm [4, 5]. This laxity measurement has since been used as an important factor to evaluate the ACL and tendon grafts. More recent studies obtained *in situ* forces and strains by attaching force transducers and strain gauges to the surface of the ACL [6, 7]. These approaches provide a quantitative measure of ACL function. While knee laxity tests provide an understanding of knee function, the results from these tests usually do not reflect the actual material properties of the ACL.

To understand the material and structural properties of soft tissue such as tangent modulus, geometric stiffness, ultimate stress to failure, and strain to failure, more quantitative mechanical tests need to be performed preferably under well-characterized deformation states. To date, numerous experimental analyses have been performed to examine the biomechanical properties of ligaments and tendons. The information obtained from these studies may then be used to search for suitable tissue grafts to replace a torn ACL. As mentioned in **Chapter 2**, researchers and clinicians have studied many tendon grafts such as

patellar tendon [8-12], Achilles tendon [13-15], quadriceps tendon [16], semitendinosus tendons [15], and gracilis tendons [15, 17]. Most tendon grafts have biomechanical properties that are less than those of the native ACL, whereas the tested patellar tendon has a maximum load of 168% and a geometric stiffness of 380% of that of the ACL [15]. It is known that tendon grafts will degrade after implantation. Given that the strength and stiffness of the PT are higher than those of the native ACL, the PT graft has been thought to be most appropriate for ACL reconstruction [18] and is currently the most common graft used to replace a torn ACL.

As described in **Chapter 2**, ligaments and tendons exhibit nonlinear elastic properties. Uniaxial load-unload tension tests or load to failure tests are performed to characterize their behavior. For these tests, researchers must consider both structural and material properties. This distinction is important (structural vs. material) since the two properties are measured and computed by different means and convey different information. Structural properties typically refer to geometric stiffness, ultimate load to failure, and displacement at failure. These properties depend on the physical size of specimens and typically are computed from the load-elongation response (Figure 2.5**A**). In contrast, material properties include tangent modulus, ultimate stress to failure, and strain to failure. These properties are not dependent on size because they are normalized by the physical size of the specimens. Material properties are calculated from the stress-strain response of the sample (Figure 2.5**B**).

4.1.1 Biomechanical characterization of the human ACL

Table 4.1 and Table 4.2 list results from previous ACL mechanics studies. The tables are intended to include information about experimental setups as much as possible to facilitate detailed discussions and criticisms. Noyes and Grood et al., 1976 are the early researchers that studied the biomechanics of the human ACL [19]. Since then, numerous studies have been conducted to characterize the biomechanical properties of the human ACL from different

perspectives. These studies suggest that experimental conditions such as specimen age, specimen orientation, and testing rate significantly affect the mechanical properties of tissues. The average tangent modulus and geometric stiffness of human ACL among these studies are 106 MPa (from 24.4 to 158 MPa) and 178 N/mm (57.2 to 308N/mm), respectively. The average ultimate load is 1070 N (from 341 to 2160 N). The ultimate strain at failure from the studies is 0.31 (from 0.24 to 0.44). Note that several specimen orientations have been used during ACL mechanical testing. Noyes et al., 1976 and Woo et al., 1991 used an anatomically aligned ACL orientation and Jones et al., 1995 used physiological orientations with knee flexion angles of 0, 10 and 30 degrees [19-21]. Jones et al., 1995 measured the stiffness and strength of the femur-ACL-tibia unit at knee flexion angles of 0, 10, and 30 degrees and at two different speeds (50 mm/min and 500mm/min) [21]. No statistical differences were found among different flexion angles or different strain rates. Aged ACLs tend to fail with a bone avulsion at the bone-ligament interface, all other specimens failed by tears in the mid-substance of the ligament [21].

Table 4.1 Summary of the human ACL biomechanical properties including geometric stiffness and tangent modulus from previous studies. (* Numbers are reported as Mean ± SD; ** Numbers are reported as Mean ± SEM; numbers in red are estimated values using average values of ACL length (38 mm) and cross sectional area (58 mm^2) from the literature. No standard deviations were reported on these estimated values.)

Studies	Specimen Age	Sample Size	ACL Orientation	Displacement Rate (mm/s)	Strain Rate (1/s)	Geometric Stiffness (N/mm)	Tangent Modulus (MPa)
Noyes and Grood 1976*	48-86	20	Test axis along the long axis of ACL; tibia 45 to the ACL axis; femur 45 to the tibia axis	38	1.00	129±39	65.3±24
	16-26	6		38	1.00	182±56	111±26
Woo et al. 1991*	22-35	9	Test axis along the long axis of ACL; tibia 45 to the ACL axis; femur 30 to the tibia axis	0.33	0.01	242±28	158
	40-50	9				220±24	144
	60-97	9				180±25	118
	22-35	9	Test axis along the axis of the tibia; ACL is aligned to the test axis; femur 30 to the testing axis			218±27	143
	40-50	9				192±17	126
	60-97	9				124±16	81
Jones et al. 1995**	42-56	7	varied, knee flexion at 0, 10 and 30 degrees	0.83, 8.3	0.02, 0.2	205±40	134
	67-82	14		0.83, 8.3	0.02, 0.2	167±56	109
	67-82	7		0.83, 8.3	0.02, 0.2	N/A	N/A
Azangwe et al. 2001**	N/A	4	Test axis along the long axis of ACL; tibia and femur parallel to the testing axis	8	0.21	73.1±1	47.9
Chandrashekar et al. 2006**	Female (26-50)	9	Test axis along the long axis of ACL; tibia 45 to the ACL axis; femur 45 to the tibia axis	38	1.00	199±88	99±50
	male (17-50)	8		38	1.00	308±89	128±35
Paschos et al. 2010**	52-88	10	Test axis along the axis of the tibia; femur 15 to the tibia axis	1.5	0.04	57.2±23.5	24.4±20.7

Table 4.2 Summary of the human ACL biomechanical properties including maximum load, maximum stress (strength) and maximum strain from previous studies. (* Numbers are reported as Mean ± SD; ** Numbers are reported as Mean ± SEM; numbers in red are estimated values using average values of ACL length (38 mm) and cross sectional area (58 mm^2) from literature. No standard deviations were reported on these estimated values.)

Studies	Load Rate (mm)	Load Rate (1/s)	Specimen Age	Maximum Load (N)	Maximum Stress (MPa)	Maximum Strain	Failure Mode
Kennedy et al. 1976**	8.33	0.22	N/A	625.9±52.0	11	0.358±0.063	mid substance
	2.08	0.055		472.8±57.9	8	0.308±0.049	mid substance
Noyes and Grood, 1976*	38	1	48-86	734±266	13.3±5.0	0.3±0.1	bone avulsion
			16-26	1730±660	37.8±9.3	0.443±0.085	mid substance
Woo et al. 1991*	3.33	0.088	22-35	2160±157	37	N/A	avulsion dominate with midsubstance
			40-50	1503±83	26	N/A	avulsion and substance dominiate
			60-97	658±129	11	N/A	midsubstance dominiate with bone avulsion
			22-35	1602±167	28	N/A	insertion failure and avulsion dominate
			40-50	1160±104	20	N/A	insertion and midsubstance dominate
			60-97	495±85	9	N/A	mid-substance a little higher than insertion failure
Jones et al. 1995**	8.3, 30 degree	0.2	42-56	1171±339	20	0.296	mid-substance
	8.3, 30 degree	0.2	67-82	1057±269	18	0.333	mid-substance
	8.3, 30 degree	0.2	67-82	341±158	6	0.232	bone avulsion
Azangwe et al. 2001**	8	0.21	N/A	556±212	10	0.242	N/A
Chandrashekar et al. 2006**	38	1	female(26-50)	1266±527	22.58±8.92	0.27±0.08	mid-substance
			male (17-50)	1818±699	26.35±10.08	0.3±0.06	mid-substance
Paschos et al. 2010**	1.5	0.04	52-88	400.1±248	7	N/A	varied

of reconstruction than the corresponding linear properties [25]. There is a large range of modulus in each gender group in their study. Donor sex, height, and body mass were found to significantly affect tangent modulus of the low-load region [25]. In addition, Cooper et al., 1993 showed that a 90 degree twist in a PT graft significantly increased the strength of the graft [9]. Hansen et al., 2010 were able to measure the mechanical properties of the anterior fascicles and posterior fascicles obtained from young men [12]. The tangent moduli, maximum stress, and maximum strain are very close to what have been measured previously in a large scope setting [12]. Haraldsson et al., 2004 claimed that they measured regional variation in tangent modulus but they actually measured the difference between the tissue-level strain and the grip-to-grip strains [10].

Table 4.4 Summary of human patellar tendon studies. (* Data used was from Johnson 1994. ** 90 degree twist was added to the specimen. * 180 degree twist was added to the specimen. # The two studies used the same data set. Data in red are estimated values using average values of PT length (40 mm) from the literature and reported cross sectional area reported from the study. No standard deviations were reported on these estimated values; SE stands for standard error.)**

Studies	Testing Environment	Preconditioning	Age	Sample Size	Specimen Size	Strain Rate (1/s)	Tangent Moduli (MPa)	Stiffness (N/mm)	Maximum Stress (MPa)	Maximum Strain
Butler 1984 and Noyes 1984	N/A	no preconditioning	26 6	7	50mm	1	305.5±59	685.2±85.6	58.3±6.1	26.5±29
Butler 1986	N/A	N/A	21-30	3	Mid-third or medial	1	643±53	N/A	68.5±6	13.5±7
France 1988*	N/A	N/A		15	Small strap		121±37	N/A	47.4±16.3	17±5
Haut 1989	In water bath 37°C	N/A	20-24	6	Half of the entire PT	1	319±27	N/A	44.5±6.1	23.4±1.4
	With water drip	N/A	20-24	6	Half of the entire PT	1	213±20	N/A	43.7±3.9	26.6±1.0
John 1994	In water bath 37°C	2% strain for 10 cycles	29-50	15	Mid third	0.08	660±266	N/A	64.7±15.0	14±6
	In water bath 37°C	N/A	64-93	15	Mid third		504±266	N/A	53.6±10	15±15
Cooper 1993	Room temp	N/A	28±7(SE)	5	Mid third-15mm wide	1	495	555.5±67.1	97.5±8.6	19.7±1.8
	Room temp	N/A	28±7(SE)	5	Mid thrid-10mm wide	1	564	455.4±56.5	95.5±16.8	17.9±1.1
	Room temp	N/A	28±7(SE)	5	Mid third-10 mm wide	1	486	424.1±66.5	77.6±17.6	15.8±4
	Room temp	N/A	28±7(SE)	5**	Mid third-15mm wide	1	564	476.9±12.4	101.3±14	18.5±3.2
	Room temp	N/A	28±7(SE)	5**	Mid third-10mm wide	1	380	391.6±34.5	64.5±20.1	17.1±3.4
	Room temp	N/A	28±7(SE)	5***	Mid third-10mm wide	1	441	423.1±25.2	70.5±19.3	17.2±3.4
	Room temp	N/A	28±7(SE)	4	Mid third-7mm wide	1	531	326.8±57.9	92.7±20.1	18.7±1.5
Blevins 1994	Room temp and spray with saline	No preconditioning	17-54	25	Medial and center third -10 mm wide	0.1	302±83	603±182	35.9±10.9	N/A
	Room temp and spray with saline	No preconditioning	17-54	25		1	310±95	519±156	37.1±11.8	N/A
Chandrashekar 2008#	Room temp and spray with saline	N/A	Male	10	Mid third	1	479±141	N/A	N/A	N/A
	Room temp and spray with saline	N/A	Female	10	Mid third	1	490±131	N/A	N/A	N/A
Chandrashekar 2012#	Room temp and spray with saline	Pre-cycled with 5000 cycles at 1.4 HZ	17-50	10	Mid third	1	565.3±180.2	N/A	61.4±20.2	0.16±0.03
	Room temp and spray with saline	No preconditioning	17-50	10	Mid third	1	513.9±136.4	N/A	59.2±16.5	0.18±0.04

4.1.3 Summary of current human tissue mechanics testing

While these human cadaver studies have given many insights into the biomechanics of ligaments and tendons, several issues may affect the accuracy of the biomechanical properties measured from these studies. The following concerns should be considered when designing a set of mechanical experiments to characterize these tissues.

1. Inconsistency in functional tests: Functional tests provide useful information such as the *in situ* ligament elongation and force produced during a physiological movement, which facilitates understanding the ACL function *in vivo* and diagnosis of an ACL deficiency [1, 3, 6, 26, 27]. However, functional tests are different from mechanical tests because they do not provide quantitative information about the material properties of the tissue. It is difficult to compare results from different studies that intend to measure the *in situ* force and elongations because these forces and elongation measurements do not take into account the physical properties (i.e. specimen size). Results from human studies are comparable due to the relatively small variations among the same species. However, comparisons across different species to draw a conclusion should be done with caution [6].

2. Inhomogeneous geometry: As described in **Chapter 2**, the ACL and other soft tissues are usually anisotropic with inhomogeneous spatial geometries and irregular bone insertions. Therefore testing the entire tissue often does not result in a uniform and well-characterized deformation state. The bundles of the ACL clearly demonstrate various length, twists, and orientations. The properties measured during ACL testing greatly depend on how the tissue and its bone ends are oriented before testing [27]. ACL and tendon grafts have been divided into multiple bundles with more uniform geometry for mechanical testing with the goal of getting more accurate biomechanical properties [27, 28]. Therefore, to obtain a more accurate and relevant material behavior of the ACL, the fiber bundle orientation and organization needs to be considered to characterize the

individual material properties of each bundle. Butler, 1989 split the ACL into 3 sub-bundles, each with two bone ends [27]. In each individual ACL sub-bundle, the maximum strain was found to be about 15% with no significant differences found among all bundles [27]. However, the inconsistent maximum strains of the entire ACL reported from previous studies range from 0.24 to 0.44 (Table 4.2). This indicates that the different bundle orientation and initial length of the ACL made it difficult to characterize the mechanical properties of the ACL. Separating the bundles and reorienting the bones to achieve an untwisted bundle configuration provides a genuine uniaxial loading configuration that facilitates accurate measurement of the actual material properties.

3. External testing factors and internal biological factors: Testing conditions are known to affect the biomechanical responses of tissues, including test humidity, tissue hydration, tissue elongation rate, and preconditioning [18, 24, 29]. Studies have also demonstrated that donor age, gender, BMI, and the physical size of a soft tissue also affect its biomechanical properties [25, 30, 31].

4. Material properties vs. Geometric properties: Many studies only reported the structural properties of tendons and ligaments and used these properties to compare the ACL and evaluate its potential [23]. Because the structural properties are dependent on physical size of the tested tissue, unless the overall dimensions of the tissue types are similar to one another, it may be difficult to carry out a standard comparison.

5. Tissue non-linearity: Soft tissues have non-linear mechanical properties. The modulus of a ligament or tendon depends on the strain level and therefore it is important to report the strain load along with tangent modulus. For example, Chandrashekar et al., 2008 showed different moduli measured at different elongations [25]. Peak ACL strains do not normally exceed 5% during daily activities including some competitive sports activities [32]. The 0-5% range includes the toe region of ligament and tendon stress-strain curves. However,

most researchers only report the material properties measured in the linear region of the stress-strain curve, which is usually beyond 10% strain. Danto and Woo 1993 used rabbit ACL and PT to demonstrate the initial modulus and tangent modulus measured at the linear region of the stress vs. strain curve. The range over which the toe region existed differed between the PT and the ACL, with the PT exhibiting shorter toe regions (0-1.5%) than that of the ACL (0-4%) [33].

6. Stress and strain measurement: Inhomogeneous tissue strain may not only exist between different bundles but also along each bundle. Bach et al., 1998 applied strain gauges on each of the bundles in a two-bundle ACL model and demonstrated that under physical external and muscular loading conditions, they consistently obtained higher strain development in posterior lateral bundle (PLB) than in anterior medial bundle (AMB) for limited ranges of flexion [7]. These strain gauges were attached to the most superficial fibers of the ligament via sutures. The mid-substance strains were much smaller than the strains near the attachment sites [15, 17, 27]. This pattern has also been seen in the MCL [34, 35]. Stouffer et al., 1985 and Butler 1989 suggested that this pattern may serve as protection from an abrupt stiffness change [36, 37]. Therefore, simply measuring the overall strain or grip-to-grip displacement does not provide accurate information to describe the tissue's response due to the intrinsic inhomogeneity and functional gradient of tissues. A more accurate strain measurement that can map the entire tissue surface strain fields will provide more valuable information to understand the tissue's biomechanical responses. Previous investigators also demonstrated distinctly different strain behaviors along different portions of native MCL [38]. MCL flexion experiments by Arms et al., 1983 demonstrated higher strain levels near bone insertions compared to the strain in the middle region where the joint line intersects [39]. Investigations on biomechanical properties of tendon to bone enthesis by Thomopoulos et al., 2006 also demonstrate an increased strain response near the tidemark in the

entheses, where the unmineralized and mineralized fibrocartilage sections meet [40].

4.1.4 Animal models for tissue biomechanics characterization

The complex biomechanical properties of ACL and tendon grafts were partially revealed by the human studies previously mentioned. While these studies showed many factors that affect the biomechanical properties of these tissues, a comprehensive understanding is hindered by the limitations associated with the human specimens such as sample size of the study, uncontrollable intrinsic donor parameters, and donor availability. It is very difficult to determine the strength and stiffness of a complex graft after implantation in humans and thus far, no known method has been proven to be able to evaluate the complex graft in human patients. Animal studies have provided a path to investigate tissue engineering strategies so that an implanted graft could be evaluated in terms of how the first few weeks of implantation affect its mechanical and biological properties [41].

Many animal models have been used for ACL related research including small animal models such as rats [42, 43], rabbits [44-46], and rhesus monkeys [19, 47], and large animal models, such as dogs [48], goats [49-51], sheep [52-54], and cows [55]. Hunt et al., 2005 commented that using small animals may be questionable as an ACL reconstruction model because they may not clinically resemble the ACL of the human [56]. The need for large animal models to develop and evaluate innovative operative treatments is well recognized. Sheep are currently being used as large animal models for orthopaedic research. They are easily managed and their stifle joint properties are anatomically similar to the human knee joint [57]. Because of the relatively large size of the joint and its mechanical, histological and molecular biological similarities, ovine stifle joint is a suitable *in vivo* model for investigations of mechanical and biological factors in joint disorders [58]. Previously, Seitz, et al., 1997 discovered that the vascular anatomy of the ovine ACL is similar to that observed in humans [59]. This study investigated the blood supply to the ACL in back limbs of Styrian mountain sheep

and demonstrated that the large vessel and microvascular anatomy of the sheep are similar to those described for humans [59]. Murray et al., 2004 also concluded that cell number density, blood vessel density, and percentage of intrinsic cells expressing smooth muscle actin, which are known to influence the response to injury in other musculoskeletal tissues, are similar between human and ovine ACL cells [60]. Sheep tend to tolerate the graft harvest and they quickly return to normal conditions. Another advantage is that they regain the majority of their knee stability in the absence of visible restrictions of motion. Little macroscopic evidence of osteoarthritis development has been seen [56]. These findings make sheep a potential animal model for studying new interventions for the repair of damaged ACL.

4.2 The viscoelastic properties of ligaments and tendons

While many studies have focused on characterizing the structural and mechanical properties of the ACL and tendon grafts, fewer studies have been dedicated to characterizing the viscoelastic properties of these tissues. Viscoelastic properties are additional intrinsic material properties that are important for the function of the tissues and various experiments have been developed to demonstrate the viscoelasticity of a material [61]. Viscoelasticity is manifest in various experiments. When subjected to a constant strain, ligaments and tendons exhibit a decreased stress profile over time, namely stress relaxation; when subjected to a constant stress, they exhibit an increased strain profile over time, namely creep. The viscoelastic behavior can also be demonstrated from a strain rate dependent response to uniaxial tension tests. A few studies have been dedicated to quantitatively characterizing the viscoelastic properties of the human ACL or patellar tendon. Several of these studies have demonstrated viscoelasticity using animal models. Thus, in this section, human cadaver and animal studies are combined together to discuss the current understanding of viscoelastic properties of ligaments and tendons.

4.2.1 Strain rate dependence of ligaments and tendons

Woo et al., 1990 showed a strain rate dependent behavior using rabbit MCL [62]. The same group later used adult rabbits to demonstrate that both ACL and PT are strain rate dependent, that is, tissues exhibit increased modulus with increased strain rate. However, the PT is more sensitive to strain rate than the ACL [33]. In Danto and Woo 1993, the tangent modulus of PT increased by 94% while the ACL initial tangent modulus increased by 31% from a slow (0.02%/s) to a fast (380%/s) elongation rate [33]. In previous studies, Pioletti et al., 1999 also showed strain rate dependence of the ACL from a series of varied strain rate uniaxial tension tests [63]. The rate dependence was significant at the toe region of the stress-strain response at corresponding strain rates. However, no significant difference was found at the linear region of the stress-strain response of each curve. These studies suggested that the tissue is significantly affected by the strain rate at the initial stress-strain response.

4.2.2 Stress relaxation and creep of ligaments and tendons

Early studies on characterizing stress relaxation behaviors of ligaments and tendons have showed an initial rapid stress relaxation followed by a gradual relaxation response which is present in the ligaments and tendons of both human and animals [29, 34, 55, 61, 64, 65]. However, these studies only measured the stress relaxation responses at a single strain level. To understand whether the viscoelastic behavior was also strain dependent, Pioletti et al., 2000 used various stress relaxation tests to compare the viscoelastic responses of human ACLs and patellar tendons [66]. They postulated that the stress relaxation responses of these tissues could be treated as strain-independent up to a certain strain level. The strain levels are tissue specific with the ACL at higher strains (16%) and the PT at lower strains (6%) [66]. Human and animal studies have shown that the strain range of the ACL during normal daily activities is within 0-5% [67-69]. Therefore, the conclusion in Pioletti et al., 2000 cannot be directly applied to the ligament and tendon viscoelastic responses at small strains. Provenzano et al., 2001, Hingorani et al., 2004, Bonifasi-Lista et al., 2006 and recently Duenwald et

al., 2010 all demonstrated that at lower strain (or stress) levels, the viscoelastic properties of tendons and ligaments from human and animals were both time- and strain-dependent in stress relaxation or creep [65, 70, 71]. Provenzano et al., 2001 and Hingorani et al., 2004 showed that MCLs from both rat and rabbit exhibited faster relaxation rates at lower strain levels (less than 5%) [70, 72]. Recently Duenwald et al., 2010 demonstrated that while ligaments relax faster as the initial strain level decreases, tendons relax slower at lower strain levels -- ligaments and tendons exhibit opposite relaxation rate tendencies [71].

This information is important when considering suitable grafts to replace ACLs. As these studies showed, tendons differ from ligaments biomechanically. It is questionable whether tendons, such as patellar tendons, would be suitable to replace the ACL. Viscoelasticity is important in daily life as stress relaxation characteristics are believed to help reduce the risk of ligament injury during prolonged static deformation [61]. Whether tendon grafts remodel and accomplish ligamentization is still under debate and little is known about whether the remodeled tendon grafts will exhibit the same viscoelastic responses as the ACL.

4.3 Experimental Analysis of Native and Engineered Rat MCLs

To evaluate the efficacy of the tissue engineered BLB constructs (described in **Chapter 3**) we used as a rat MCL replacement, we designed and conducted cyclic uniaxial tensile tests on the engineered constructs after 1 month and 2 months of implantation. The contralateral native MCL was also evaluated for baseline comparison. To accurately measure local strain, micro glass beads were applied to the tissue surface and used as surface markers. Digital image correlation analysis was then applied to obtain accurate local strains and 2D strain contours. One-month and two-month implantations were performed with the engineered BLBs. The experimental data demonstrated that the tangent moduli of the BLB one-month explants increased by a factor of 2.4 over *in vitro* controls, to a value equivalent to those observed in 14-day-old neonatal rat

MCLs. These BLB one-month explants also exhibited a functionally graded response that closely matched native MCL inhomogeneity, indicating the constructs functionally adapted *in vivo*.

4.3.1 Cyclic uniaxial tensile tests

Cyclic tensile tests on BLB constructs and native MCLs were conducted to obtain viscoelastic responses to multiple load/unload cycles, calculate tangent modulus during the initial load excursion, examine the mechanical heterogeneity of the ligament response, and evaluate the mechanical integrity of the engineered enthesis. An in-house designed tensiometer was employed to conduct the cyclic tension. A chamber located in the middle of the tensiometer had two grips protruding into the chamber that were connected to stepper motors. The chamber was filled with saline to test the specimens in hydrated conditions. The bones at the ends of the specimens were secured into the grips by clamping pressure where by the ligament and enthesis regions were positioned away from the grips to eliminate stress or strain concentrations on these tissues. The specimen diameter was measured at several positions along the length using an inverted microscope (Axiovert 25 at X50 magnification; Carl Zeiss, Thornwood, NY), allowing the average diameter of the ligament portion to be calculated. Blue microsphere fiduciary markers (25 μm diameter, 403-025 IMT, Irvine, CA) were brushed on the surface of the ligament portion of the constructs for digital image correlation analysis of tissue displacements to provide highly accurate calculations of the tissue strain field along the entire ligament. Images of the deforming tissues were taken using a 1.4 megapixel digital video camera (Basler, Ahrensburg, Germany) mounted on the microscope. 3D BLB and native MCL samples were loaded in the tensiometer under cyclic tension loading (0-10% strain, 0.01 Hz) and the synchronized force and image recordings were compiled and controlled by LabVIEW software (National Instruments, Austin, TX) on a Dell Precision 300 computer. Five load-unload cycles were conducted to characterize the overall non-linear viscoelastic response based on the average strain along the section length of the ligament

portion of the BLBs and native MCLs. These same cyclic loading data were used with the local strain field measurements to examine the functionally graded response of the engineered or native ligament. A maximum strain of 10% was chosen to examine the cyclic response within the MCL.

Force versus digital image data were converted to nominal stress versus nominal strain. The stress was computed by normalizing the load data by the average cross-sectional area of the samples. Strain data were analyzed using the image processing functions in the imaging software package MetaMorph, a 2D Digital Image Correlation method, and a preprocessing data smoothing technique in MATLAB [The MathWorks, Inc. Natick, MA]. The images generated during the tests were loaded as a stack into MetaMorph, and the object tracking function generated displacement value sheets of targeted markers. Nominal strains between markers were calculated and smoothed with a Savitzky-Golay filtering method to reduce any vibration effects [The MathWorks, Inc. Natick, MA]. Smoothed strain data were combined with the synchronized nominal stress data to create the cyclic nominal stress vs. nominal strain response curves for each specimen. The (maximum) tangent modulus was determined by calculating the maximum value of the slope of the nominal stress versus nominal strain response of the initial load cycle. Displacement continuity was verified across the engineered enthesis of BLB samples to verify structural integrity over the cyclic strain range.

Five sequential load-unload tension response curves are shown for *in vitro* 3D BLB constructs **(**Figure 4.1**A)**, 3D BLB one-month explants **(**Figure 4.1**B)**, and native 14-day neonatal rat MCL **(**Figure 4.1**C)**. The *in vitro* constructs displayed the characteristic non-linear soft tissue response that included an initial toe region followed by strain hardening. The ligament tangent modulus of these constructs was 14.3±3.0 MPa (n=4; Figure 4.2). They also displayed hysteresis in the initial load-unload response, characteristic of viscoelastic materials, and the subsequent cycles overlapped the first. After one month of implantation, the

ligament explants grew physically in size and their tangent modulus increased on average by a factor of 2.4 to 34.6±17.1 MPa (n=4; Figure 4.2). The BLB explants had a cross sectional area of 0.25±0.17mm^2, which is approximately 2 fold greater than that of 14-day neonatal rat MCL (0.12±0.06mm^2). The toe region in the mechanical response of the BLB explants transitioned to strain hardening more gradually and at lower strain levels than those of *in vitro* controls and strain softening behavior was observed in some specimens. The BLB constructs *in vitro* and upon explantation all demonstrated mechanically viable entheses that withstood the cyclic strain protocol without separation or tearing of the interface. The native 14-day neonatal MCL exhibited a similar cyclic loading response **(**Figure 4.1**C)** to that of the 3D BLB explants **(**Figure 4.1**B)** including a similar transition from the toe region to strain hardening and approximately the same tangent stiffness as the BLB explants, 47.6±22.9 MPa (n=5; Figure 4.2).

A.

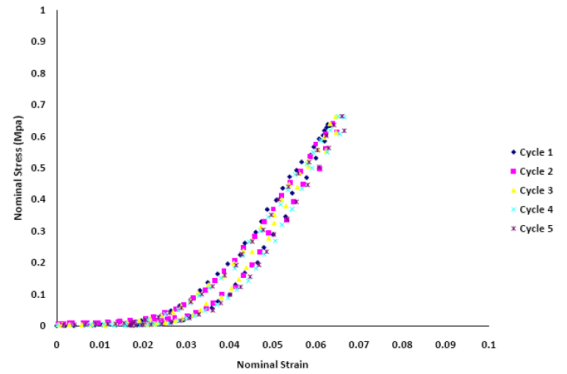

B.

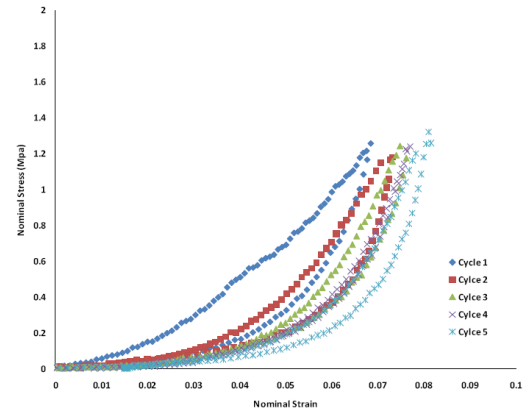

C.

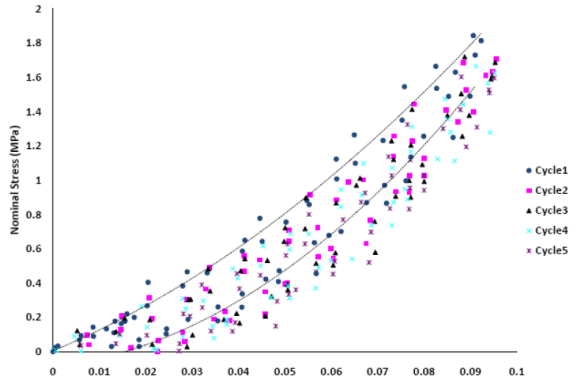

Figure 4.1 Nominal stress versus nominal strain cyclic response curves for *in vitro* 3D BLBs, 3D BLB explants and 14-day native MCLs. (A) Stress-strain response of the *in vitro* 3D BLBs shows that the non-linear cyclic response includes a toe region, strain hardening and hysteresis. (B) Stress-strain response of 3D BLB explants after 4 weeks as MCL replacement tissues on a stress scale that is (approximately) twice that in (A), indicating an increase in mechanical stiffness of the construct during *in vivo* implantation. The non-linear response includes hysteresis and an earlier and more gradual transition to strain hardening than in the *in vitro* BLBs. (C) Stress-strain response of native 14-day neonatal MCL shows similar non-linear stress-strain cyclic behavior to that observed in the 3D BLB explants.

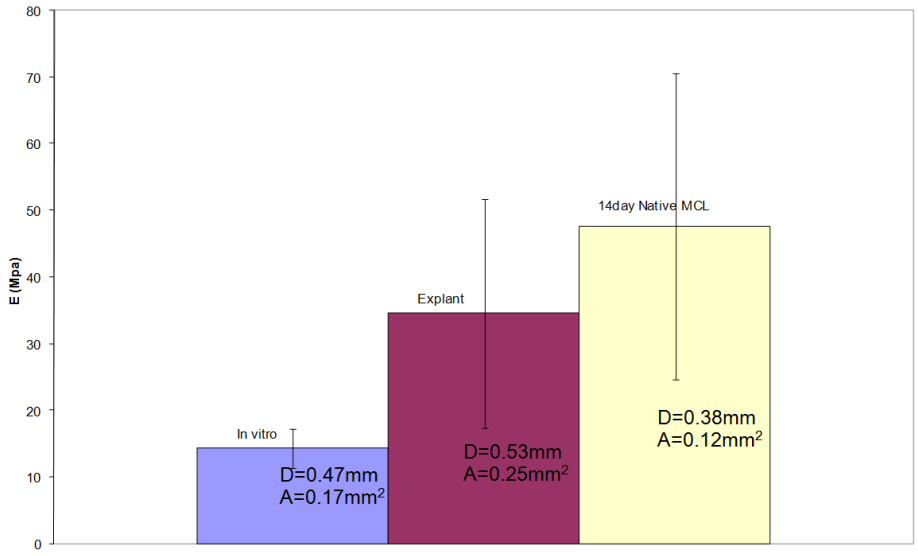

Figure 4.2 Comparison of tangent stiffness, average diameter and cross sectional area of *in vitro* 3D BLBs, 3D BLB explants and 14-day native MCLs.

The peak load experienced by the BLB explant in Figure 4.1**B** during cyclic tension testing was P_{MAX} = 0.7 N, measured at a peak strain of ε = 0.083. The native MCL in Figure 5**C** experienced P_{MAX} = 0.25 N during a similar test protocol and measured at ε = 0.095. The cross-sectional area of a BLB explant and hence its geometric stiffness (P_{MAX}/peak strain) exceeds that of the native MCL by a factor of approximately 2.0, therefore the BLB explant carried a higher load than the native MCL at a similar strain level.

4.3.2 Inhomogeneous and functional gradient characterization

Representative local mechanical response curves are shown for *in vitro* 3D BLB constructs (Figure 4.3**A**), 3D BLB one-month explants (Figure 4.3**B**) and native adult rat MCL (Figure 4.3**C**). Regions were chosen from 2-4 mm long sections near the bone insertions and from the mid-section along the ligament portion. Local stress vs. strain response curves from both ends and the mid-section of the *in vitro* constructs lie on top of each other, indicating a homogeneous mechanical response. However after one month of implantation,

the 3D BLB constructs developed an inhomogeneous strain response along their length. The mid-section of the ligament portion is relatively stiff (curves shown in blue) compared to the ends of the ligament where it inserted to the bones (curves shown in red), showing a functionally graded strain response *in vivo*. The native adult rat MCL exhibited a similar functionally graded pattern to that of the BLB explants; the ends of ligament are more compliant and the middle section is stiffer.

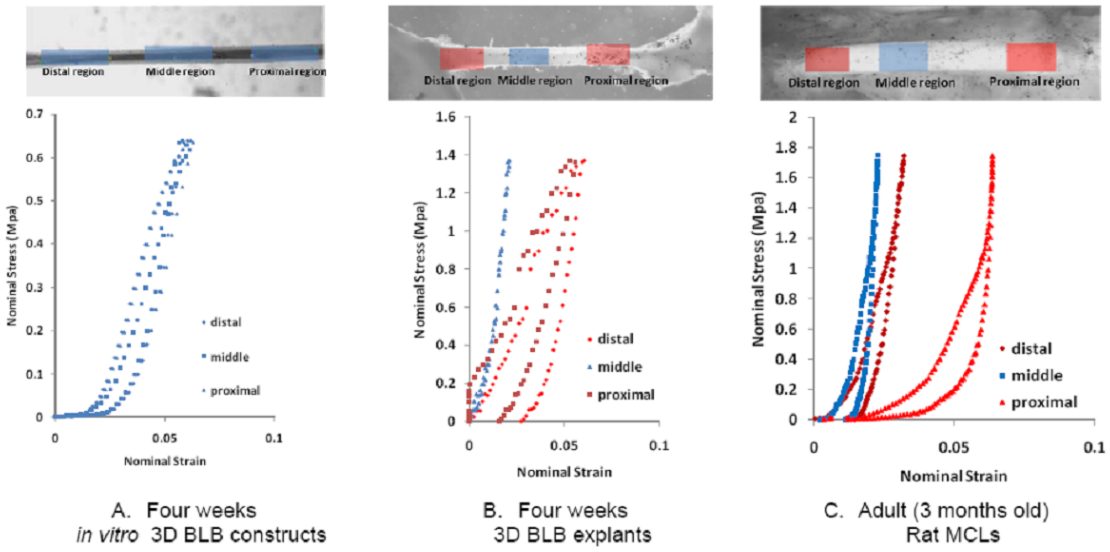

Figure 4.3 Localized stress vs. strain analysis of 3D BLB constructs *in vitro* (A), 3D BLB explants (B) and native rat MCL (C) with corresponding regions shown in the specimen photos. Developed for four weeks *in vitro* 3D BLB constructs show uniform strain response. After one month of implantation, strain responses are localized in 3D BLB explants, showing a functional gradient that is also indicated in native MCL. Regions that are closer to bones are relatively more compliant than the ligament mid-sections in both 3D BLB explants and native MCLs.

4.3.3 Remarks

The tissue engineering approach presented in this study avoids the use of a scaffold, commonly used incurrent tissue engineering approaches, and adopts a design rubric based on the concept of displacement or strain controlled rather than load (or stress) controlled mechanical requirements of knee ligaments. Maximum strain levels during rehabilitation exercises in humans have been estimated at 0.05 (or 5%), which is approximately 25% of the failure strain in

native knee ligament [73]. Our *in vitro* 3D BLB constructs are capable of withstanding repeated strain cycles in excess of 0.05. We tested the hypotheses that these constructs were capable of surviving the strain levels placed on the MCL of an adult rat during normal ambulatory motion and that the initial compliance of the ligament regions of the 3D BLB will allow cells within the construct to experience strains *in vivo* and deposit ligamentous extracellular matrix (ECM). None of the 3D BLB constructs failed *in vivo*. All implanted constructs were found to be well integrated to the native bone at the tibial and femoral insertions. After one month *in vivo* the explanted BLB constructs showed physical growth from an average area of 0.17±0.04mm^2*in vitro* to 0.25±0.17mm^2. Type 1 collagen was present throughout the cross section of the ligament portion of the 3D BLB explants. The changes in size and collagen constitution resulted in an increased geometrical stiffness P_{MAX}/length = 0.01N/mm in vitro vs. P_{MAX}/length = 0.09 N/mm in 3D BLB explants as well as an increased tangent modulus of 14.3±3.0 MPa *in vitro* vs. 34.6±17.1 MPa in explants. The geometric stiffness of the 3D BLB explants significantly increased and had the same value compared to the stiffness of the 14-day native MCL (P_{MAX}/length = 0.09 N/mm). The tangent modulus of the 3D BLBs increased significantly from *in vitro* to explant values (p=0.0309) and the tangent modulus of the 3D BLB explants did not differ significantly from that of the native MCLs (47.6±22.9 MPa). None of the four 3D BLB explants failed during cyclic loading to approximately 10% strain indicating mechanically viable engineered interfaces (entheses). The average mechanical response is not sufficient to fully characterize the mechanical properties of ligament and tendon. Our present results for native adult MCL show a heterogeneous or functionally graded mechanical response that is consistent with previous MCL studies [38-40]. Results from our implantation show the engineered 3D BLB constructs adapted a functionally graded mechanical response *in vivo* that matches the heterogeneity of native MCL.

The current design requirements of engineered tissue for ligament replacement aim to restore stability to the knee at the time of replacement. Many

recent studies have shown that neither autogenous grafts nor scaffold-based engineered approaches ever attain the strengths of uninjured controls and that a large percentage (40-78%) of engineered ligaments have failed after a period of time *in vivo* [73]. We are unaware of a previously published study in which the mechanical properties of an engineered ligament improved over time *in vivo*. We have speculated that the conditions required for rapid growth of normal collagen in ligament *in vivo* differ significantly from those required for collagen content maintenance. In particular, we targeted extensibility to withstand physiological strain levels and compliance to allow transduction of cellular signals, as two important design features of our engineered constructs. We further hypothesized that the ideal engineered ligament construct would exhibit non-linear viscoelasticity, including strain rate dependence and hysteresis in cyclic loading, to more closely resemble the response of native tissue.

In summary, following implantation, 3D BLB constructs grew in thickness and the cross sectional area was on average 2 fold larger than that of the 14-day neonatal MCLs. The ligament region of the rat 3D BLB constructs showed an increased tangent modulus by a factor of 2.4. Load comparisons at the maximum cyclic strain levels of 10% during tensile testing reveal the 3D BLB constructs were actually carrying higher loads without failure.

4.4 Experimental characterization of sheep native ACL, patellar tendon, patellar tendon autograft explants and engineered BLB explants

The encouraging results obtained from the rat MCL replacement study motivated us to evaluate the efficacy of our tissue engineering strategy as an ACL graft. We fabricated the engineered BLB to match the size of a sheep ACL and performed an ACL replacement using the sheep model (**Chapter 3**). The morphological and histological characterizations of these engineered BLB constructs after *in vivo* recovery showed rapidly improved biological properties that resembled those of the native ACL. To compare the mechanical properties and functions of the engineered BLB to the native ACL and the commonly used

patellar tendon autografts, we performed experiments to characterize the function, material properties, and viscoelastic properties of these tissues. In our ACL studies, we have conducted two separate studies with different objectives. In an earlier study, we utilized the tissue engineered BLB in the sheep model with a 6-month *in vivo* recovery time to evaluate the efficacy of the engineered BLB used as an ACL replacement. The promising results from the study led us to continue with a longer *in vivo* study (9-month) to compare our tissue engineered BLB with a commonly used PT autograft and evaluatethe potential of the engineered BLB as an ACL replacement graft.

4.4.1 Uniaxial tension tests and knee laxity analysis

In the 6-month study, uniaxial tension testing was then conducted on the BLB explants and on ACL specimens from both operated and non-operated animals to obtain the tensile extensibility, stiffness and strength using an MTS 810 servo hydraulic test system with a 25 kN load cell. A 6 mm hole was drilled on the proximal end of the femur and the distal end of the tibia. Two 6 mm stainless steel bars were inserted into the holes drilled on the bones for attachment to the metal grips on the MTS so that the femur and tibia were fixed in a 0º flexion angle. The grips hung into a trough to submerge the specimen in saline allowing testing in a hydrated state. Initially, there was no pretension applied along the axis of the specimen. A Grasshopper IEEE-1394b digital camera was used for synchronized image acquisition. Ink markers were applied to the surface of all tissues to track the displacement. The samples were subjected to five continuous load-unload cycles at a constant strain rate of 0.05/s followed by loading until failure and the synchronized force and image recordings were compiled using LabVIEW.

In vitro BLB constructs were tested using a customized tensiometer designed in our lab and a 5 N load cell as described previously in **Section 4.3.1**. The samples were subjected to five continuous load-unload cycles at constant strain rate followed by loading until failure and the synchronized force and image

recordings were again compiled using LabVIEW. Image J and Metamorph software was used for displacement calculation via digital image correlation analysis of image data from a Basler A102fc digital video camera.

In the mechanics experiments, the secondary slope of the raw load vs. particle displacement response curve determined the geometric stiffness. The data were then converted to nominal stress (load/CSA) vs. nominal strain (change in separation of image data/initial separation). The (maximum) tangent modulus was determined by calculating the secondary slope of the nominal stress vs. nominal strain response curve.

In the 9-month study, we improved our testing apparatus with (1) a new grip system that can vary the knee testing angle, (2) a customized *in vivo* drawer tester that can measure the joint laxity at a given knee flexion angle, and (3) a new local strain deformation capture system that can track the full-field tissue surface strain contours. These improvements helped us to obtain the most accurate stress and strain measurements to characterize and compare the biomechanical properties of BLB explants, patellar tendon autograft (PTG) explants, native ACL, and native PT.

A customized anterior drawer tester using MTS 810 servohydraulic test system equipped with a 25kN load cell was fabricated to measure the knee laxity at 45 degrees (Figure 4.4). The bones were secured by two ¼ in screws through the grips. The knee with grips was installed onto the MTS. India Ink markers were brushed onto the femur and tibia to enable measurement of displacement. A 0.5mm/s displacement rate was applied to the tibia until a 50 N force was achieved. A grasshopper IEEE-1394b digital camera was utilized to record synchronized camera images during the tests. Metamorph software was used for displacement calculation by tracking the markers on the specimens.

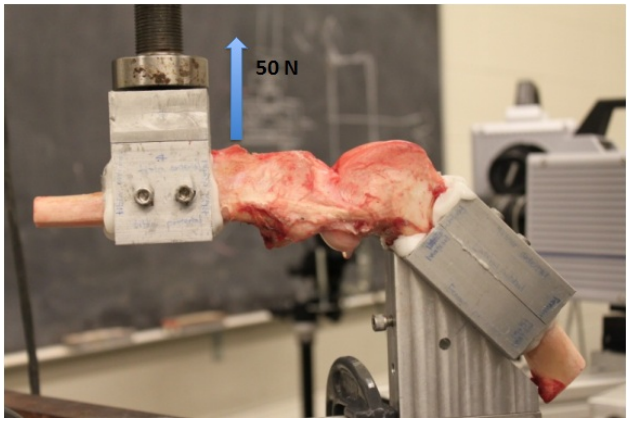

Figure 4.4 Customized anterior drawer tester designed and fabricated to measure the *in vitro* knee laxity at a 45 degree knee flexion angle. The tibia grip was fixed at 0 degrees and the femur grip was fixed at 45 degrees. A force was applied perpendicular to the tibia shaft from the MTS at a displacement rate of 0.5mm/s. Once the force reached 50 N, the displacement of femur and tibia location was recorded to measure knee anterior tibia translation.

After anterior drawer tests, all tissue was removed leaving only the ACL or its replacement graft attached. Measurements including length, width and thickness were recorded. The femur was repositioned at 60 degrees and tibia was at 90 degrees in the sagittal plane so that the knee flexion angle was 30 degrees. Blue Kote Aerosol (N.W.Naylor Co. Morris, NY) was sprayed onto the specimen surface for optical displacement measurement using digital image correlation (DIC) (Figure 4.5**A**). A tattooed speckle pattern was also developed for surface markers for DIC (Figure 4.5**B**). Both methods were used to compute full-field strain contours from digital image correlation. Uniaxial tension tests were then conducted on the BLB explant, the PTG explant, and ACL specimens to obtain the tensile extensibility and stiffness. A Photron high-speed camera was used for synchronized image acquisition. The samples were subjected to multiple load-unload cycles at constant strain rates. Finally the specimens were loaded until failure. Correlated Solution VIC-2D software was used for local displacement calculation and full-field strain contours via digital image correlation analysis of the camera image data.

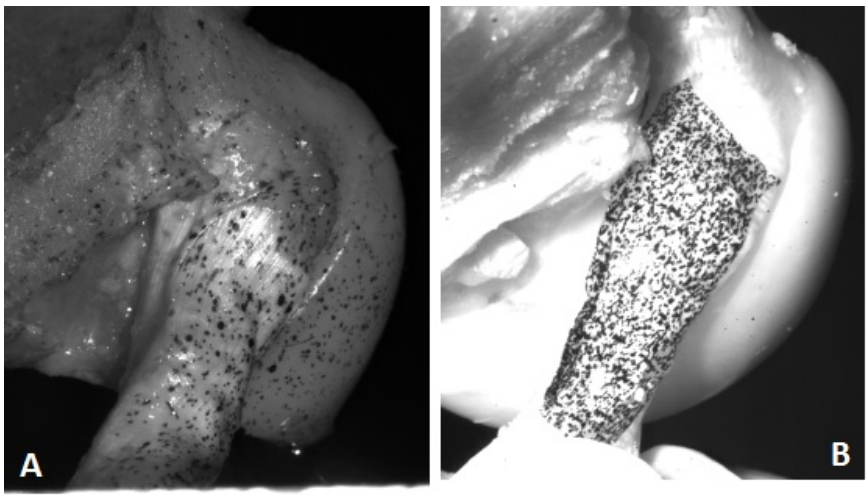

Figure 4.5 Speckle patterns on the tissue surface to facilitate accurate tissue local deformation measurement. The pattern on (A) is generated by spraying Blue Kote Aerosol on the surface of the tissue. The pattern on (B) is generated by attaching a pre-patterned tattoo transfer to the surface of the tissue.

In the mechanics experiments, the secondary slope of the raw load vs. particle displacement response curve determined the geometric stiffness. The data were then converted to nominal stress (load/CSA) vs. nominal strain (change in separation of image data/initial separation). The (maximum) tangent modulus at a strain range of 0.04-0.08 was determined by calculating the secondary slope of the nominal stress vs. nominal strain response curve.

4.4.2 Results from uniaxial tension tests in the 6-month study

We conducted mechanical loading tests by prescribing a displacement ramp to a given strain level and then reversing to zero strain at the same rate (a strain-controlled load-unload tension test). The tangent modulus (the slope of the stress-strain curve at specified strain range) of the BLB explants at six months (N=3) averaged 130.0±17.2 MPa (strain range: 0.10 – 0.35), the modulus of the contralateral ACL, 250.7±8.5 MPa (N=3; strain range: 0.10 – 0.35), and the tangent modulus of ACLs from non-operated animals was found to be 232±11 MPa (N=2; strain range: 0.10 – 0.35), see Figure 4.6**A**. We also measured geometric stiffness (the slope of the load-displacement curve at a specified

displacement) and found it was 359.0±150.6 N/mm for the BLB explants and 379.2±73.6 N/mm for the contralateral ACL (Figure 4.6**B**). The geometric stiffness was a function of the CSA and composition of the graft, both of which varied in the developing BLB explants at six months. Prior to implantation the BLB constructs had a tangent modulus of 1.4±0.14 MPa (N=3; strain range: 0.2 – 0.3). These data indicate that after six months *in vivo* as an ACL replacement, the BLB constructs increased in mechanical properties by a factor of over 90 to attain 52% of the tangent modulus and 95% of the geometric stiffness of an adult contralateral ACL.

We measured the initial responses to an imposed strain of 0.15 in the BLB explants at six months vs. the animal-matched adult contralateral ACL (Figure 4.6**C** and **D**). These data demonstrate that the initial stress-strain response of the BLB explant at six months is more compliant than the native ACL in the 0% to 10% strain range (the physiologically relevant *in vivo* range) but that the load-displacement response curves of the BLB explant and the adult contralateral ACL are quantitatively and qualitatively similar. The load-displacement results indicate that at six months the BLB explants are capable of carrying physiologically relevant loads, accurately matching the biomechanics of adult ACL. The stress-strain results demonstrate that the tissue of the BLB is not yet fully remodeled to that of adult ACL because the BLB is more compliant than the adult ACL. More time *in vivo* or a rehabilitation protocol may allow complete remodeling of the BLB to an adult ACL phenotype.

We conducted mechanical loading tests by prescribing a displacement ramp to a given strain level and then reversing to zero strain at the same rate (a strain-controlled load-unload tension test). These load-unload experiments were conducted on animal-matched ACLs and patellar tendons of two month-old (N=2) and adult (N=1) sheep (Figure 4.7). Both tissues exhibit non-linear viscoelasticity with hysteresis in the load-unload response. At small strains the stress-strain response curves of the patellar tendon and ACL diverge and the patellar tendon

is seen to have a higher tangent modulus (slope of the stress-strain loading curve) as shown for example by the grey line segments in (Figure 4.7) at all strain levels beyond 0.002 (0.2%). These data are in agreement with recent data on patient-matched human ACLs and patellar tendons, which also demonstrated a greater tangent modulus for the patellar tendon [25].

Strength of Bone/Graft and Bone/ACL Complexes: Three BLB explants at six months and contralateral ACLs were loaded until failure after completion of the load-unload and stress relaxation experiments. In all cases failure occurred by failure of the tibia in the grip of the testing system, therefore no failure loads can be recorded for our BLB explants or the contralateral ACLs. However the maximum loads before bone failure in the grips occurred were recorded and the average values are 676.3±356.4 N (N=3) for the BLB explants and 970.7±384.1 N (N=3) for the contralateral ACLs. The maximum loads expected *in vivo* are conservatively estimated at 250 N (the load at 10% strain). Although BLB strengths could not be determined, they clearly exceed the *in vivo* loads. All of the seven implanted BLB constructs integrated with native bone, and all survived the implantation experiments intact.

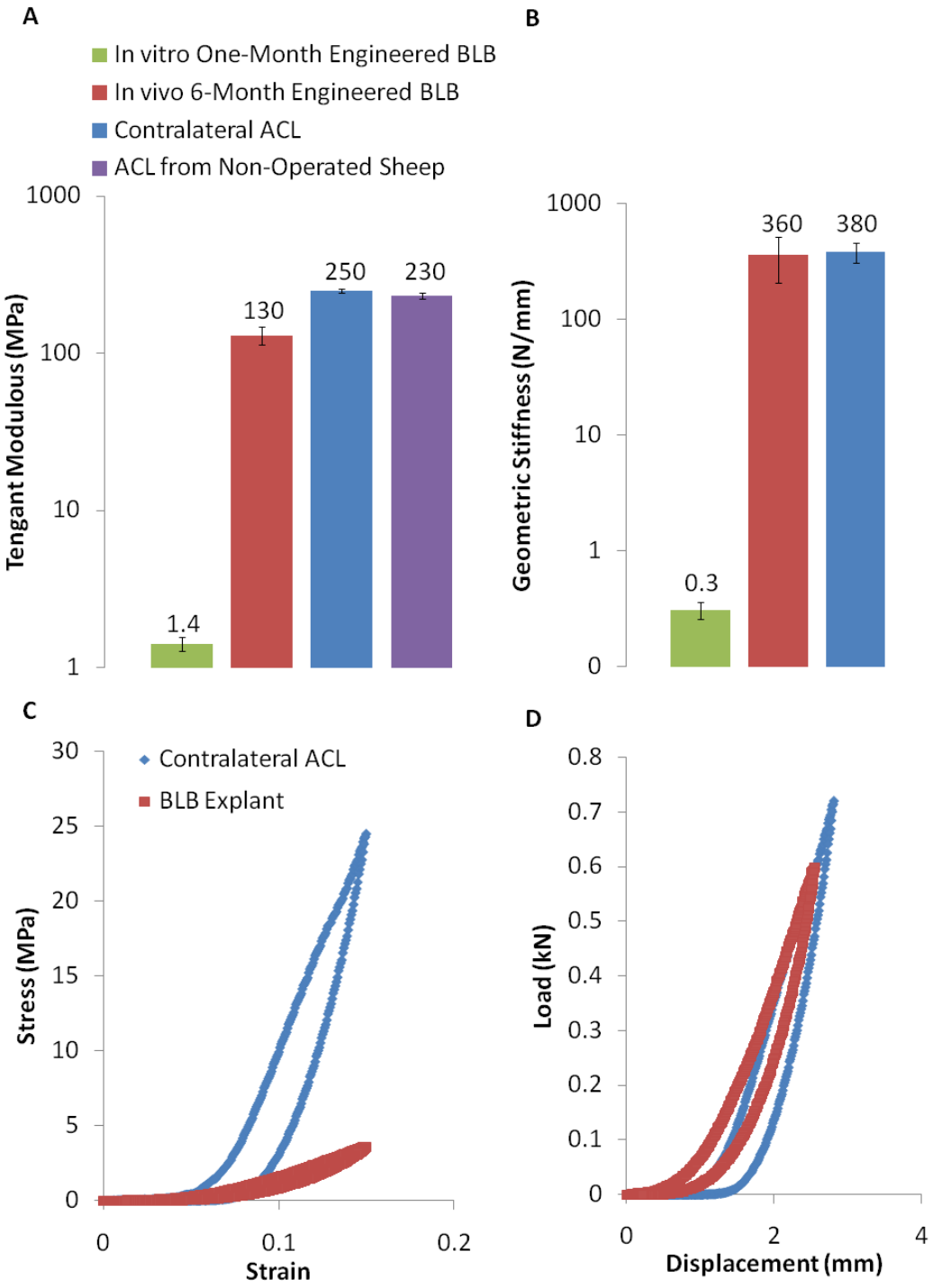

Figure 4.6 Stiffness of BLB explants after implantation and contralateral ACLs at six months of adult sheep. (A) Tangent modulus of the linear portion of the stress-strain response curves over a strain range of 0.10 to 0.35. (B) Corresponding geometric stiffness (C) Stress-strain relationship and (D) Load-displacement curves detailing the initial responses (physiological or <5% strain) of BLB explants and adult CL ACL.

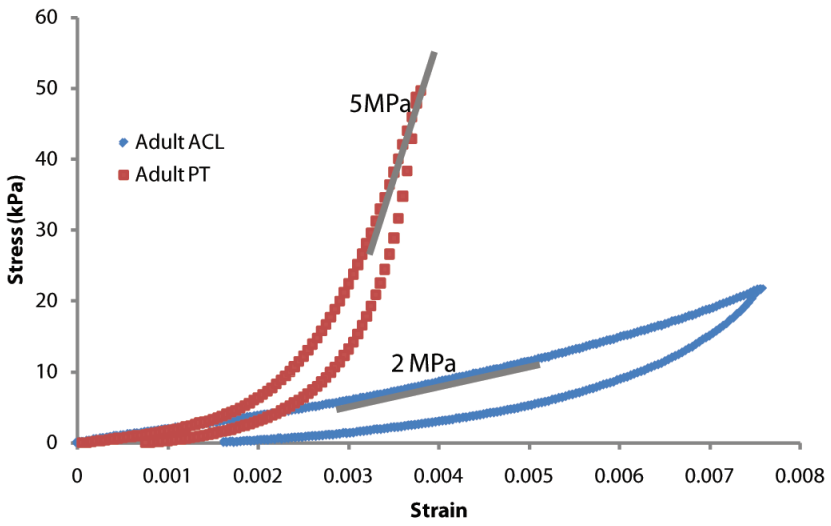

Figure 4.7 Representative stress - strain response curves of a patellar tendon and an ACL from the same animal.

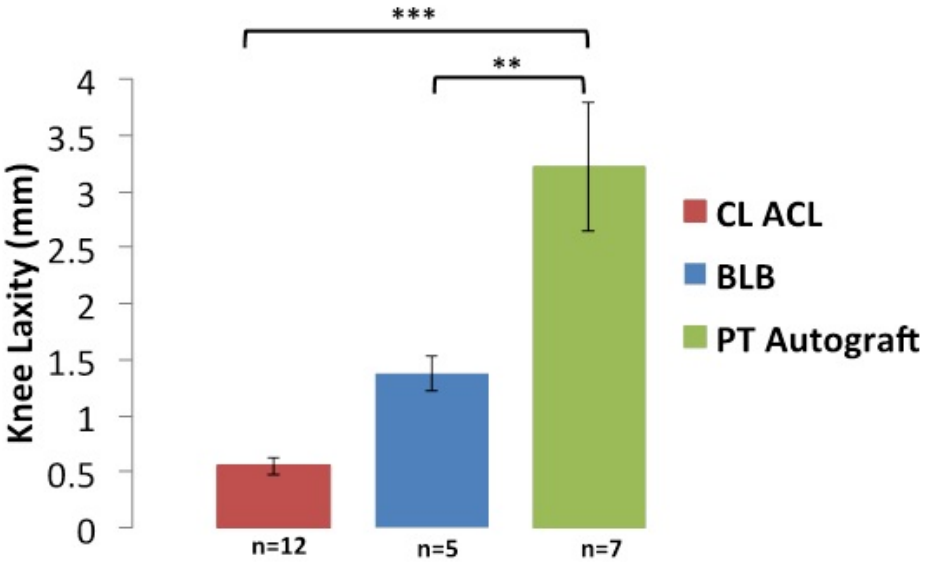

Figure 4.8 Knee laxity measurements from anterior drawer tests show no significant difference between the BLB knee after 9 months and the contralateral ACL knee. There are significant differences between the PT autograft (PTG) receiving knee after 9 months and the contralateral ACL knee, and between the PT autograft receiving knee and BLB knee after 9 months. ** p<0.025, *** p<0.001

4.4.3 Results from knee laxity and uniaxial tension tests in the 9-month study

Knee Laxity: The anterior tibial translation of the BLB knee after 9 months was 1.4±0.2 mm (N=5), the PTG knee was 3.2±0.6 mm (N=7), and the contralateral knee was 0.6±0.1 mm (N=12) (Figure 4.8). The PTG knees were significantly more lax than the BLB knees (*p<0.025*) and the contralateral knees (*p<0.001*). No significant difference was found between BLB and the contralateral knee laxities (p=0.56).

Mechanical properties: The geometric stiffness (the slope of the load-displacement curve at specified displacement) was 205.7±21.8 N/mm for the contralateral ACL, 122.8±38.2 N/mm for the BLB explants, 77.0±23.8 N/mm for the PTG, and 348.3± 24.3 N/mm for the native PT (Figure 4.9). The tangent modulus (the slope of the stress-strain curve at specified strain range) of the contralateral ACL averaged 110.4±7.6 MPa (N=14; strain range: 0.04 – 0.08), the BLB explants at 9 months, 57.4±16.9 MPa (N=7; strain range: 0.04 – 0.08), PTG, 35.3 ± 12.6 MPa (N=7; strain range: 0.04 – 0.08), and native PT, 190.0±13.2MPa (N=3; strain range: 0.04 – 0.08; Figure 10**B**). These data show that after 9 months in vivo as an ACL replacement, the BLB constructs increased in mechanical properties by factor of 40 to attain 52% of the tangent modulus and 60% of the geometric stiffness of an adult contralateral ACL. In contrast, the PTG decreased in mechanical properties to 32% of the tangent modulus and 37% of the geometric stiffness of the contralateral ACL.

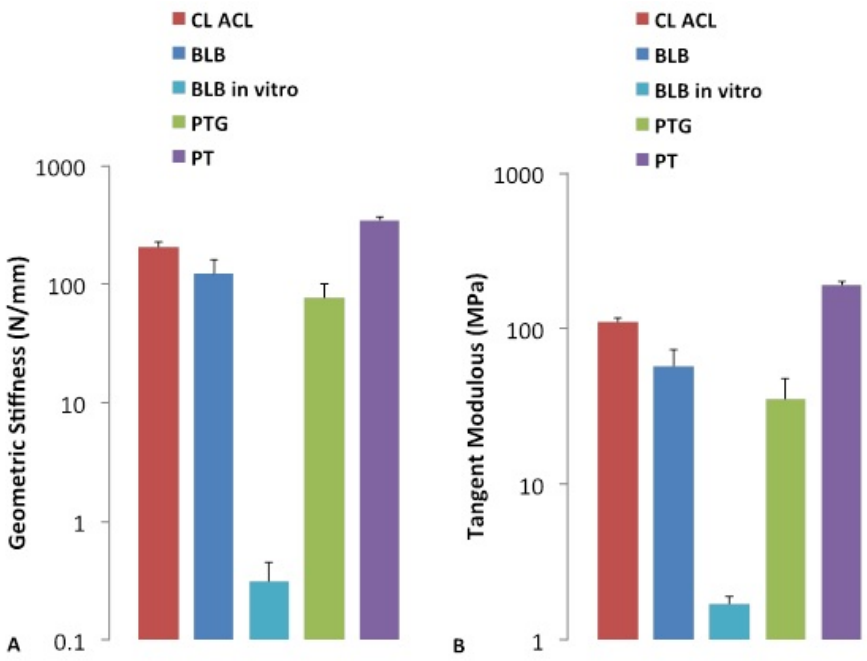

Figure 4.9 Geometric stiffness (A) and tangent modulus (B) of BLB before, and after 9 months *in vivo*, PTG after 9 months in vivo, contralateral ACLs and PTs of adult sheep. Geometric stiffness of the force-displacement curves was measured over a displacement range of 0.6 mm to 2.0 mm. Tangent modulus of the stress-strain curves was measured over a strain range of 0.04 to 0.08.

Full-field strain contours of BLB explant, PTG explant, Native ACL and PT:

The full-field axial strain contours of all tissue captured during axial loading show the ACL (left knee) is a heterogeneous material with the highest strain levels at the distal end of the ACL (Figure 4.10**A**). The BLB (right knee) contours are practically a mirror image of the CL ACL with the highest strain levels at the distal end of the BLB (Figure 4.10**B**). The PT is a relatively homogenous material (Figure 4.10**C**). The strain contour of the PTG after 9 months of recovery did not develop a functional gradient similar to that of native ACL (Figure 4.10**D**).

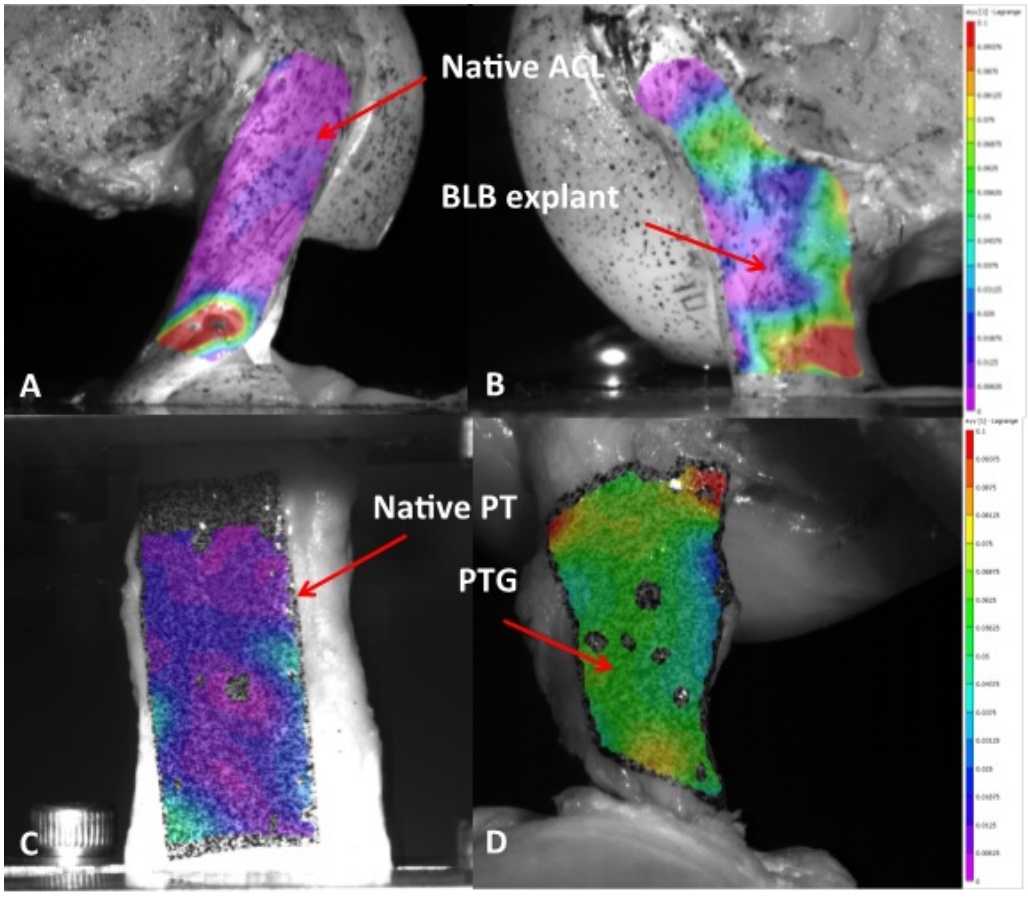

Figure 4.10 Full-field displacement contours of native ACL (A), BLB explant after 9-month recovery (B), native PT (C) and PTG after 9-month recovery. The contours are presented at the same strain magnitude with the red color representing the highest strain (10%).

4.4.4 Viscoelastic characterization

In the 6-month study, stress relaxation tests were conducted to obtain the viscoelastic responses of BLB and native ACL and patellar tendon specimens using an RSA III Dynamic Mechanical Analyzer (DMA) (TA Instruments, New Castle, DE) equipped with a 35 N load cell. Prior to testing, the BLB and ACL were isolated from the knee with the femur and tibia attached. Both femur and tibia were trimmed to approximately 20 mm X 20 mm X 15 mm in order to fit into the DMA grips. Care was taken to keep the soft tissue intact during the trimming process. Blue Kote Aerosol (Dr. Naylor) was sprayed onto the specimen surface for optical displacement measurement using digital image correlation as shown in Figure 4.11. Measurements including length, width and

thickness were recorded before the tests. The DMA was controlled using TA Orchestrator software provided by TA Instruments. A Grasshopper IEEE-1394b digital camera was employed for synchronized image acquisition. The samples were subjected to continuous load-unload cycles at constant strain rate (0.01/sec) followed by stress relaxation at three different strain levels. Times, loads and synchronized camera images were recorded. During the tests, the specimens were kept in a hydrated state by dripping DPBS onto the specimen.

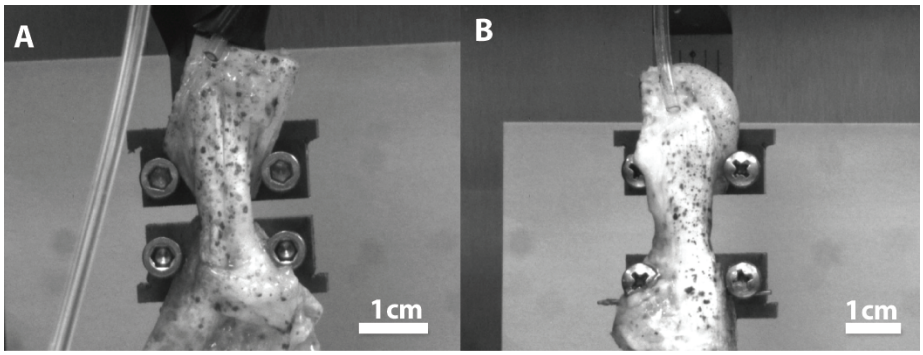

Figure 4.11 Spray were applied to the surface of the ACL (A) and BLB (B) for displacement markers.

The non-linear stress relaxation response of the BLB explants after six months as ACL replacements in the sheep (N=1) was compared to those of the native ACL in the contralateral knee (N=1) and to adult patellar tendons (N=2). The results for an animal-matched ACL and BLB pair are shown in Figure 4.12**A** and **B**. The stress relaxation response of the BLB explant is virtually indistinguishable from that of the contralateral ACL indicating the BLB is capable of maintaining physiologically relevant viscoelastic characteristics of adult ACL after six months as an ACL replacement in the sheep. The patellar tendon stress relaxation results are shown in Figure 4.12**C** to differ from those of the ACL and our BLB explants in important ways. The initial rate of patellar tendon stress relaxation increases with increased initial strain and the relaxation rate reaches a steady state at long times, whereas for the ACL and the BLB explant the rate of relaxation decreases with increased initial strain.

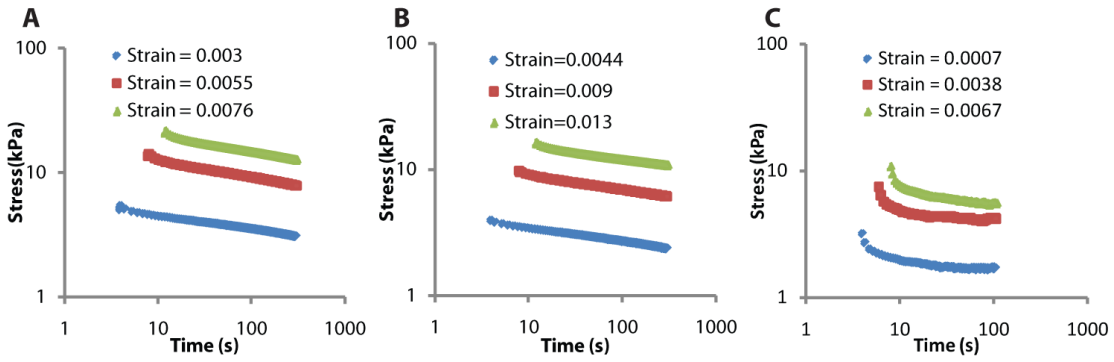

Figure 4.12 Stress relaxation as a function of initial strain for animal-matched (A) ACL and (B) BLB explant in adult sheep at 6 months and (C) adult patellar tendon.

4.4.5 Summary of the 6-month and 9-month studies

Our multi-phasic engineered ligament and bone tissues can be fabricated from an autogenic source but without the donor site morbidity associated with patellar tendon and hamstring autografts. Tissue availability is not a limiting factor with this approach due to a plentiful and easily accessible allogenic cell source as well. The lack of immune rejection of our constructs after implantation indicates that allogenic rather than autogenic sources of BMSCs may be used.

The elasticity requirements of engineered ligament at the time of replacement remain under debate [73-76]. The current paradigm is to match or exceed native ligament stiffness and strength in order to immediately restore stability to the knee [75]. However, recent evidence suggests stiff scaffolds shield the cells within these structures from strains required for proper signal induction and hence, growth of neoligamentous tissue [74-76]. The result is loss of cell viability with time *in vivo* and increased joint laxity [73, 76]. Moreover, the stresses during normal ACL function do not typically exceed 20% of ACL strength [73] suggesting that current engineering approaches are over-designed for strength, especially if eventual collagen growth and remodeling is expected with time. Therefore an engineered ligament that is compliant upon implantation such that its cells are not strain shielded would promote cell growth, remodeling of tissues and eventual ligamentization. In our approach, the animals were not

restrained during healing. During the early healing period, the BLB implants do not need to sustain a physiological load, they need to be able to accommodate knee motion without tearing. Because our BLBs are compliant upon implantation, they can sustain a physiological length change during knee motion. Also, because they are viscoelastic, they recover that length change upon unloading. The BLB constructs were fabricated at a slightly larger length than the expected intra-articular span and at the time of implantation the ends of the bone sections were aligned with the insertion edges of the bones, allowing the intra-articular region to quickly retension itself, providing a perfect patient-specific fit. This allowed us to fabricate one size construct for any size knee.

After 6 months of *in vivo* recovery, we have shown that the BLB grafts can sustain very large loads, well-beyond physiological limits, and also the same load magnitudes that the contralateral ACLs can withstand. The average cross sectional area of *the in vivo* BLB is 57.5±48.7 mm^2 and the cross sectional area of the contralateral ACL is 27.7±4.3 mm^2. The initial cross sectional area of the BLBs prior to the surgery is 7.1±1.0 mm^2. The size of the bone tunnel needed to accommodate the BLB graft was less than that typically used clinically (see Section 3.3.1). Our results suggest the thinner bone tunnel may heal faster and it may accelerate the growth and remodeling of the BLBs. Therefore the implication of BLBs increasing in size *in vivo* over time is significant. We demonstrate that a full-sized graft is not needed if a thinner graft can develop rapidly *in vivo*. Statistically, the six month *in vivo* BLB is not significantly larger than the native ACL. The large standard of deviation is due to the large cross sectional area of one BLB explant. The cross sectional area of the BLB explants at 9-months PO is 37.0±5.5 mm^2. It had a much smaller standard deviation. The BLBs have developed to match the same size of the ACL at 9-months PO.

The tangent modulus of ACLs from non-operated animals was found to be 232±11 MPa (N=2). The moduli of non-operated animals were not significantly different from those of the contralateral ACLs from operated animals. We have

compared our modulus results with values from the literature [56, 77, 78]. The reported geometric stiffness values for sheep ACL were converted to tangent moduli using the geometric properties provided [56, 77, 78] and the average value was found to be 130±15 MPa. This value is lower than our results and the differences are due to the fact that we measure the actual tissue level displacement directly and non-invasively. The literature results recorded the grip-to-grip displacement that neglected the compliance within the system and non-physiological issues associated with mechanical testing such as slip, tearing and stress concentrations at the grips, which add complication to the measured value of stiffness/modulus, therefore lowering both stiffness and modulus.

The patellar tendon autograft is a common source of tissue for ACL repair. Recently the biomechanical properties of the ACL and the patellar tendon have been compared within the physiological range of 5% strain [25, 33] and the results suggest that current ACL grafts are often over-designed for stiffness (Figure 4.7). Our multi-phasic constructs rapidly increased stiffness and strength *in vivo* in response to stresses and strains placed on them to attain physiologically relevant mechanics. We believe the initial compliance of the intra-articular region of the graft allowed the graft to strain at relatively low stress levels. This deformability was conducive to mechanotransduction of the cells within the intra-articular region. It had the added benefit of transferring very low loads to the regions of the graft within the bone tunnels in the weeks after surgery during which bone tunnel healing occurs, eliminating the need for metal fixation screws to hold the graft in place.

At six months as an ACL replacement in the sheep some of the BLB grafts contained fascicles of type I collagen that were highly aligned and resembled the collagen fascicle structure and alignment of native adult ACL. Moreover, native ACL has a characteristic viscoelastic relaxation response that is not shared by patellar tendon grafts; our multi-phasic BLB constructs did exhibit qualitatively and quantitatively similar stress relaxation responses to those of native ACL.

These results indicate that the patellar tendon is not an ideal biomechanical replacement for the ACL, not only because it is too stiff, but also because its time dependent properties are very different at the time of implantation from those of native ACL. This has important implications for the risk of re-injury when using a patellar tendon graft, especially at high strain rates of loading such as in an impact event, because the viscoelastic or time dependent properties govern the high strain rate response. The viscoelastic response of the patellar tendon graft is initially fundamentally different from that of native ACL. The relevance of the patellar tendon data is that it is not biomechanically similar to ACL despite the fact that the patellar tendon is adult, native connective tissue. The goal is also to establish that the BLB constructs have the proper nonlinear viscoelastic properties compared to those of native tissue which are not matched by current ACL repair techniques utilizing patellar tendon grafts. This result has the further significance of addressing how arduous a task it is to accurately match the very important non-linear viscoelastic properties of the native ACL with a graft – engineered or otherwise.

Tissue engineering grafts for ACL repair has been increasingly focused recently. For instance, Cooper et al., 2007 had developed synthetic braided scaffolds as grafts for ACL repair [79]. Synthetic scaffolds are not needed in our method. One of the disadvantages of using synthetic scaffold is that the degradation rate of the scaffold *in vivo* often exceeds the desired rates. Infiltration of collagen fibers are seen in these types of scaffolds *in vivo*, however, the overall mechanical properties decrease rapidly over time because of the rapidly biodegrading scaffold. On the other hand, our scaffold-less self-assembled BLB grafts grow rapidly *in vivo* and the mechanics of the *in vivo* BLB increase by a factor of 90 compared to that of the *in vitro* BLB prior to the implantation. In addition, the integration of the ends of the graft to native bone was not evaluated in Cooper el al. 2007. There is no evidence showing that the synthetic graft formed a strong enthesis between the graft and the native bone,

whereas our BLB has shown early markers of enthesis after only 2 months of implantation.

These BLB constructs are viscoelastic and contain contractile cells. Prior to implantation, they are longitudinally constrained and carry an internal tensile stress. Upon implantation into the bone tunnel, the BLB undergoes viscoelastic deformation to restore passive tension. The initial compliance of the intra-articular region of the BLB and its ability to maintain self-tension allow it to accommodate knee motion and the necessary intra-articular length. A previous report demonstrated the possibilities of the scaffold-less tissue engineering technology [80]. The lack of comparison to the commonly used graft (PT) left the potential of this technology unknown. The results of the current study suggest that at 9 months these scaffold-less constructs surpass the PTG in mechanical, vascular and neural developments (details of vascular and neural developments can be found in **Chapter 3**). Interference screws commonly used in human ACL repair were not used in these PTG knees because of the study design comparison of the intra-articular histology and mechanics between the BLB and PTG required the same fixation in both. Interference screws could not be used with the BLB because of the soft structure of the BLB. Therefore suture fixation was used in both the BLB and PTG for consistency. However, previous studies evaluating PT autografts and allografts with interference screws using goat also showed a significantly increased knee laxity compared to the contralateral knees after 6 months *in vivo* [51].

Promising mechanical results were achieved despite low loads applied to the ACL during the low level of activity normally seen in sheep. Increasing the loading in the post-operative phase may accelerate and facilitate the development of the engineered construct. The BLB appears to be able to respond to its environment opening the possibilities for manipulating the joint forces responsible for BLB development through designed rehabilitation programs.

The geometric stiffness of the a graft is a function of the CSA and composition of the graft, both of which vary in the developing grafts at 9 months. PTGs had a more compliant geometric stiffness but a larger CSA than the BLBs suggesting that BLBs and PTGs remodeled and developed via different pathways *in vivo*. The inhomogeneity of the full-field strain deformation developed in the BLB (Figure 4.10) suggests BLB remodeling is more than just extracellular matrix deposition.

The stress-strain results demonstrate that the BLB is not yet fully remodeled to that of adult ACL, suggesting more time in vivo or a more rigorous rehabilitation program may allow complete remodeling of the BLB to an adult ACL phenotype. The 6-month study had an n=3 to evaluate the survival of the BLB in vivo and to determine if the mechanical properties if the BLB would improve. The standard deviation among these biomechanical results was relatively high. This study shows the BLB can be implanted arthroscopically and its mechanical properties actually surpass those of the PTG in the sheep model. This study is a step towards determining the feasibility of bringing this translational work to human clinical trials.

4.5 Experimental characterization of sheep ACL bundles

As mentioned earlier in **Chapter 2**, the ACL has a complicated spatial geometry including a twist (Figure 4.13**A**) and multiple-bundle (Figure 4.13**B**) features. Human ACLs have been treated as double-bundle (anterior medial and posterior lateral bundles) or triple-bundle (anterior lateral, anterior medial, and posterior lateral bundles) [1, 27, 81,82]. In sheep ACL, the bundle separation is more distinct and therefore can be treated as a double-bundle (Figure 4.13**B**). In our previous study, the native sheep ACL is used as a control group to compare the tissue engineered BLB explant and the patellar tendon autograft. It is difficult to separate these grafts into sub-bundles after *in vivo* recovery since no obvious separation could be found on these grafts. Therefore, a bundle separation on the

contralateral native ACL in these studies was not performed. As previously mentioned in this chapter, to obtain more accurate material properties, better experimental characterizations should be performed. Therefore, we have performed a separate study to characterize the mechanical properties of the native sheep ACL. The anterior tibial translation test (ATT) was first performed to understand the ACL response in a physiological loading condition. After ATT, the entire ACL was reoriented in order to perform a uniaxial tension test. Then, each bundle was characterized from uniaxial tension tests and stress relaxation tests, as described in the next section.

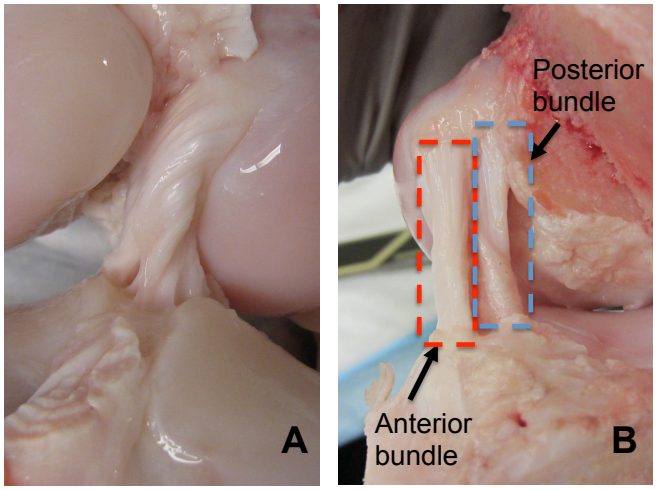

Figure 4.13 The twisted (A) and double-bundle (B) features of the sheep ACL. (A) a posterior view of the sheep ACL; (B) the distinction between the anterior and posterior bundle after the tibia was internally rotated 90 degrees.

4.5.1 Experimental setup: anterior tibial translation and bundle uniaxial tension tests

Anterior Tibial Translation (ATT): Sheep knees were thawed at room temperature overnight. With the knee joint still intact, the femur and tibia were first fixed into the grips. The samples with grips were then installed into the servo hydraulic material test system 810 (MTS) such that the natural knee position at 45 degree flexion angle (tibia remained horizontal and femur in 45° angle) was preserved by fixing the locations of the grips on the MTS. Then, the knee was uninstalled from the grips and all uninvolved tissue and the medial condyle were

removed leaving only the native ACL attached to the femur and tibia for mechanical characterization. The femur-ACL-tibia unit was then fixed into the grips again and reinstalled into the MTS using the natural knee position recorded previously. Prior to tests, a speckle pattern print using a temporary tattoo transfer paper was applied to the entire surface of the ACL to serve as displacement markers. During tests, a 50 N force was applied perpendicularly to the tibia shaft at strain rates of 0.005/s, 0.05/s and 0.5/s. A high-speed camera was employed to record the tissue-level displacement (Figure 4.14). The displacement data that were recorded were implemented into the VIC-2D 2010 software to obtain full-field strain contours.

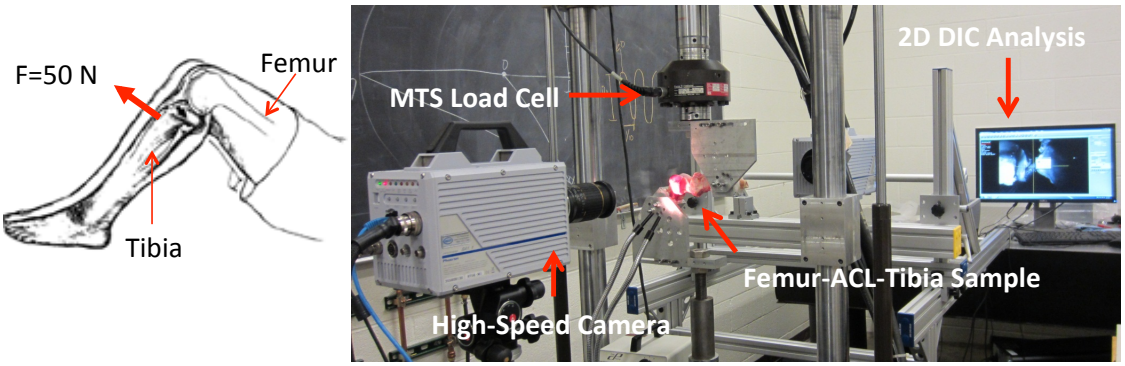

Figure 4.14 Experimental setup of the anterior tibial translation test

Single bundle experimental characterization: After the ATT tests on the native ACL, specimens were subjected to uniaxial tension tests for mechanical characterization. The ACL was first separated into two bundles, anterior and posterior, along the natural separation starting near the tibial insertion. Then, several cuts on the tibia were made (Figure 4.15**A**) to release the anterior bundle from the rest of the specimen (Figure 4.15**B**). Uniaxial load-unload tests at 0.05/s were performed first on the posterior bundle, then on the anterior bundle. As previously described, the speckle pattern was again applied to the surface of each bundle before the tests were performed. The high-speed camera was employed to measure the tissue level displacement.

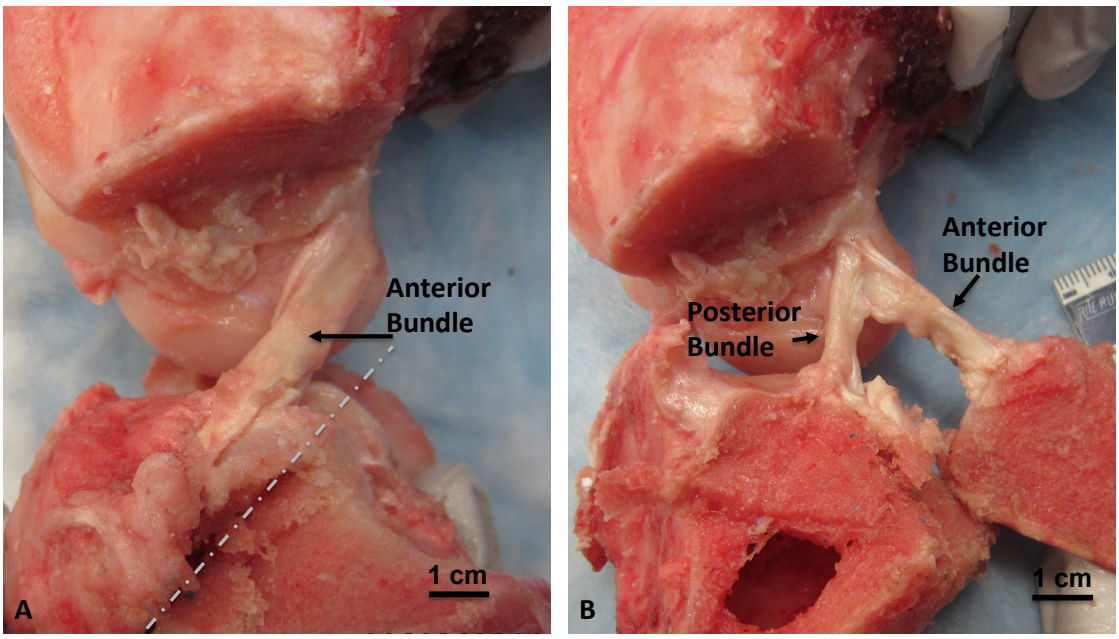

Figure 4.15 Sheep anterior bundle and posterior bundle separation: (A) the cut made on the tibia to release the anterior bundle from the rest of the ACL; (B) the posterior bundle and anterior bundle geometry.

4.5.2 Full-Field strain contours of the native ACL during ATT

During an anterior tibial translation test, the native ACL exhibited inhomogeneous strain fields, demonstrated by the full-field strain contours of the native ACL (Figure 4.16). The contours showed large deformations near the proximal insertion and in the mid-substance. The maximum in-plane shear strains were calculated from the normal strains ε_x, ε_y, and shear strain ε_{xy} obtained from DIC analysis. The location of the maximum shear strain was found to be between the mid-substance and ACL proximal insertion. Clinical examinations reported that during an ACL injury incident, the tearing site of the ACL is commonly seen near the proximal insertion or mid-substance [83]. Ductile materials such as the ACL often fail when a critical shear strain is exceeded. The location of the maximum in-plane shear strain from our results is in agreement with the clinical examination, indicating that our experiment is a valid experimental setup to examine the ACL failure mechanism.

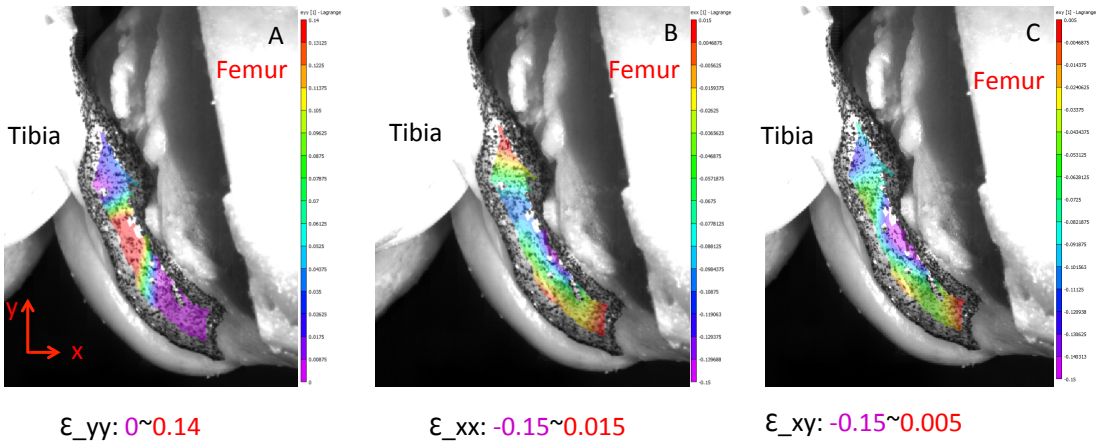

Figure 4.16 Full field strain contours of the ACL during an anterior tibial translation test: (A) Normal strain in y direction (force direction); (B) Normal strain in x direction; and (C) in-plane shear strain.

One limitation in our current study is that during the ATT tests, the strains at failure were not measured; all ACL samples were not subjected to failure tests. The loads and displacements were kept within a normal range of motion in order to avoid ACL failure. This is because the ACL sample needed to be kept intact for the single bundle mechanics analysis following the ATT tests. We intended to conduct all tests on the same sample. In this fashion, we were hoping to use the biomechanical properties characterized from each bundle to predict the results in ATT from the sample ACL. A study that focuses on the failure mechanism of the knees during the ATT test is needed in future analysis.

4.5.3 Mechanics of the AM bundle and PL bundle

Overall, the results indicate that the anterior bundle is stiffer than the posterior bundle. Very little hysteresis was found when examining the single bundles. Within the normal strain range (5%), the stress-strain curve of the anterior bundle exhibited higher curvature compared to that of the posterior bundle (Figure 4.17). Figure 4.18 and Figure 4.19 demonstrated the full field strain contours of the AM and PL bundles. The small strain magnitude in in-plane strain contours of the AM bundle (Figure 4.18 **C**) and the PL bundle (Figure 4.19 **C**) indicated that by separating the ACL into AM and PL bundle, we are able to orientate the AM and PL bundles in a uniaxial orientation. The mechanical tests

under this configuration provide us the most accurate and well characterized fields stress and strain for computing material properties.

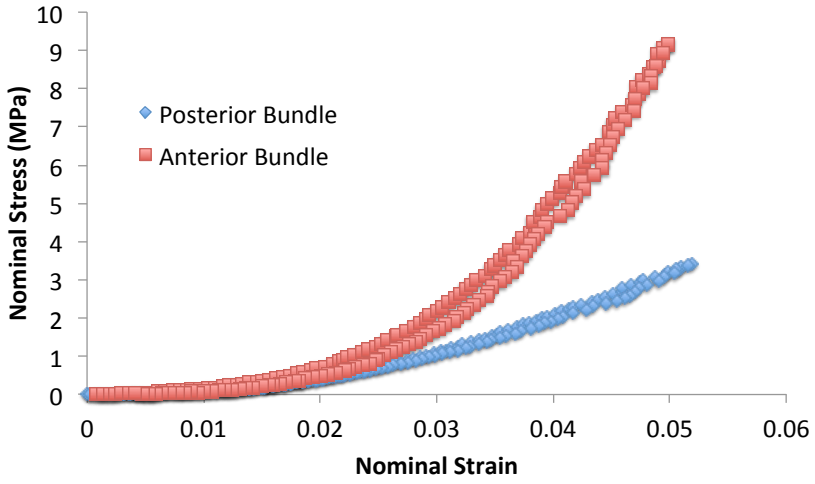

Figure 4.17 Average stress-strain responses from the anterior bundle and posterior bundle of the same ACL.

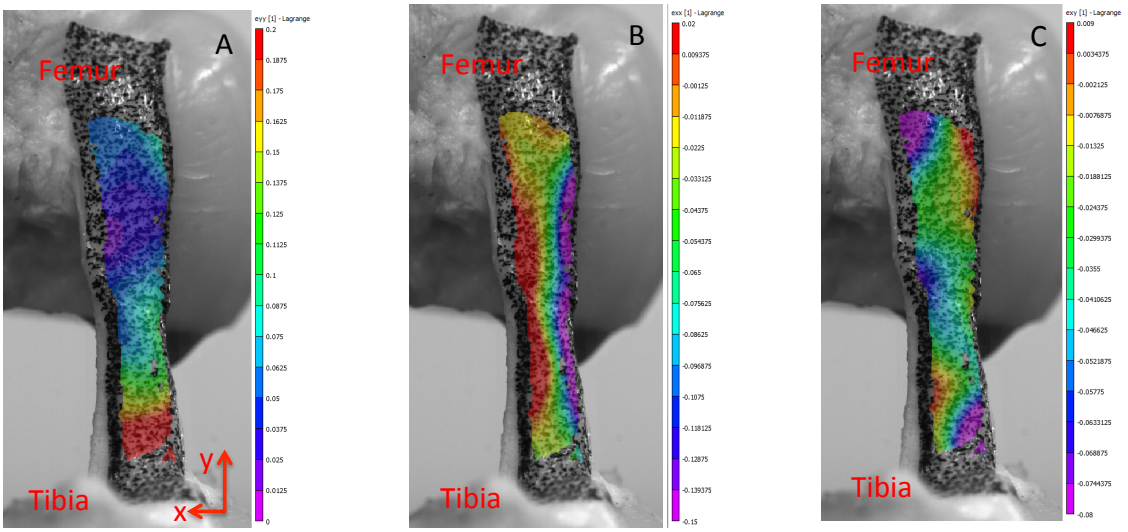

Ɛ_yy: 0~0.2 Ɛ_xx: -0.15~0.02 Ɛ_xy: -0.08~0.01

Figure 4.18 Full-field strain contours of the anterior bundle of the ACL during an uniaxial tension test: (A) Normal strain in y direction (force direction); (B) Normal strain in x direction; and (C) in-plane shear strain.

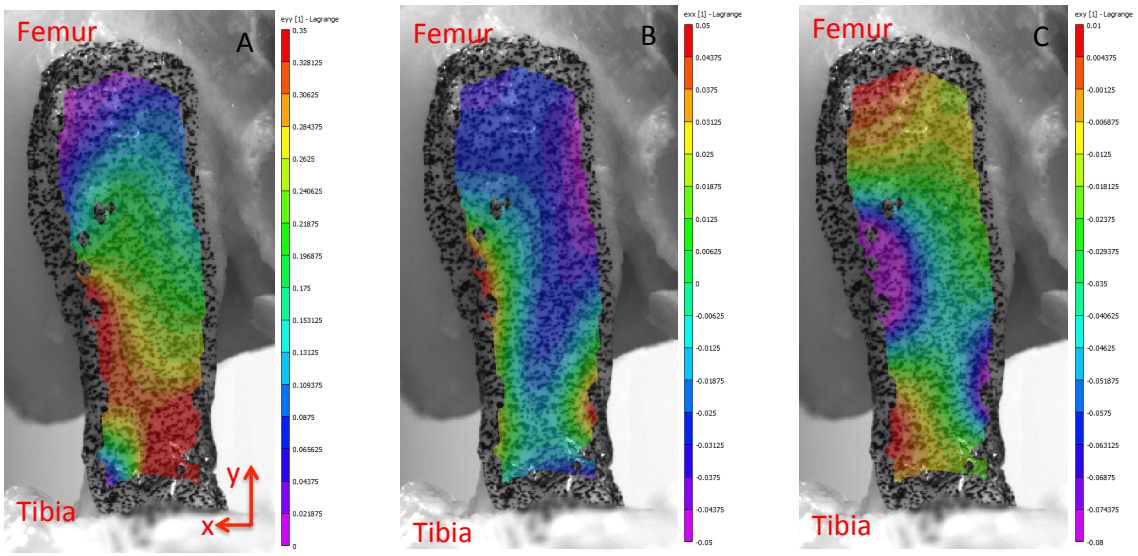

ε_yy: 0~0.35 ε_xx: -0.05~0.05 ε_xy: -0.08~0.01

Figure 4.19 Full-field strain contours of the posterior bundle of the ACL during an uniaxial tension test: (A) Normal strain in y direction (force direction); (B) Normal strain in x direction; and (C) in-plane shear strain.

The higher tangent modulus found in the anterior bundle in our study is in agreement with early studies presented by Butler et al., 1992 [28]. An ACL hydroxyproline analysis study showed that the density of the collagen near insertion sites was less than that found in the mid-substance of the ACL [84]. A lower collagen density could cause more compliant mechanical properties. The full-field strain contours of the ACL are in agreement with this study. The mechanism of the ultrastructure and composition of ligaments and tendons affecting the viscoelastic responses are still under investigation. Studies using mouse tail tendon have shown greater stress relaxation with reduced proteoglycans and associated glycosaminoglycans [85, 86]. In contrast to these mouse tail studies, Chimich et al., 1992 showed that ligaments with higher water content demonstrated greater relaxation than ligaments with lower water content [87]. A possible explanation for the decreased stress relaxation rate from Oza et al., 2006 was that as tissues were subjected to higher strains, more fluid was driven out of the ligaments, causing the ligament to response more elastically [88].

4.5.4 Remarks

The different uniaxial tension mechanical responses of the anterior and posterior bundles of the ACL may have further implications in a 3D kinematics setting. We are surprised to discover the different stress relaxation responses between the anterior and posterior bundles. The possible reasons that cause the differences need to be elucidated to fully understand the biomechanical properties of the ACL.

4.6 Summary

The biomechanical requirements of an ACL graft at the time of implantation were examined with the aim of developing an engineered ACL graft that would rapidly grow and remodel *in vivo* to present the histological and biomechanical characteristics of an adult, native ACL. We have demonstrated that our BLB constructs, with their initially compliant intra-articular region, do not require fixation screws to achieve a rapid *in vivo* interface with the native bone, thus becoming vascularized and innervated. Some of the BLB constructs develop highly organized collagen fascicles and after 6 months *in vivo*, exhibit the physiologically relevant viscoelastic properties of adult ACLs. The viscoelastic properties of an ACL graft have been largely overlooked in previous studies, but they are a critical aspect of the restoration of biomechanical function to prevent graft failures. Our ongoing studies will compare the non-linear viscoelastic characteristics of BLB grafts to patellar tendon autografts at longer recovery time points.

Studies have shown that the modulus and strength of the human PT, the commonly used ACL graft, are much greater than those of the human ACL. The PT has been shown to be more sensitive to strain rate than the ACL. Stress relaxation tests demonstrated that ligaments and tendons exhibit relaxation patterns that differ from each other. These data all indicate that the PT may not be the optimal solution for ACL replacement. Our current experimental data from sheep ACL and PT are in agreement with previous published data in terms of the different relaxation patterns between ligaments and tendons. Moreover, the

stress profiles over time for the ACL and PT showed more complicated behavior than those found in rat MCL and porcine digital tendon studies, suggesting that the relaxation pattern may be tissue-specific. Our tissue engineered BLB constructs showed very promising mechanical properties compared to the native tissue in the rat MCL replacement study and the sheep ACL replacement study, demonstrated by their rapidly increased tangent modulus and geometric stiffness. The stress relaxation comparison between the engineered BLB and native ACL in sheep studies showed little difference in relaxation patterns. We have also developed local strain deformation and full-field strain contour characterizations using digital image correlation analysis. The strain fields measured in our studies demonstrated that both native MCL and ACL are functionally graded, whereas the native PT is not. The functional gradients generated in the tissue engineered BLBs along their surfaces closely resembled those found in the native tissue, indicating that the tissue engineered BLB had remodeled *in vivo* and possibly underwent a "ligamentization" process, showing a more promising solution to replace an injured ACL than what the current PT graft offers.

4.7 References

1. Girgis, F.G., J.L. Marshall, and A. Monajem, *The cruciate ligaments of the knee joint. Anatomical, functional and experimental analysis.* Clinical orthopaedics and related research, 1975. **106**: p. 216-231.

2. Norwood, L.A. and M.J. Cross, *Anterior cruciate ligament: functional anatomy of its bundles in rotatory instabilities.* The American Journal of Sports Medicine, 1979. **7**(1): p. 23-26.

3. Arnoczky, S.P., J.R. Matyas, and J.A. Buckwalter, *Anatomy of the anterior cruciate ligament.* Clinical orthopaedics and related research, 1983. **172**: p. 19-25.

4. Zantop, T., et al., *Anterior cruciate ligament anatomy and function relating to anatomical reconstruction.* Knee Surg Sports Traumatol Arthrosc, 2006. **14**(10): p. 982-92.

5. Woo, S.L., et al., *The effectiveness of reconstruction of the anterior cruciate ligament with hamstrings and patellar tendon . A cadaveric study comparing anterior tibial and rotational loads.* The Journal of bone and joint surgery. American volume, 2002. **84-A**(6): p. 907-14.

6. Xerogeanes, J.W., et al., *A functional comparison of animal anterior cruciate ligament models to the human anterior cruciate ligament.* Annals of Biomedical Engineering, 1998. **26**(3): p. 345-352.

7. Bach, J.M., M.L. Hull, and H.A. Patterson, *Direct measurement of strain in the posterolateral bundle of the anterior cruciate ligament.* Journal of Biomechanics, 1997. **30**(3): p. 281-283.

8. Butler, D.L., M.D. Kay, and D.C. Stouffer, *Comparison of Material Properties in Fascicle-Bone Units From Human Patellar Tendon and Knee Ligaments.* Journal of Biomechanics, 1986. **19**(6): p. 425-432.

9. Cooper, D.E., et al., *The Strength of the Central 3rd Patellar Tendon Graft - a Biomechanical Study.* American Journal of Sports Medicine, 1993. **21**(6): p. 818-824.

10. Haraldsson, B.T., et al., *Region-specific mechanical properties of the human patella tendon.* Journal of applied physiology, 2005. **98**(3): p. 1006-1012.

11. Couppe, C., et al., *Mechanical properties and collagen cross-linking of the patellar tendon in old and young men.* Journal of applied physiology (Bethesda, Md.: 1985), 2009. **107**(3): p. 880-886.

12. Hansen, P., et al., *Lower strength of the human posterior patellar tendon seems unrelated to mature collagen cross-linking and fibril morphology.* Journal of applied physiology, 2010. **108**(1): p. 47-52.

13. Waggett, A.D., et al., *Characterization of collagens and proteoglycans at the insertion of the human Achilles tendon.* Matrix biology : journal of the International Society for Matrix Biology, 1998. **16**(8): p. 457-70.

14. Cooper, J.A., Jr., et al., *Evaluation of the anterior cruciate ligament, medial collateral ligament, achilles tendon and patellar tendon as cell sources for tissue-engineered ligament.* Biomaterials, 2006. **27**(13): p. 2747-54.

15. Noyes, F.R., et al., *Biomechanical analysis of human ligament grafts used in knee-ligament repairs and reconstructions.* The Journal of bone and joint surgery. American volume, 1984. **66**(3): p. 344-52.

16. Staubli, H.U., et al., *Quadriceps tendon and patellar ligament: cryosectional anatomy and structural properties in young adults.* Knee surgery, sports traumatology, arthroscopy : official journal of the ESSKA, 1996. **4**(2): p. 100-110.

17. Butler, D.L., et al., *Effects of structure and strain measurement technique on the material properties of young human tendons and fascia.* Journal of Biomechanics, 1984. **17**(8): p. 579-96.

18. Haut, R.C. and A.C. Powlison, *The Effects of Test Environment and Cyclic Stretching on the Failure Properties of Human Patellar Tendons.* Journal of Orthopaedic Research, 1990. **8**(4): p. 532-540.

19. Noyes, F.R. and E.S. Grood, *Strength of Anterior Cruciate Ligament in Humans and Rhesus-Monkeys.* Journal of Bone and Joint Surgery-American Volume, 1976. **58**(8): p. 1074-1082.

20. Hollis, J.M., S. Takai, and S.L. Woo, *The effects of knee motion and external loading on the length of the anterior cruciate ligament (ACL): a kinematic study.* Journal of Biomechanical Engineering, 1991. **113**(2): p. 208-214.

21. Jones, R.S., et al., *Mechanical properties of the human anterior cruciate ligament.* Clinical Biomechanics, 1995. **10**(7): p. 339-344.

22. Wilson, T.W., M.P. Zafuta, and M. Zobitz, *A biomechanical analysis of matched bone-patellar tendon-bone and double-looped semitendinosus and gracilis tendon grafts.* The American Journal of Sports Medicine, 1999. **27**(2): p. 202-207.

23. Hamner, D.L., et al., *Hamstring tendon grafts for reconstruction of the anterior cruciate ligament: biomechanical evaluation of the use of multiple strands and tensioning techniques.* The Journal of bone and joint surgery. American volume, 1999. **81**(4): p. 549-57.

24. Blevins, F.T., et al., *The effects of donor age and strain rate on the biomechanical properties of bone-patellar tendon-bone allografts.* The American Journal of Sports Medicine, 1994. **22**(3): p. 328-333.

25. Chandrashekar, N., et al., *Low-load behaviour of the patellar tendon graft and its relevance to the biomechanics of the reconstructed knee.* Clinical Biomechanics, 2008. **23**(7): p. 918-25.

26. Kennedy, J.C., H.W. Weinberg, and A.S. Wilson, *Anatomy and Function of Anterior Cruciate Ligament - as Determined by Clinical and Morphological*

Studies. Journal of Bone and Joint Surgery-American Volume, 1974. **A 56**(2): p. 223-235.

27. Butler, D.L., *Anterior cruciate ligament: Its normal response and replacement.* Journal of Orthopaedic Research, 1989(7): p. 910-921.

28. Butler, D.L., et al., *Location-dependent variations in the material properties of the anterior cruciate ligament.* Journal of Biomechanics, 1992. **25**(5): p. 511-518.

29. Johnson, G.A., et al., *Tensile and Viscoelastic Properties of Human Patellar Tendon.* Journal of Orthopaedic Research, 1994. **12**(6): p. 796-803.

30. Beynnon, B.D., et al., *The relationship between menstrual cycle phase and anterior cruciate ligament injury: a case-control study of recreational alpine skiers.* Am J Sports Med, 2006. **34**(5): p. 757-64.

31. Chandrashekar, N., J. Slauterbeck, and J. Hashemi, *Effects of cyclic loading on the tensile properties of human patellar tendon.* Knee, 2012. **19**(1): p. 65-68.

32. Beynnon, B.D., R.J. Johnson, and B.C. Fleming, *The science of anterior cruciate ligament rehabilitation.* Clinical orthopaedics and related research, 2002. **402**: p. 9-20.

33. Danto, M.I. and S.L. Woo, *The mechanical properties of skeletally mature rabbit anterior cruciate ligament and patellar tendon over a range of strain rates.* Journal of orthopaedic research : official publication of the Orthopaedic Research Society, 1993. **11**(1): p. 58-67.

34. Woo, S.L.Y., *Mechanical-Properties of Tendons and Ligaments .1. Quasi-Static and Non-Linear Viscoelastic Properties.* Biorheology, 1982. **19**(3): p. 385-396.

35. Woo, S.L., et al., *Measurement of mechanical properties of ligament substance from a bone-ligament-bone preparation.* Journal of orthopaedic research : official publication of the Orthopaedic Research Society, 1983. **1**(1): p. 22-9.

36. Butler, D.L., et al., *Surface strain variation in human patellar tendon and knee cruciate ligaments.* Journal of Biomechanical Engineering, 1990. **112**(1): p. 38-45.

37. Stouffer, D.C., D.L. Butler, and D. Hosny, *The relationship between crimp pattern and mechanical response of human patellar tendon-bone units.* J Biomech Eng, 1985. **107**(2): p. 158-65.

38. Warren, L.F., J.L. Marshall, and F. Girgis, *Prime static stabilizer of medial side of knee.* Journal of Bone and Joint Surgery-American Volume, 1974. **A 56**(4): p. 665-674.

39. Arms, S., et al., *Strain measurement in the medial collateral ligament of the human knee: an autopsy study.* Journal of Biomechanics, 1983. **16**(7): p. 491-6.

40. Thomopoulos, S., et al., *Collagen fiber orientation at the tendon to bone insertion and its influence on stress concentrations.* Journal of Biomechanics, 2006. **39**(10): p. 1842-1851.

41. Singhatat, W., et al., *How four weeks of implantation affect the strength and stiffness of a tendon graft in a bone tunnel: a study of two fixation devices in an extraarticular model in ovine.* The American Journal of Sports Medicine, 2002. **30**(4): p. 506-513.

42. Maeda, A., et al., *Remodeling of allogeneic and autogenous patellar tendon grafts in rats.* Clinical orthopaedics and related research, 1997. **335**: p. 298-309.

43. Goh, K.L., et al., *Ageing changes in the tensile properties of tendons: influence of collagen fibril volume fraction.* Journal of Biomechanical Engineering, 2008. **130**(2): p. 021011.

44. Goldberg, V.M., A. Burstein, and M. Dawson, *The influence of an experimental immune synovitis on the failure mode and strength of the rabbit anterior cruciate ligament.* The Journal of bone and joint surgery. American volume, 1982. **64**(6): p. 900-6.

45. Woo, S.L.Y., et al., *Effects of Knee Flexion on the Structural-Properties of the Rabbit Femur-Anterior Cruciate Ligament-Tibia Complex (Fatc).* Journal of Biomechanics, 1987. **20**(6): p. 557-563.

46. Ballock, R.T., et al., *Use of Patellar Tendon Autograft for Anterior Cruciate Ligament Reconstruction in the Rabbit - a Long-Term Histologic and Biomechanical Study.* Journal of Orthopaedic Research, 1989. **7**(4): p. 474-485.

47. Clancy, W.G., et al., *Anterior and Posterior Cruciate Ligament Reconstruction in Rhesus-Monkeys - a Histological, Micro-Angiographic, and Biomechanical Analysis.* Journal of Bone and Joint Surgery-American Volume, 1981. **63**(8): p. 1270-1284.

48. Figgie, H.E., et al., *The Effects of Tibial Femoral Angle on the Failure Mechanics of the Canine Anterior Cruciate Ligament.* Journal of Biomechanics, 1986. **19**(2): p. 89-91.

49. Oster, D.M., et al., *Primary and Coupled Motions in the Intact and the Acl-Deficient Knee - an Invitro Study in the Goat Model.* Journal of Orthopaedic Research, 1992. **10**(4): p. 476-484.

50. Shino, K., et al., *Replacement of the Anterior Cruciate Ligament by an Allogeneic Tendon Graft - an Experimental-Study in the Dog.* Journal of Bone and Joint Surgery-British Volume, 1984. **66**(5): p. 672-681.

51. Jackson, D.W., et al., *A comparison of patellar tendon autograft and allograft used for anterior cruciate ligament reconstruction in the goat model.* The American Journal of Sports Medicine, 1993. **21**(2): p. 176-85.

52. Bosch, U., et al., *The Relationship of Mechanical-Properties to Morphology in Patellar Tendon Autografts After Posterior Cruciate Ligament Replacement in Sheep.* Journal of Biomechanics, 1992. **25**(8): p. 821-830.

53. Bosch, U. and W.J. Kasperczyk, *Healing of the Patellar Tendon Autograft After Posterior Cruciate Ligament Reconstruction - a Process of Ligamentization - an Experimental-Study in a Sheep Model.* American Journal of Sports Medicine, 1992. **20**(5): p. 558-566.

54. Rogers, G.J., et al., *Measurement of the Mechanical-Properties of the Ovine Anterior Cruciate Ligament Bone Ligament Bone Complex - a Basis for Prosthetic Evaluation Rid A-7014-2008.* Biomaterials, 1990. **11**(2): p. 89-96.

55. Donahue, T.L.H., et al., *Comparison of viscoelastic, structural, and material properties of double-looped anterior cruciate ligament grafts made from bovine digital extensor and human hamstring tendons.* Journal of Biomechanical Engineering-Transactions of the Asme, 2001. **123**(2): p. 162-169.

56. Hunt, P., et al., *A model of soft-tissue graft anterior cruciate ligament reconstruction in sheep.* Archives of orthopaedic and trauma surgery, 2005. **125**(4): p. 238-248.

57. Radford, W.J.P., A.A. Amis, and A.C. Stead, *The Ovine Stifle as a Model for Human Cruciate Ligament Surgery.* Vet Comp Orthop Trauma, 1996. **9**: p. 134-139.

58. Tapper, J.E., et al., *In vivo measurement of the dynamic 3-D kinematics of the ovine stifle joint.* Journal of Biomechanical Engineering, 2004. **126**(2): p. 301-305.

59. Seitz, H., et al., *Vascular anatomy of the ovine anterior cruciate ligament. A macroscopic, histological and radiographic study.* Archives of orthopaedic and trauma surgery, 1997. **116**(1-2): p. 19-21.

60. Murray, M.M., A. Weiler, and K.P. Spindler, *Interspecies variation in the fibroblast distribution of the anterior cruciate ligament.* The American Journal of Sports Medicine, 2004. **32**(6): p. 1484-1491.

61. Kwan, M.K., T.H.C. Lin, and S.L.Y. Woo, *On the Viscoelastic Properties of the Anteromedial Bundle of the Anterior Cruciate Ligament.* Journal of Biomechanics, 1993. **26**(4-5): p. 447-452.

62. Woo, S.L., et al., *The effects of strain rate on the properties of the medial collateral ligament in skeletally immature and mature rabbits: a biomechanical and histological study.* J Orthop Res, 1990. **8**(5): p. 712-21.

63. Pioletti, D.P., L.R. Rakotomanana, and P.F. Leyvraz, *Strain rate effect on the mechanical behavior of the anterior cruciate ligament-bone complex.* Medical engineering & physics, 1999. **21**(2): p. 95-100.

64. Yamamoto, E., K. Hayashi, and N. Yamamoto, *Mechanical properties of collagen fascicles from the rabbit patellar tendon.* J Biomech Eng, 1999. **121**(1): p. 124-31.

65. Bonifasi-Lista, C., et al., *Viscoelastic properties of the human medial collateral ligament under longitudinal, transverse and shear loading.* Journal of Orthopaedic Research, 2005. **23**(1): p. 67-76.

66. Pioletti, D.P. and L.R. Rakotomanana, *On the independence of time and strain effects in the stress relaxation of ligaments and tendons.* J Biomech, 2000. **33**(12): p. 1729-32.

67. Beynnon, B.D. and B.C. Fleming, *Anterior cruciate ligament strain in-vivo: A review of previous work.* Journal of Biomechanics, 1998. **31**(6): p. 519-525.

68. Fleming, B.C., et al., *The effect of weightbearing and external loading on anterior cruciate ligament strain.* Journal of Biomechanics, 2001. **34**(2): p. 163-170.

69. Holden, J.P., et al., *In vivo forces in the anterior cruciate ligament: direct measurements during walking and trotting in a quadruped.* J Biomech, 1994. **27**(5): p. 517-26.

70. Provenzano, P., et al., *Nonlinear ligament viscoelasticity.* Ann Biomed Eng, 2001. **29**(10): p. 908-14.

71. Duenwald, S.E., R. Vanderby, Jr., and R.S. Lakes, *Stress relaxation and recovery in tendon and ligament: experiment and modeling.* Biorheology, 2010. **47**(1): p. 1-14.

72. Hingorani, R.V., et al., *Nonlinear viscoelasticity in rabbit medial collateral ligament.* Annals of Biomedical Engineering, 2004. **32**(2): p. 306-312.

73. Frank, C.B. and D.W. Jackson, *The science of reconstruction of the anterior cruciate ligament.* The Journal of bone and joint surgery. American volume, 1997. **79**(10): p. 1556-76.

74. Petrigliano, F.A., D.R. McAllister, and B.M. Wu, *Tissue engineering for anterior cruciate ligament reconstruction: a review of current strategies.* Arthroscopy : The Journal of Arthroscopic & Related Surgery : Official Publication of the Arthroscopy Association of North America and the International Arthroscopy Association, 2006. **22**(4): p. 441-451.

75. Freeman, J.W., M.D. Woods, and C.T. Laurencin, *Tissue engineering of the anterior cruciate ligament using a braid-twist scaffold design.* Journal of Biomechanics, 2007. **40**(9): p. 2029-2036.

76. Mascarenhas, R., *Anterior cruciate ligament reconstruction: a look at prosthetics-past, present and possible future.* McGill Journal of Medicine, 2008. **11**(1): p. 29-37.

77. Dustmann, M., et al., *The extracellular remodeling of free-soft-tissue autografts and allografts for reconstruction of the anterior cruciate ligament: a comparison study in a sheep model.* Knee surgery, sports traumatology, arthroscopy : official journal of the ESSKA, 2008. **16**(4): p. 360-369.

78. Meller, R., et al., *Histologic and Biomechanical Analysis of Anterior Cruciate Ligament Graft to Bone Healing in Skeletally Immature Sheep.* Arthroscopy: The Journal of Arthroscopic & Related Surgery, 2008. **24**(11): p. 1221-1231.

79. Cooper, J.A., Jr., et al., *Biomimetic tissue-engineered anterior cruciate ligament replacement.* Proceedings of the National Academy of Sciences of the United States of America, 2007. **104**(9): p. 3049-54.

80. Ma, J., et al., *Three-dimensional engineered bone-ligament-bone constructs for anterior cruciate ligament replacement.* Tissue engineering.Part A, 2012. **18**(1-2): p. 103-116.

81. Arnoczky, S.P., *Anatomy of the anterior cruciate ligament.* Clinical orthopaedics and related research, 1983. **172**: p. 19-25.

82. Amis, A.A. and G.P. Dawkins, *Functional anatomy of the anterior cruciate ligament. Fibre bundle actions related to ligament replacements and injuries.* The Journal of Bone and Joint Surgery, 1991. **73**(2): p. 260-267.

83. Sherman, M.F., et al., *The long-term follow-up of primary anterior cruciate ligament repair - defining a rationale for augmentation.* American Journal of Sports Medicine, 1991. **19**(3): p. 243-255.

84. Mommersteeg, T.J.A., et al., *Nonuniform distribution of collagen density in human knee ligaments.* Journal of Orthopaedic Research, 1994. **12**(2): p. 238-245.

85. Elliott, D.M., et al., *Effects of altered matrix proteins on quasilinear viscoelastic properties in transgenic mouse tail tendons*, Annals of Biomedical Engineering, 2003. **31**(5): p. 599-605.

86. Robinson, P.S., et al., *Strain-rate sensitive mechanical properties of tendon fascicles from mice with genetically engineered alterations in collagen and decorin*, Journal of Biomechanical Engineering, 2004. **126**(2): p. 252-257

87. Chimich, D., et al., *Water content alters viscoelastic behaviour of the normal adocescent rabbit medial collateral ligament*, Journal of Biomechanics, 1992. **25**(8): p. 831-833, 835-837

88. Oza, A.L., R. Vanderby, and R.S. Lakes, *Creep and relaxation in ligament: Theory, methods and experiment*, ed. G.A. Holzapfel and R.W. Ogden 2006. 397.

CHAPTER 5

Computational Modeling of Native and Engineered Ligaments and Tendons I. Constitutive models

The mechanisms by which soft collagenous tissues such as ligament and tendon respond to mechanical deformation include nonlinear elasticity and viscoelasticity. These contributions to the mechanical response are modulated by the content and morphology of structural proteins such as type I collagen and elastin, other molecules such as glycosaminoglycans, and fluid. Our BLB constructs, engineered from bone marrow stromal cells and their autogenous matricies, exhibit histological and mechanical characteristics of native tissues of different levels of maturity. In order to (1) establish whether the constructs have optimal mechanical function for implantation and utility for regenerative medicine and (2) establish stress strain relationships to prescribe accurate tissue behavior in finite element studies, constitutive relationships for the constructs and native tissues must be established. The most commonly used model, the quasi-linear viscoelastic (QLV) formulation, does not fully describe the mechanical responses of ligaments and tendons. Here a micromechanical approach incorporating collagen and elastic elastin is used to describe the soft tissue. The model captures the nonlinear viscoelastic responses of these tissues using a limited number of parameters that can be interpreted in terms of physical properties of collagen fibers and elastin. The parameters used to model the tissue engineered ligament response are similar to those found for the native ACL, indicating that the microstructure of the tissue engineered ligament graft has developed in vivo to match that of the native ACL.

5.1 Current constitutive Models for Ligaments and Tendon

As mentioned in **Chapter 4**, one important goal of tissue engineering grafts for ACL replacement is that the biomechanical response of the graft matches that of the native ACL. To quantitatively compare the biomechanical response of the native ACL, engineered ACL, and tendon grafts, a constitutive model that can accurately describe the nonlinear viscoelastic behavior of these tissues is required. The constitutive model can be further implemented in a finite element framework to investigate the biomechanical responses of the native and engineered ligaments and tendons in a complicated physiological loading condition such as the anterior tibial translation that isolates the ACL. In **Chapter 4**, experimental analysis revealed that ligaments and tendons have non-linear viscoelastic responses. Moreover, these studies demonstrated that the creep rate of the ligaments and tendons depends on the stress level and the relaxation rate depends on the strain level [1-3]. Various viscoelastic constitutive laws have been proposed to capture these responses. These are briefly reviewed below.

5.1.1 Generalized Maxwell model

Linear elastic springs and viscous dashpots are used in various combinations to describe the linear viscoelastic response. A Maxwell fluid element is a series combination of a linear spring and linear dashpot. The generalized Maxwell model (Figure 5.1) consists of multiple Maxwell elements in parallel. The model has been used to model inorganic polymer viscoelasticity and has been proposed for soft tissue [4-6]. In this modeling approach the multiple spring-dashpot elements are often thought of as representing the aligned fibrous structures of ligament or tendon. A generalized description of the model in 1D is expressed in **Eq. 5.1**, where σ is stress, ε is strain*, t is time,* k_i is the Young's modulus of the i^{th} linear spring and η_i is the viscosity of the i^{th} linear dashpot. The model includes an additional spring element with modulus k_m to capture the solid-like response. The advantage of this model is that it is simple and convenient to implement into computer programs and to auto-search the parameters to fit the experimental data. However, this model requires a fairly large number of parameters in order to capture the nonlinear viscoelastic

responses of tissues. Because the parameters are determined by numerically fitting test data, the fitted parameters do not reflect the physiologic structure of soft tissue [7].

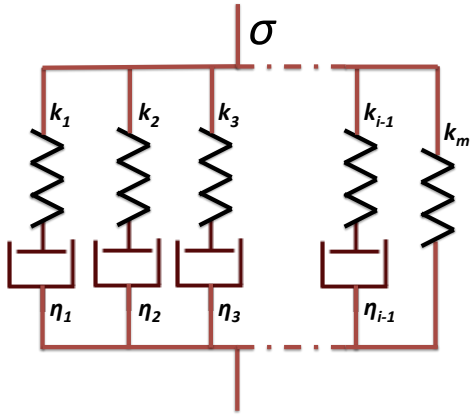

Figure 5.1 Generalized Maxwell model

$$\boldsymbol{\sigma(\varepsilon,t)=\left[k_1 exp\frac{-k_1 t}{\eta_1}+k_2 exp\frac{-k_2 t}{\eta_2}+\cdots+k_{i-1} exp\frac{-k_{i-1} t}{\eta_{i-1}}+k_m\right]\cdot\varepsilon}$$

Eq. 5.1

5.1.2 Quasi-Linear Viscoelastic (QLV) Model

To capture the nonlinear responses with a reduced number of parameters, Fung's quasi-linear viscoelasticity (QLV) theory has been widely used [8]. QLV theory assumes that the relaxation or creep response can be separated into strain-dependent and time-dependent components, as described in 1D in **Eq. 5.2**:

$$\sigma(\varepsilon,t)=\int_0^t E_t(t-\tau)\frac{d\sigma}{d\varepsilon}\frac{d\varepsilon(t)}{d\tau}d\tau$$

Eq. 5.2

Where E_t is the reduced relaxation function that depends on time and $\frac{d\sigma}{d\varepsilon}$ is the instantaneous elastic response. Both functions are obtained by curve-fitting the experimental data. The QLV model is widely used in current viscoelastic characterization of soft tissue [9-14]. The QLV model is able to fit a single set of experimental data [15] such as a stress relaxation experiment. However, this model cannot fully describe or predict stress or strain profiles at different constraint levels with the same set of parameters due to the fact that the reduced

relaxation function E_t is a function that depends on time only whereas the actual tissue response includes a strain dependent relaxation function [1-3, 16].

5.1.3 Schapery's single integral nonlinear model

Schapery's single integral nonlinear theory, or modified superposition theory, is another model proposed recently that describes the nonlinear strain and time dependent tissue viscoelastic responses [1, 2]. The modified superposition theory is similar to Schapery's single integral nonlinear theory and therefore in this paper, we use Schapery's single integral theory to demonstrate this class of constitutive models. In 1D uniaxial loading, Schapery's theory can be expressed as:

$$\sigma(\varepsilon,t) = h_e(\varepsilon)E_e\varepsilon + h_1(\varepsilon)\int_0^t \Delta E(\rho(t)-\rho'(\tau))\frac{dh_2(\varepsilon)\varepsilon}{d\tau}d\tau$$

Eq. 5.3

where the reduced time ρ and reduced time variable of integration ρ' are functions of strain and time and are defined as:

$$\rho = \int_0^t \frac{dt'}{a_e[\varepsilon(t')]} \; and \; \rho' = \int_0^\tau \frac{dt'}{a_e[\varepsilon(t')]}$$

E_e is the final value of the elastic modulus and ΔE is the transient modulus during the relaxation between the initial and final values of the elastic modulus. h_e, h_1, h_2 and a_e are strain-dependent material properties, and τ is the variable of integration. A power law equation $\Delta E(\rho) = C\rho^n$ is used to fit a stress relaxation curve and the other material properties are fitted using the rest of the relaxation curves. To fit four different curves, a total of ten parameters is used and the relaxation function is obtained from curve-fitting the relaxation profile at the lowest strain level. The model has been applied to ligament and can describe its strain and time dependent response [1-3, 16]. However, the relaxation function in the model is not unique. In fact, for four different relaxation curves, four different relaxation functions can be fit and therefore four separate sets of parameters

would describe this behavior, indicating the method is essentially a curve-fitting based methodology.

The 1D models discussed above describe the uniaxial response of ligaments and tendons. They must be extended to 3D formulations to be used within a finite element framework or even to consider a different mode of deformation analytically, such as the anterior tibial translation deformation that results in ACL tears. Extending these models to 3D is likely to require the involvement of more parameters for describing the tissue responses in other orientations because, for instance, anisotropy is not addressed in these models in their present form. QLV viscoelastic models and modified QLV models have been implemented into 3D finite element modeling [17]. These continuum models are able to describe the tissue behavior in 3D settings with curve-fitted parameters. However, because the QLV and modified QLV models are based on the separable relaxation function, they cannot fully predict the time and strain dependent responses of soft tissue.

5.2 Micromechanical Modeling of Non-Linear Viscoelasticity

As described in **Chapter 2**, ligaments and tendons have densely organized networks of collagen fibers as their major components, with small amounts of elastin and proteoglycans. Since the mechanical behavior of ligaments and tendons is determined by their constituents and microstructures, a model that takes these constituents and microstructures into consideration may better describe their complicated nonlinear viscoelastic responses. In recent studies, researchers have proposed several constituent-based and microstructurally-based constitutive models with the goal of fully describing the nonlinear viscoelastic ligaments and tendons.

To address this desire for a non-linear viscoelastic model that can capture the 3D response of ligament and tendon with a reduced number of parameters, and moreover can potentially be predictive, we have taken a micromechanics

approach that describes the deformation of aligned structural proteins such as collagen and elastin. Since these are macromolecules, we describe their elastic response in terms of hyperelastic formulations that have been shown to be predictive of the non-linear elasticity of biopolymers and inorganic elastomers alike [18-31].

The recent invention of instruments such as the atomic force microscope (AFM), the magnetic levitation force microscope (MLFM), and optical tweezers (OT), has made it possible to characterize the molecular-level mechanical responses of single biopolymer molecules. A recent study performed using AFM has shown highly nonlinear elastic behavior of long-chain DNA molecules, collagen molecules, and elastin protein molecules [32]. These experimental results have been successfully fitted with entropic elastic models such as the worm-like chain model, the freely jointed chain model, and the Mackintosh semi-flexible chain model [32].

With the thermodynamics considerations, the elasticity of a network of long chain molecules at a constant temperature during stretch can be treated almost entirely due to the entropy change [33] . The entropy for a long-chain biopolymer *s* can be described as:

$$s = k_B \ln(\Omega)$$

Eq. 5.4

where Ω is the number of available configurations, k_B is the Boltzmann's constant. The tension along the chain, f_{chain}, is then described as:

$$f_{chain} = -\Theta \frac{\partial \Delta s}{\partial r}$$

Eq. 5.5

where r is the end-to-end separation of the chain and Θ is the absolute temperature. The number of available configurations decreases as the chain is stretched, causing a decrease in entropy and an increase in the chain stiffness [33]. Based on this, several entropy based models have been established and they have successfully captured nonlinear force-stretch responses of many

biopolymers. Their mechanical responses can be categorized into three regimes: flexible, semi-flexible, and stiff [33]. For example, MacKintosh et al., 1995 proposed a model that describes the nonlinear behavior of semi-flexible biopolymers at small strains well [23]. This model has been implemented in an eight-chain framework [34] to capture the response of an f-actin network [22].

5.2.1 Flexible chain models

A freely jointed chain (FJC) model is proposed to characterize the flexible polymers with long contour lengths [35]. As shown in Figure 5.2, the freely jointed chain consists of N segments with a length of l. Therefore, the total contour length of a flexible biopolymer L_C is Nl. r is the end-to-end separation of the chain. For $r < Nl/3$, r can be expressed using the Gaussian error function $p(r) = (3Nl^2/2\pi)^{3/2}\exp(-3r^2/2Nl^2)$. Therefore, the chain entropy becomes $s = k_B \ln(p(r)dV)$ from Eq. 5.4. Based on Eq. 5.5 the force of such a chain generated during stretching is described as: $f_{Gaussian} = \frac{3k\Theta}{Nl^2}r$. Finally, a network of such flexible chains with a Gaussian error function gives the strain energy density:

$$U_{Gaussian} = \frac{nk_B\Theta}{2}({\lambda_1}^2 + {\lambda_2}^2 + {\lambda_3}^2 - 3)$$

Eq. 5.6

where $nk_B\Theta$ is the rubbery modulus, n is the number of chains per unit volume, and λ_i is the stretch in the i^{th} principal direction of the network.

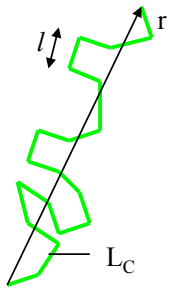

Figure 5.2 Schematic illustration of a freely jointed chain

When the chain deformation approaches the contour length, the Gaussian error assumption breaks down. Non-Guassian behavior is captured from

Langevin chain statistics derived by Kuhn and Grün [36]. The probability density function is valid for $r < Nl$ and is given as:

$$\ln p(r) = c - N(\frac{r}{Nl}\beta + ln\frac{\beta}{\sinh\beta})$$

where $\beta = \mathcal{L}^{-1}(\frac{r}{Nl})$ is the inverse Langevin function, where the Langevin function is defined as $\mathcal{L}(x) = \coth x - 1/x$

$$f_{FJC} = \frac{k_B\Theta}{l}\beta$$

Using a Padé approximation $\mathcal{L}^{-1}(x) = x\frac{3-x^2}{1-x^2} + 0(x^6)$ [37], the above equation can be expressed as:

$$f_{FJC} = \frac{k_B\Theta}{l}\frac{r}{Nl}\left(\frac{3-(r/Nl)^2}{1-(r/Nl)^2}\right)$$

The worm-like chain (WLC) model, derived from Kratky-Porod expression [38], has also been used to successfully characterize the force-extension behavior of long chain molecules [32, 39]. The WLC model [39] is:

$$f_{WLC} = \frac{k_B\Theta}{a}\left[\left(\frac{r}{L_C}\right) + \frac{1}{4(1-r/L_C)^2} - \frac{1}{4}\right]$$

where a is the persistence length $a = \mathrm{K}/k_B\Theta$, L_C is again the contour length and K is the bending stiffness of the chain. The model has been successfully used to capture the force-extension responses of single stranded RNA molecules [40] and double stranded DNA molecules [39], where $L_C \gg a$.

5.2.2 Semi-flexible chain models

MacKintosh used the Kratky-Porod expression to derive the total energy of a semi-flexible chain that has a persistence length on the order of its contour length. The initial chain length, the value of r at f=0 is found to be $r_0 = L_C(1 - L_C/6a)$. With the Padé approximation mentioned earlier, the force expression is derived as [22]:

$$f_{Mac} = \frac{k_B\Theta}{a}(\frac{1}{4(1-r/L_C)^2})\left(\frac{L_C/a - 6(1-r/L_C)}{L_C/a - 2(1-r/L_C)}\right)$$

In these semi-flexible chain models, since the persistence length a is a function of bending stiffness as mentioned above, a represents the stiffness of the chain. As shown in Figure 5.3, variations in persistence lengths lead to differences in mechanical response [33]. A smaller persistence length results in a longer toe region with a relatively compliant initial mechanical response, while a larger persistence length leads to a shorter toe region and a relatively stiffer response.

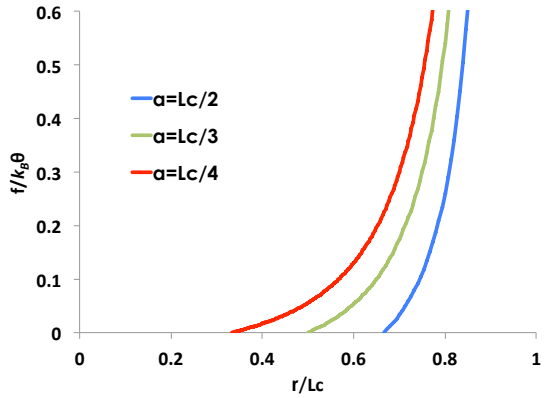

Figure 5.3 The effect of persistence length on the force vs. extension response of a MacKintosh single chain model.

These chain models have the robust capability to capture a large variety of single chain molecules. Since the microstructure of ligaments and tendons is composed of network of single chain molecules, these chain models provide an obvious basis for ligament and tendon models. They can be incorporated into a 3D representative volume element model.

5.2.3 Arruda-Boyce 8-chain network model for 3D deformation

A network of biopolymers can be treated as an idealized network structure as described by the Arruda-Boyce 8-chain model. The model was originally proposed to describe the 3D deformation in elastomers and glassy thermoplastics [34, 41]. The 8-chain model has since been extended and modified to capture the collagen network in skin tissue by Bischoff et al., 2000

[31] and Kuhl et al., 2005 [42]. It was further extended to the elastin network in vascular tissue by Zou et al., 2009 [43]. The cubic structure represents the Arruda-Boyce isotropic representative volume element (RVE). Each chain originates from the center of the RVE to one corner. The cube faces align with the principal stretch directions during deformation in Figure 5.4**.** The stretch on each chain λ_{chain} in the network is therefore given as:

$$\lambda_{chain} = \sqrt{\frac{{\lambda_1}^2 + {\lambda_2}^2 + {\lambda_3}^2}{3}} = \sqrt{\frac{I_1}{3}} = \sqrt{\frac{tr(\mathbf{B})}{3}}$$

Eq. 5.7

where λ_i is the stretch in the i^{th} principal direction, $I_1 = {\lambda_1}^2 + {\lambda_2}^2 + {\lambda_3}^2$ is the first invariant of the stretch tensor, and $\mathbf{B} = \mathbf{F}\mathbf{F}^{\mathrm{T}}$ is the left Cauchy-Green tensor, in which $\mathbf{F} = \frac{\boldsymbol{dx}}{\boldsymbol{dX}}$ is the deformation gradient of a material point $\mathbf{x}$ in the stretched configuration and $\mathbf{X}$ in the reference configuration.

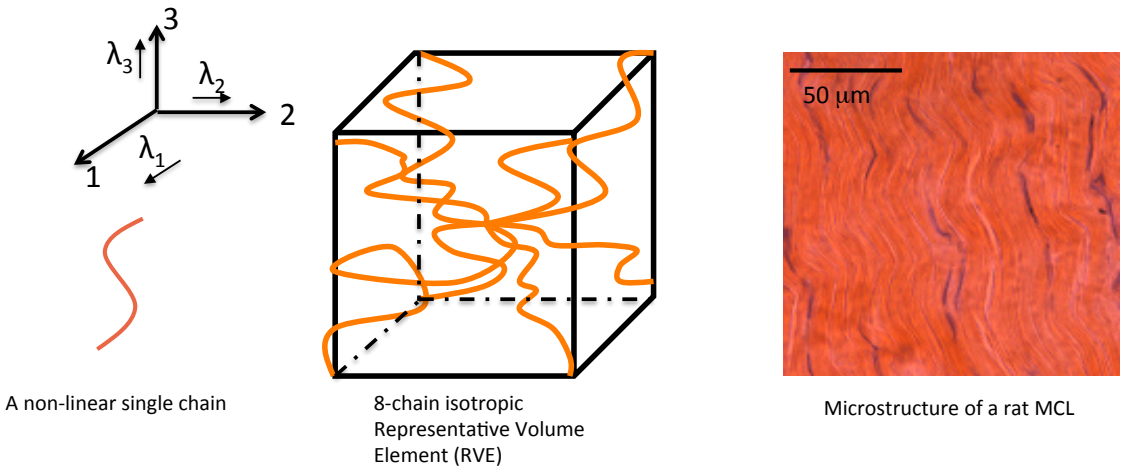

Figure 5.4 An eight-chain network model with eight nonlinear single chains resembles the microstructure of the extracellular matrix found in a ligament or tendon.

Depending on the model used for the individual chains, the strain energy density per unit volume for the 8-chain model with n chains per unit volume is given in **Table 5.1**:

Table 5.1 Strain energy density function of flexible and semi-flexible chains in the Arruda-Boyce 8-chain network.

Single chain	Strain energy density in the 8-chain network
FJC	$U_{FJC} = nk_B\Theta\left\{\frac{\lambda_{chain}}{\sqrt{N}}\beta_{chain} + ln\frac{\beta_{chain}}{\sinh\beta_{chain}}\right\},\ \beta_{chain} = \mathcal{L}^{-1}(\frac{\lambda_{chain}}{\sqrt{N}})$
WLC	$U_{WLC} = \frac{nk_B\Theta}{a}L_C\left[\frac{1}{2}\left(\frac{r_0\lambda_{chain}}{L_C}\right)^2 + \frac{1}{4(1-r_{chain}/L_C)} - \frac{1}{4}\left(\frac{r_0\lambda_{chain}}{L_C}\right)\right]$
Mac	$U_{Mac} = \frac{nk_B\Theta}{a}\left\{\frac{a}{4(1-r_0\lambda_{chain}/Lc)} - a\left[ln\left({L_C}^2 - 2aL_C + 2ar_0\lambda_{chain}\right) - \ln\left(aL_C - ar_0\lambda_{chain}\right)\right] - c\right\}$

The Cauchy stress can be found by differentiating the strain energy density function as follows:

$$\mathbf{T} = 2\frac{\partial U}{\partial I_1}\mathbf{B} - p\mathbf{I}$$

where p is the hydrostatic pressure required for material incompressibility. Based on **Table 5.1** and **Eq. 5.6**, the Cauchy stress of a Gaussian chain network, a freely jointed flexible chain network, and a MacKintosh semi-flexible chain network are given as follows:

$$\mathbf{T}_{Gauss} = nk_B\Theta\mathbf{B} - p\mathbf{I}$$

Eq. 5.8

$$\mathbf{T}_{FJC} = \frac{nk_B\Theta}{3}\left(\frac{3-{\lambda_{chain}}^2/N}{1-{\lambda_{chain}}^2/N}\right)\mathbf{B} - p\mathbf{I}$$

Eq. 5.9

$$\mathbf{T}_{Mac} = \frac{nk_B\Theta}{3a}\frac{r_0}{\lambda_c}\left(\frac{1}{4(1-\lambda_c r_0/L_c)^2}\right)\left(\frac{L_c/a - 6(1-\lambda_c r_0/L_c)}{L_c/a - 2(1-\lambda_c r_0/L_c)}\right)\mathbf{B} - p\mathbf{I}$$

Eq. 5.10

A representative stress-strain response of each model is shown in Figure 5.5**A** and a zoomed-in view of these responses at low stretch is provided in Figure 5.5**B**. The Mackintosh 8-chain semi-flexible model is initially much more compliant than either the Gaussian model or the freely jointed chain model. As the stretch increases, the slope of the Mackintosh chain increases drastically,

whereas the slopes of the Gaussian and FJC chains stays at the same level with a minor decrease in the small stretch regime.

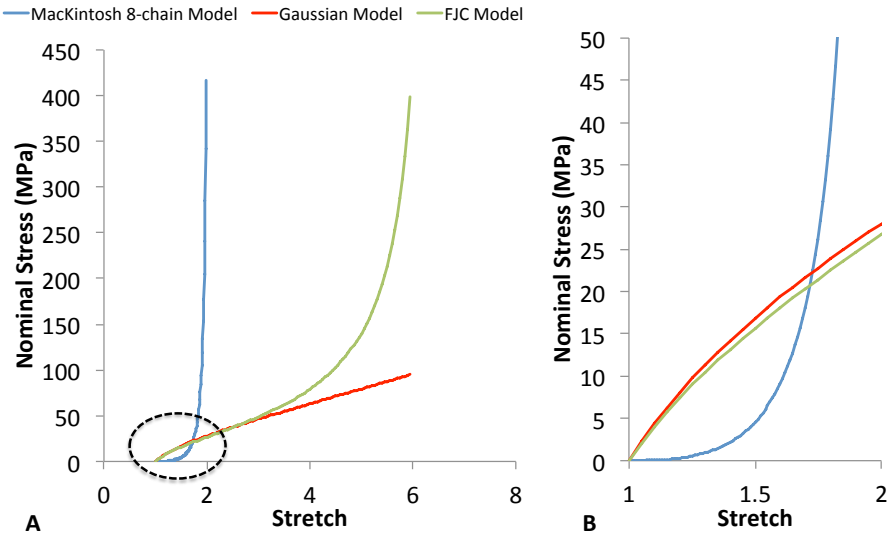

Figure 5.5 Representative stress-strain response curves of a MacKintosh 8-chain model, Gaussian model, and a FJC model (A); (B) shows the low-stretch responses of these models.

5.2.4 3D Non-linear viscoelastic model

Ligaments and tendons are largely comprised of aligned viscoelastic collagen fibers and nonlinear elastic elastin networks. To capture their structure and nonlinear viscoelastic behavior, we have developed a micromechanical model incorporating collagen and elastin to describe the non-linear viscoelastic response of ACLs and our tissue engineered grafts.

5.2.4.1 Nonlinear three-element model

The simplest viscoelastic model that can capture solid-like behavior is the standard linear solid model, the 1D analog of which has two linear springs and a linear dashpot. The configuration of this model can be represented with springs of stiffness as k_1 and k_2 and a dashpot with viscosity η_1 as in Figure 5.6**A**. The model describes the linear viscoelastic behavior of solids well. In the extension to 3D, each spring becomes a 3D linear elastic stress-strain relationship (i.e. Hooke's Law) and the dashpot becomes a 3D linear viscous element. Since

ligaments and tendons have nonlinear viscoelastic responses, we substitute a nonlinear MacKintosh semi-flexible network of Figure 5.6**B** for one linear spring and a nonlinear Gaussian spring for the other linear spring to capture the response of a homogeneous non-linear viscoelastic tissue.

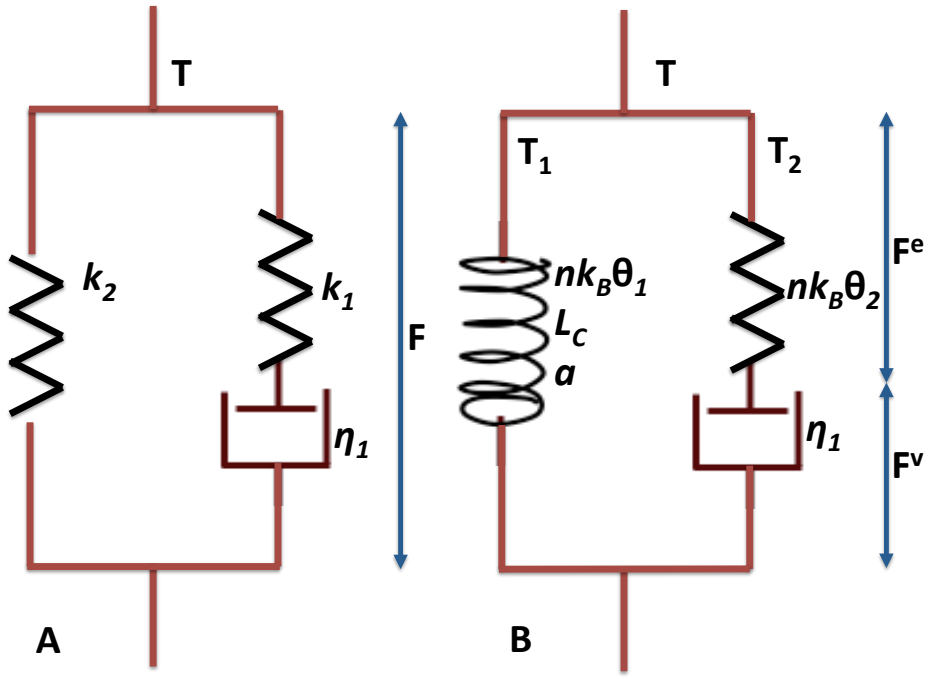

Figure 5.6 By substituting the linear springs in a standard three-element model (A) with nonlinear springs, a nonlinear solid model (B) can be used to capture the nonlinear viscoelastic responses of soft tissue.

In this model, a non-linear spring 2 and linear viscous dashpot in series is in parallel with another non-linear spring 1. To model the engineered and native tissue, a network of MacKintosh chains [22, 23] is used for spring 1 and a Gaussian chain network (see Treloar for example [35]) is utilized in spring 2. $\mathbf{F}^e$ is the elastic part of the deformation tensor and $\mathbf{F}^v$ is the viscous part. From compatibility, the total deformation $\mathbf{F}$ can be decomposed as $\mathbf{F} = \mathbf{F}^e\mathbf{F}^v$. The equilibrium of the system gives the total Cauchy stress as $\mathbf{T} = \mathbf{T_1} + \mathbf{T_2}$, where $\mathbf{T_1}$ is the Cauchy stress generated from spring 1 and $\mathbf{T_2}$ is the Cauchy stress generated from spring 2. The Cauchy stress on spring 1 is given by a MacKintosh semi-flexible chain network in **Eq. 5.10** and the Cauchy stress on

spring 2 is given by a Gaussian chain network in **Eq. 5.8**. The linear dashpot constitutive equation is $\mathbf{D}^v = \frac{\boldsymbol{\sigma}_2'}{\eta^*}$ where $\mathbf{D}^v$ is the viscous shear strain rate, $\eta^*$is the constant shear viscosity and $\boldsymbol{\sigma}_2'$ is the equivalent shear stress on spring 2. The network deformation is assumed to be isochoric and incompressible.

A rate formulation is employed to compute the stress vs. strain responses of various tissues to a cyclic load/unload test. Briefly, time and total stretch are prescribed so that $\mathbf{F}^v$ can be explicitly computed based on the rate of deformation of the viscous dashpot updated from the previous step. $\mathbf{F}^e$ is therefore updated in the current time step and then used to compute the stresses. Once the total stress is calculated, the rate of deformation is again updated for the viscous stretch computation in the next step.

This micromechanical model was applied to rat MCL and BLB constructs. The parameters were determined from the results of uniaxial cyclic load/unload tests conducted using *in vitro* and *in vivo* engineered BLB constructs and native neonatal rat MCL. The numerical and experimental results are shown in Figure 5.7. Model parameters used for obtaining the numerical results are listed in Table 5.2. By varying the stiffness of the two nonlinear springs and the viscosity of the dashpot, the micromechanical model is robust enough to capture the mechanical responses of *in vitro* and *in vivo* engineered constructs and native MCLs. The presented computational model of connective tissue has been used to explore the rich mechanical response of native and engineered MCL. The parameters found using the current model have the capability to connect the numerically fitted responses with the physical properties of native and engineered MCLs.

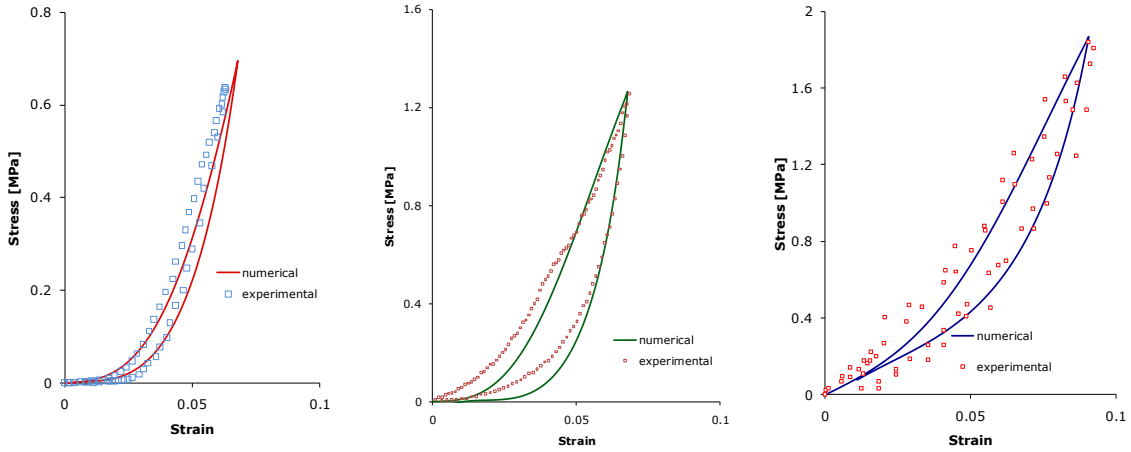

Figure 5.7 Micromechanical modeling of engineered *in vitro* BLB constructs (A), engineered one-month *in vivo* BLB constructs (B) and 14-day old rat neonatal MCL (C).

Table 5.2 Model parameter comparison among the in vitro rat BLB, one-month rat BLB explant, and 14-day old neonatal rat MCL.

	MacKintosh Spring			Gaussian Spring	Dashpot
	nk_BT_1(MPa)	Lc	a	nkT_B_2 (MPa)	η_1
***in vitro* Engineered BLB**	55	10	2	0.1	200
1-mo *in vivo* Engineering BLB	150	10	2	0.1	1000
14-day old Rat MCL	55	10	2	2.5	150

We have also examined various possibilities for characterizing the nonlinear viscoelasticity of soft tissue with this model using data from literature. To characterize different nonlinear strain-dependent stress relaxations of ligaments and tendons, we took advantage of the tangent modulus of these nonlinear springs being strain-dependent and consequently constructed two constitutive models (Figure 5.8). Ligaments tend to relax slower as the strain level increases [1]. By connecting a Gaussian spring in series with a linear dashpot (Figure 5.8**A**), the relaxation rate contributed from this spring-dashpot series exhibits decreasing relaxation rates with increasing strain levels (Figure 5.8**C**). On the other hand, tendons tend to relax faster as the strain levels

increases [2]. By connecting a MacKintosh spring in series with a linear dashpot (Figure 5.8**B**), the relaxation rate contributed from this series exhibits increasing relaxation rates with increasing strain levels (Figure 5.8**D**). The capabilities of the proposed models were examined by applying them to data from the literature as shown in Figure 5.9. We were able to qualitatively capture and predict the non-constant stress relaxation rates of ligaments and tendons using a limited number of parameters that are physiologically relevant. Our previous work has shown ligament and tendon strain behaviors are more complicated than those presented in Provenzano et al., 2001 and Duenwald et al., 2009. In particular, the tissue exhibits a heterogeneous mechanical response and the initial stress relaxation rate is much faster than the rate at a later time course [3]. These experimental observations from experiments inspired us to propose a more accurate model with the aim of fully capturing the nonlinear viscoelastic responses of ligaments and tendons.

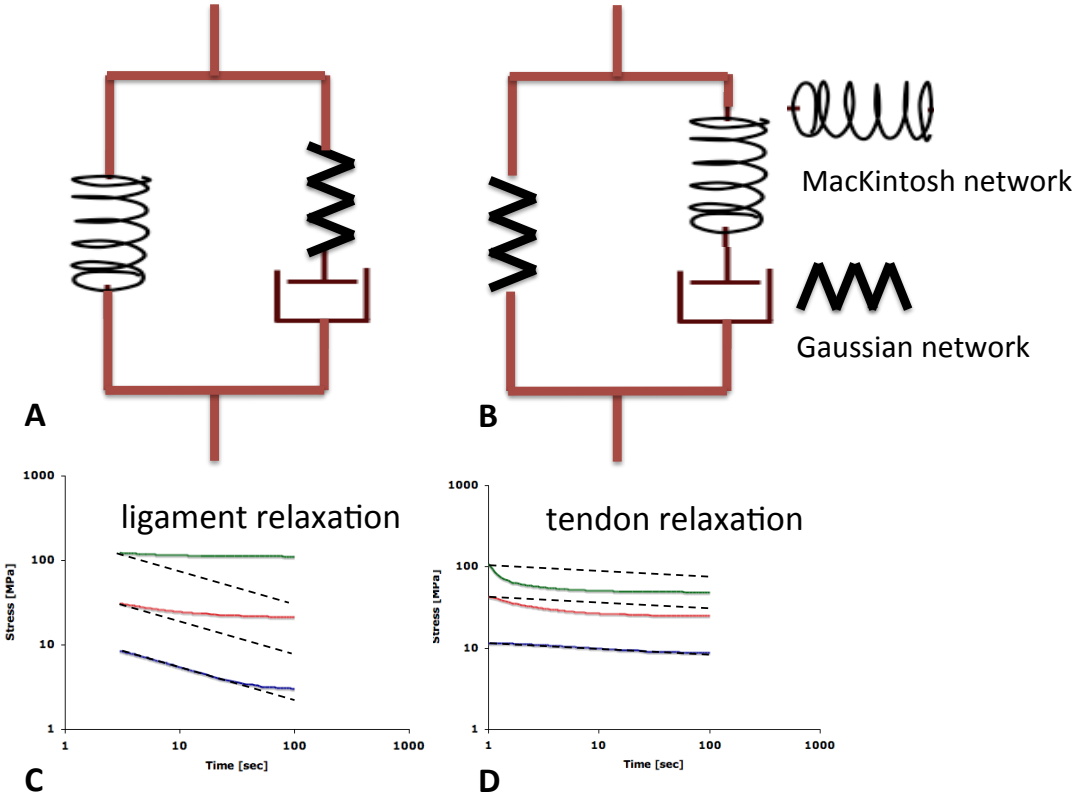

Figure 5.8 By switching the locations of the MacKintosh spring and the Gaussian spring, the nonlinear three-element model can capture the different strain-dependent relaxation behaviors of ligaments and tendons

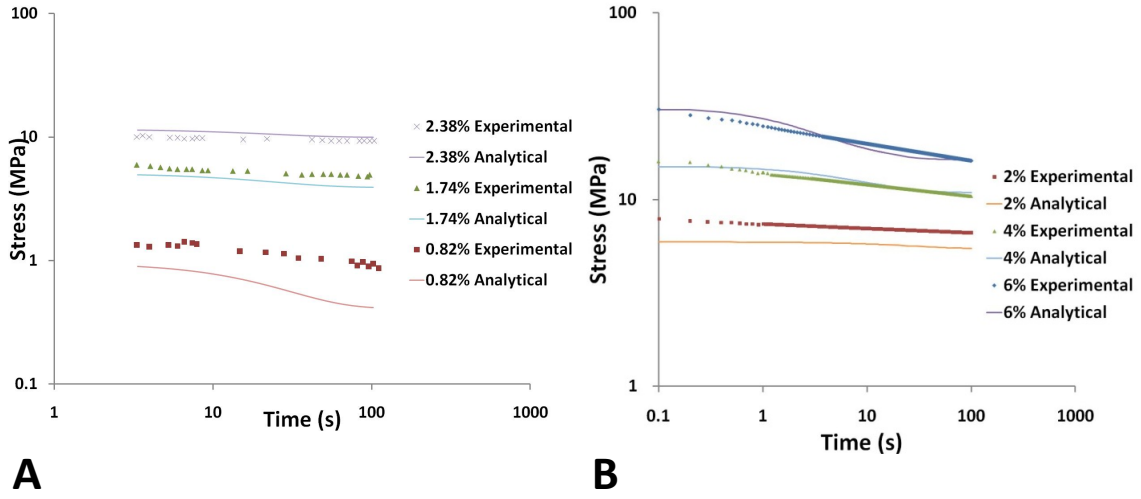

Figure 5.9 Model predictions from literature results in (A) ligament and (B) tendon [1, 2].

5.2.4.2 Nonlinear five-element model

Our previous stress relaxation experiments have demonstrated that ACLs and tissue engineered grafts have a distinct bi-linear relaxation responses as shown in Figure 5.10 that may be captured by two Gaussian elastic networks and two linear viscous elements. Therefore, the proposed 3D model consists of five elements, a nonlinear elastic network, two linear elastic networks and two linear viscous elements (Figure 5.11).

In this model $\mathbf{F}_B^e$ and $\mathbf{F}_C^e$ are the elastic parts of the deformation gradient tensors and $\mathbf{F}_B^v$ and $\mathbf{F}_C^v$ are the viscous parts. From compatibility, the total deformation $\mathbf{F}$ is $\mathbf{F} = \mathbf{F}_B^e\mathbf{F}_B^v = \mathbf{F}_C^e\mathbf{F}_C^v$. The equilibrium of the system gives the total Cauchy stress as $\mathbf{T} = \mathbf{T}_A + \mathbf{T}_B + \mathbf{T}_C$, where $\mathbf{T}_A$ is the Cauchy stress in the nonlinear spring network A, given by **Eq. 5.10**, and $\mathbf{T}_B$ and $\mathbf{T}_C$ are the Cauchy stresses in the Gaussian spring networks B and C. The Cauchy stress tensor in each Gaussian network is given by **Eq. 5.8**. The linear dashpot constitutive equation for viscous element B, C is $D_{B,C}^v = \frac{\mathbf{T}'_{B,C}}{\eta_{B,C}}$ where $D_{B,C}^v$ is the viscous shear strain rate, $\eta_{B,C}$ is the constant shear viscosity and $\mathbf{T}'_{B,C}$ is the equivalent shear stress. The network deformation is assumed to be incompressible. The model

implementation and parameter determination will be presented in the next section.

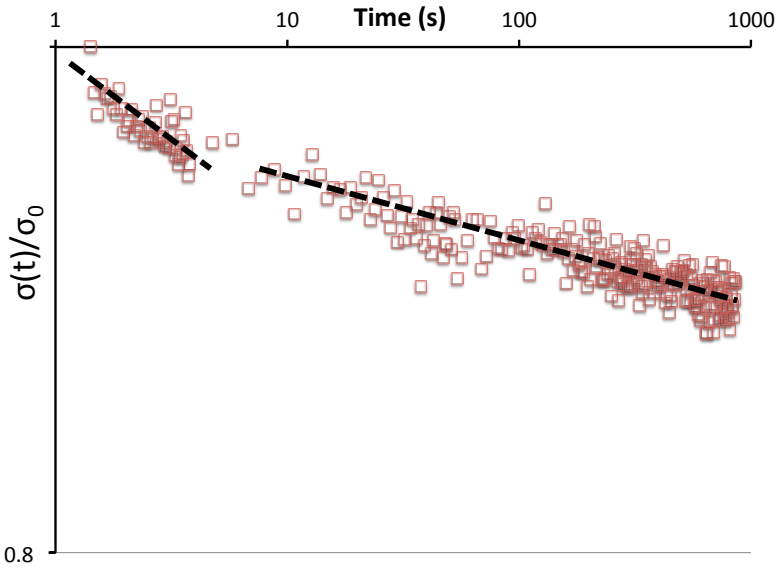

Figure 5.10 Bi-linear stress relaxation response of a native ACL

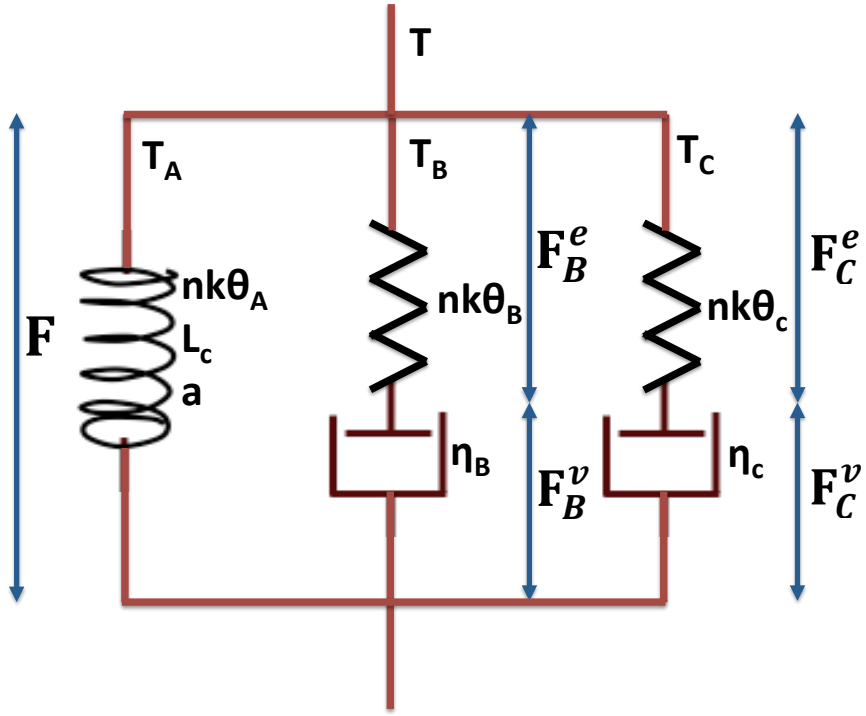

Figure 5.11 A five-element nonlinear viscoelastic 3D constitutive model

5.3 Determination of the Parameters of the five-element model

Stress and strain data from the uniaxial test and the final value of the stresses from each stress relaxation test conducted on the same specimen are used to determine the model parameters. As shown in Figure 5.12, first, the parameters of the MacKintosh 8-chain model, L_C, a, and $nk\Theta$, are determined by fitting the equilibrium response, ie. the fully relaxed stress vs. strain values from the stress relaxation tests. These are shown as black dots and fit to a nonlinear elastic MacKintosh model shown by the solid purple line in the figure. With these three parameters determined, the contributions of the two Gaussian springs (yellow and blue curves) are added to the model to fit the uniaxial test data. The rate of the uniaxial test is 0.05/s therefore one load-unload test ends within 4 seconds. The hysteresis of the uniaxial load-unload response can be fit using the viscosity of a fast linear dashpot. Finally, using the three sets of stress relaxation data, the parameters associated with the linear series spring-dashpot systems are adjusted so that the same set of seven parameters can fit all three stress relaxation response curves as well as the uniaxial tension response obtained from the same specimen. The rate formulation, described previously in section **5.2.4.1**, is again employed to compute the stress vs. strain responses of various tissues to a cyclic load/unload test.

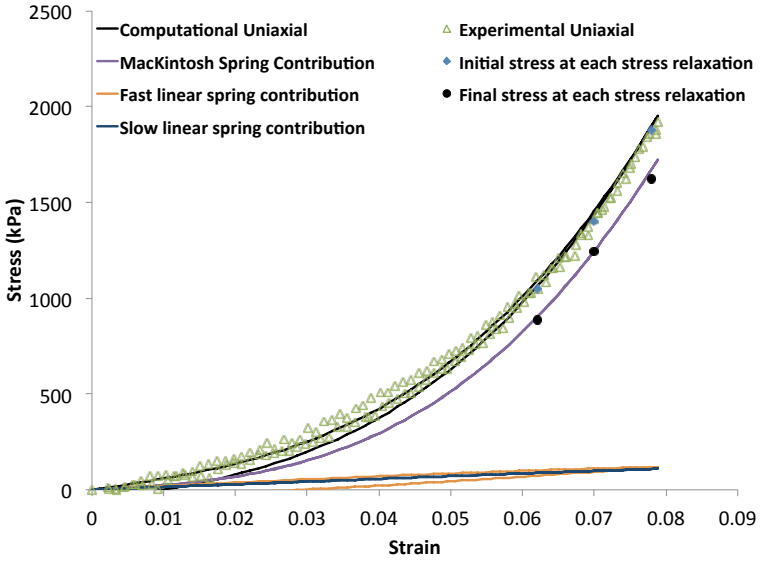

Figure 5.12 Parameter fitting scheme of the proposed five-element viscoelastic constitutive model

5.4 Predicted biomechanical properties of native and engineered ligaments and tendons using the nonlinear 5-element model

The micromechanical model proposed herein captures the uniaxial load-unload responses of the native ACL (Figure 5.13**A**), the engineered BLB explant (Figure 5.13**C**), and PTG explant at 9-months (Figure 5.13**E**). Experimental results of the native PT demonstrated that the PT cannot be predicted using the proposed model with two Gaussian springs. After changing one of the Gaussian springs to a nonlinear MacKintosh spring, the model was able to successfully capture the stress relxation responses of the native PT (Figure 5.13**G**). With the same sets of parameters, the model predicts the stress relaxation responses (Figure 5.13 **B**, **D**, **F**, and **H**).

The parameters used to predict the BLB explant response are very similar to those used to predict the native ACL response (Table 5.3). A total of 7 parameters are needed to capture these responses, but unlike the model previously discussed in this chapter, the current formulation is 3D and additional model parameters are not needed to describe other deformation states.

Table 5.3 Model parameter comparison among the native ACL, BLB explant at 9-months, PTG explant at 9-months, and native PT.

	MacKintosh Spring			Fast Gaussian Spring	Fast Dashpot	Slow Gaussian Spring			Slow Dashpot
	nkT_A (MPa)	Lc	a	nkT_B (MPa)	η_B	nkT_C (Mpa)			η_C
Native ACL	50	12.5	8	5	1000	8			280000
Engineered BLB	50	12.4	8	3.5	1000	2			150000
PT autograft	250	12	8.3	2	2500	2			100000
	MacKintosh Spring			Fast Gaussian Spring	Fast Dashpot	Mackintosh Spring			Slow Dashpot
	nkT_A (Mpa)	Lc_A	a_A	nkT_B (Mpa)	η_B	nkT_C (MPa)	Lc_C	a_C	η_C
Native PT	1.8	11.8	12.5	3	8000	1600	12	12.5	1600000

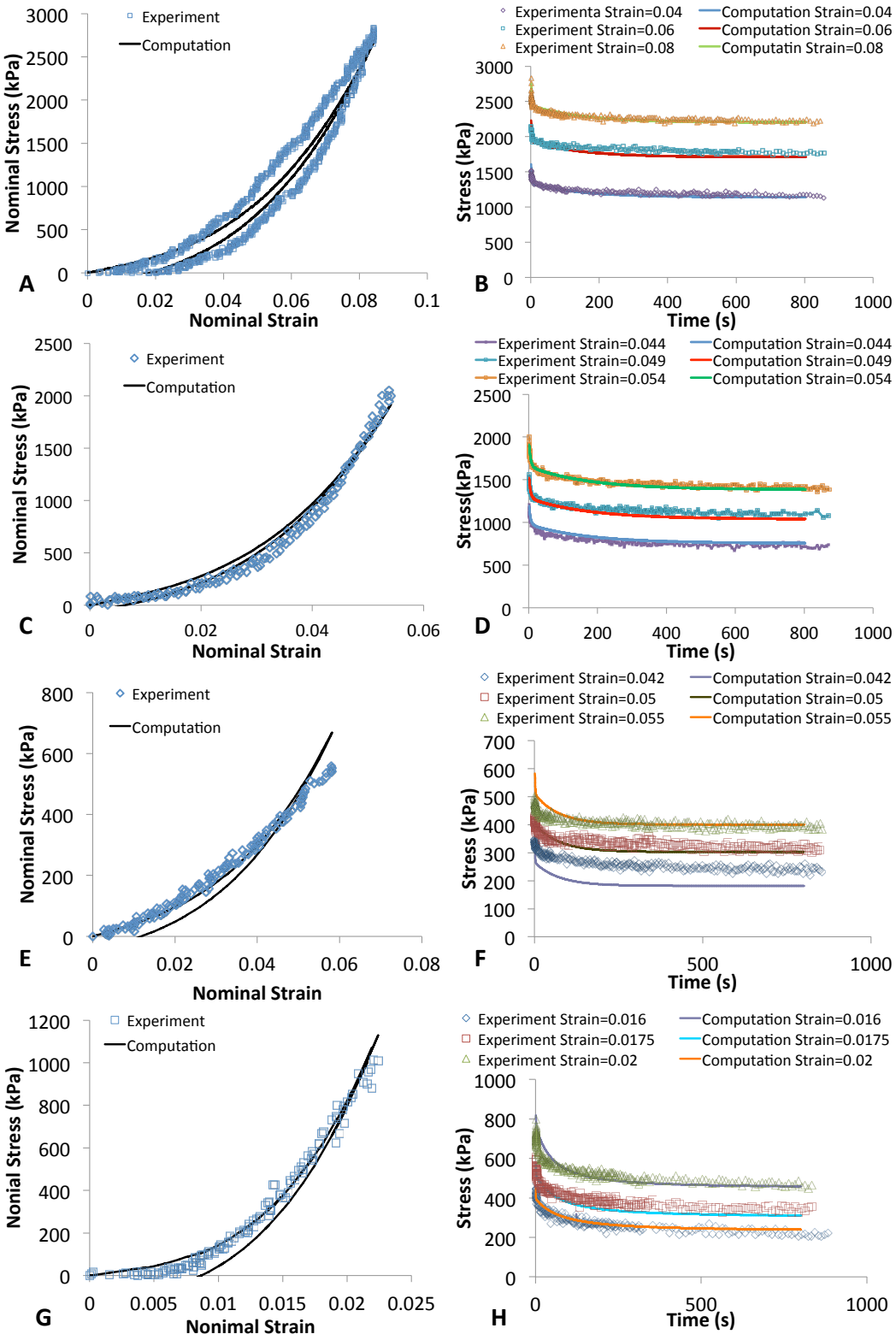

Figure 5.13 Experimental and computational responses of a native ACL (A, B), engineered BLB explant after 9-month (C, D), PTG explant after 9-month (E, F), and native PT (G, H).

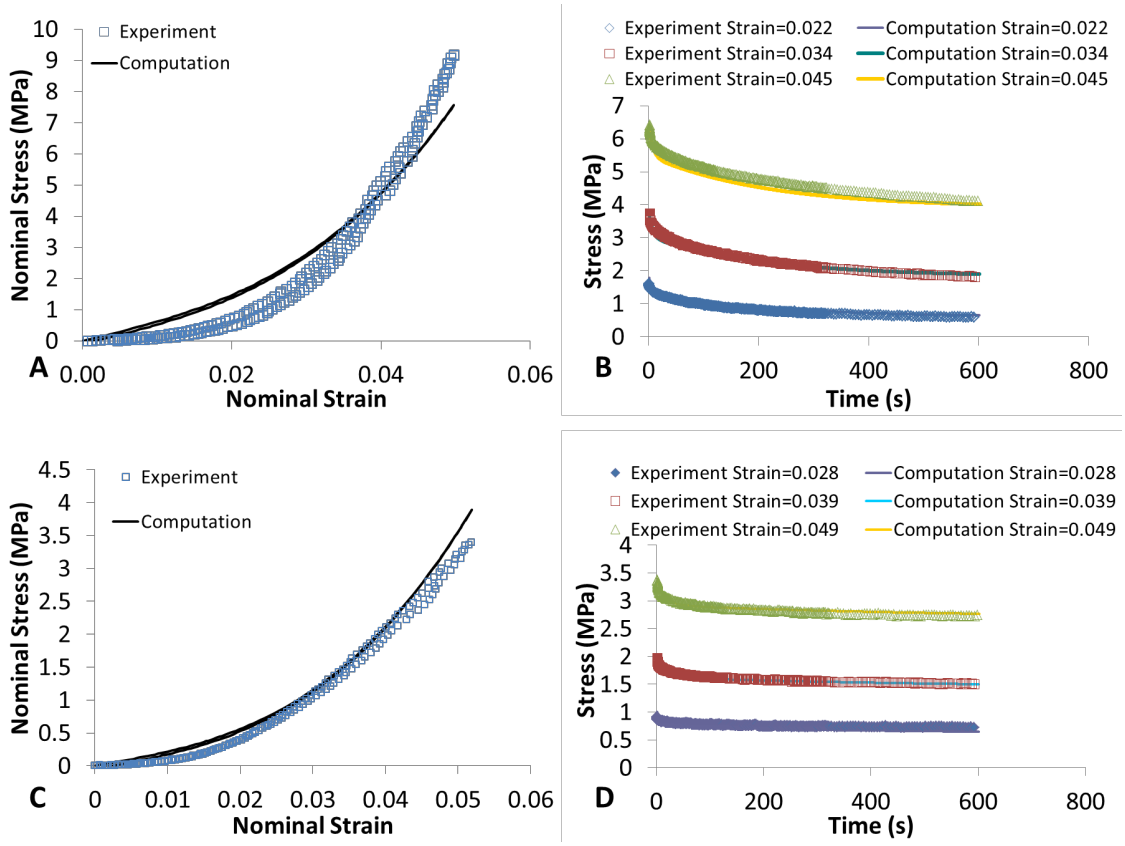

Figure 5.14 Experimental and computational responses of the anterior (A and B) and the posterior bundle (C and D) from the same sheep ACL.

Previously we developed a three-element viscoelastic model for describing ligament and tendon response. This simple model qualitatively captured the nonlinear viscoelastic responses of ligaments and tendons. Experimental data from stress relaxation experiments demonstrate that these soft tissues possess a bi-linear relaxation pattern. This finding is in agreement with the results from collagen related research done by Shen et al., 2011 and by Yang et al., 2012 [44, 45]. Therefore, we added another linear series spring-dashpot system to the existing model as this two time constant feature fits the data well as seen in Figure 5.13 and Figure 5.14. The nonlinear strain-dependent viscoelastic responses of ligaments and tendons are captured by the nonlinear MacKintosh network representing the collagen components of the structure.

The model was constructed based on the physical microstructure of the native and engineered tissue. Earlier studies showed that the center of the ACL has a higher type I collagen density than the two insertion ends [46]. Histological analysis also revealed that collagen fibers are more aligned than the rest of the regions. Near the distal insertion end, a more wavy crimp region of the collagen was found [47]. These physical observations can all be reflected by the parameters in the proposed model. In a nonlinear MacKintosh network, $nk\Theta$ is the chain density which is the density of type I collagen in the ACL. The contour length L_C is the total length of the single collagen chain. A more wavy crimp region can be interpreted as a longer contour length of the collagen fibers at this region. The high correlation between the parameters of the model and the morphological parameters was demonstrated from the well matched functionally graded mechanical responses (Figure 5.15).

Parameters	Average	Proximal	Mid	Distal
nkΘ (Mpa)	10000	28000	40000	10000
a	8	4	5.4	6.1
Lc	5.4	5	4.5	17

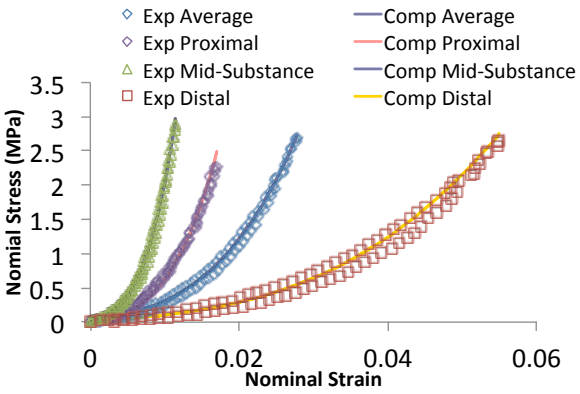

Figure 5.15 Functionally graded prediction of the anterior bundle of the native ACL.

Our previous study shows the tissue engineered BLB, after 9 months of *in vivo* recovery, has developed a similar microstructure to that of the native ACL as indicated from longitudinally and sectionally stained tissue samples for both collagen and elastin [3]. The parameters of our microstructural constitutive model are in agreement with previous biological and mechanical studies. Model parameters used to capture the native ACL and engineered BLB response show the three parameters for the MacKintosh network are indeed very similar, indicating the engineered BLBs have remodeled *in vivo* and have developed

mechanical properties that are very similar to that of the native ACL. The BLB parameters indicate a more compliant response than do those of the ACL, indicating a longer recovery time may be needed for our BLBs to fully develop to native ACLs.

The seven model parameters needed to capture the non-linear response of these tissues are intended to capture the full 3D response of these tissues, however they assume initial isotropy. However, the modeling framework does allow for initial anisotropy (Figure 5.16), without adding several more parameters. A transversely isotropic ligament or tendon would incur an additional parameter, which is the ratio of the representative volume element dimensions in the direction of the fibers versus perpendicular to them. In ongoing work, we intend to implement this model into a commercially available finite element program to simulate the complicated inhomogeneous response of the knee during an anterior tibial translation, the motion that results in ACL failure. We will assess the initial anisotropy requirements needed to capture this response.

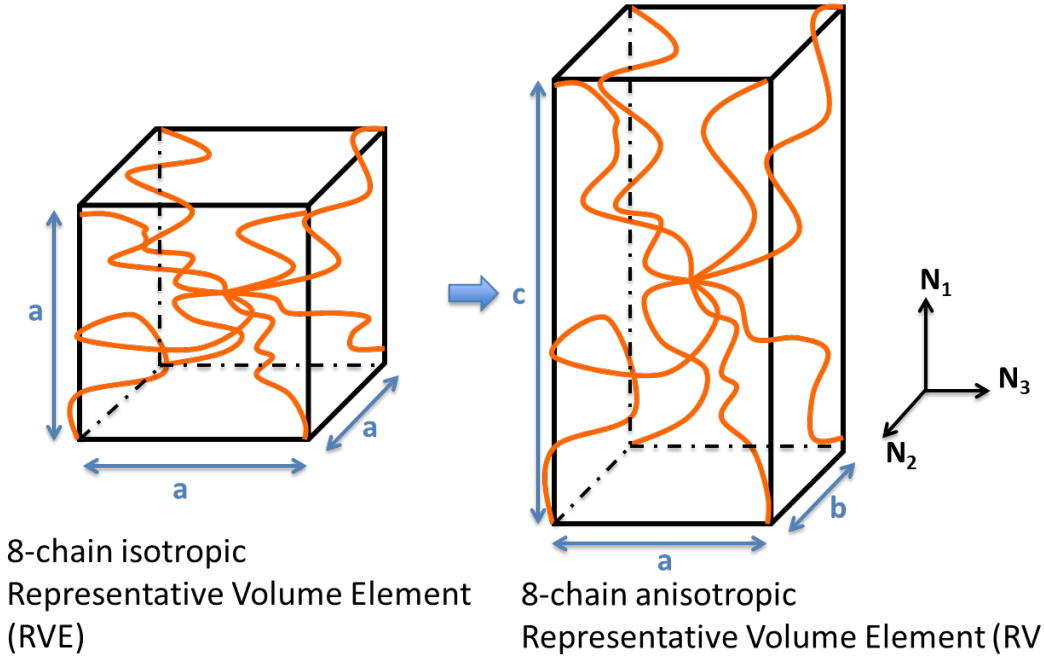

Figure 5.16 An anisotropic representative volume element for a network of semi-flexible chains [27, 28]

5.5 Conclusions

Experimental results show the mechanical response of ligaments and tendons is nonlinear, viscoelastic, and functionally graded. Moreover, engineered ligaments used as an ACL replacement rapidly develop *in vivo* to obtain similar structure and function as compared to native ACL. Our micromechanical model of connective tissue has been used to explore the rich mechanical response of native and engineered ligaments from a microstructural point of view and is in agreement with the findings in histological studies.

5.6 References

1. Provenzano, P., et al., *Nonlinear ligament viscoelasticity.* Ann Biomed Eng, 2001. **29**(10): p. 908-14.

2. Duenwald, S.E., R. Vanderby, Jr., and R.S. Lakes, *Stress relaxation and recovery in tendon and ligament: experiment and modeling.* Biorheology, 2010. **47**(1): p. 1-14.

3. Ma, J., et al., *Three-dimensional engineered bone-ligament-bone constructs for anterior cruciate ligament replacement.* Tissue engineering.Part A, 2012. **18**(1-2): p. 103-116.

4. Chhabra, A., et al., *Anatomic, radiographic, biomechanical, and kinematic evaluation of the anterior cruciate ligament and its two functional bundles.* The Journal of bone and joint surgery. American volume, 2006. **88 Suppl 4**: p. 2-10.

5. Corr, D.T., et al., *A nonlinear generalized Maxwell fluid model for viscoelastic materials.* Journal of Applied Mechanics-Transactions of the Asme, 2001. **68**(5): p. 787-790.

6. Petersen, W., et al., *Biomechanical evaluation of two techniques for double-bundle anterior cruciate ligament reconstruction: one tibial tunnel versus two tibial tunnels.* Am J Sports Med, 2007. **35**(2): p. 228-34.

7. Zantop, T., et al., *The role of the anteromedial and posterolateral bundles of the anterior cruciate ligament in anterior tibial translation and internal rotation.* Am J Sports Med, 2007. **35**(2): p. 223-7.

8. Petersen, W. and T. Zantop, *Partial rupture of the anterior cruciate ligament.* Arthroscopy, 2006. **22**(11): p. 1143-5.

9. Johnson, G.A., et al., *Tensile and Viscoelastic Properties of Human Patellar Tendon.* Journal of Orthopaedic Research, 1994. **12**(6): p. 796-803.

10. Freeman, J.W., et al., *Tissue engineering of the anterior cruciate ligament: the viscoelastic behavior and cell viability of a novel braid-twist scaffold.* Journal of biomaterials science.Polymer edition, 2009. **20**(12): p. 1709-1728.

11. Oza, A.L., R. Vanderby, and R.S. Lakes, *Creep and relaxation in ligament: Theory, methods and experiment*, ed. G.A. Holzapfel and R.W. Ogden 2006. 397.

12. Sarver, J.J., P.S. Robinson, and D.M. Elliott, *Methods for quasi-linear viscoelastic modeling of soft tissue: Application to incremental stress-relaxation experiments.* Journal of Biomechanical Engineering-Transactions of the Asme, 2003. **125**(5): p. 754-758.

13. Abramowitch, S.D. and S.L. Woo, *An improved method to analyze the stress relaxation of ligaments following a finite ramp time based on the quasi-linear viscoelastic theory.* Journal of Biomechanical Engineering, 2004. **126**(1): p. 92-97.

14. Abramowitch, S.D., et al., *An evaluation of the quasi-linear viscoelastic properties of the healing medial collateral ligament in a goat model.* Annals of Biomedical Engineering, 2004. **32**(3): p. 329-335.

15. Weiss, J.A. and J.C. Gardiner, *Computational modeling of ligament mechanics.* Critical reviews in biomedical engineering, 2001. **29**(3): p. 303-71.

16. Hingorani, R.V., et al., *Nonlinear viscoelasticity in rabbit medial collateral ligament.* Annals of Biomedical Engineering, 2004. **32**(2): p. 306-312.

17. Pioletti, D.P., et al., *Viscoelastic constitutive law in large deformations: application to human knee ligaments and tendons.* Journal of Biomechanics, 1998. **31**(8): p. 753-757.

18. von Lockette, P.R., E.M. Arruda, and Y. Wang, *Mesoscale modeling of bimodal elastomer networks: Constitutive and optical theories and results.* Macromolecules, 2002. **35**(18): p. 7100-7109.

19. von Lockette, P.R. and E.M. Arruda, *Computational annealing of simulated unimodal and bimodal networks.* Computational and Theoretical Polymer Science, 2001. **11**(6): p. 415-428.

20. von Lockette, P.R. and E.M. Arruda, *Topological studies of bimodal networks.* Macromolecules, 1999. **32**(6): p. 1990-1999.

21. von Lockette, P.R. and E.M. Arruda, *A network description of the non-Gaussian stress-optic and Raman scattering responses of elastomer networks.* Acta Mechanica, 1999. **134**(1-2): p. 81-107.

22. Palmer, J.S. and M.C. Boyce, *Constitutive modeling of the stress-strain behavior of F-actin filament networks.* Acta Biomaterialia, 2008. **4**(3): p. 597-612.

23. Mackintosh, F.C., J. Kas, and P.A. Janmey, *ELASTICITY OF SEMIFLEXIBLE BIOPOLYMER NETWORKS.* Physical Review Letters, 1995. **75**(24): p. 4425-4428.

24. Boyce, M.C. and E.M. Arruda, *Swelling and mechanical stretching of elastomeric materials.* Mathematics and Mechanics of Solids, 2001. **6**(6): p. 641-659.

25. Boyce, M.C. and E.M. Arruda, *Constitutive models of rubber elasticity: A review.* Rubber Chemistry and Technology, 2000. **73**(3): p. 504-523.

26. Bischoff, J.E., E.M. Arruda, and K. Grosh, *A rheological network model for the continuum anisotropic and viscoelastic behavior of soft tissue.* Biomechanics and Modeling in Mechanobiology, 2004. **3**(1): p. 56-65.

27. Bischoff, J.E., E.M. Arruda, and K. Grosh, *Orthotropic hyperelasticity in terms of an arbitrary molecular chain model.* Journal of Applied Mechanics-Transactions of the Asme, 2002. **69**(2): p. 198-201.

28. Bischoff, J.E., E.M. Arruda, and K. Grosh, *Finite element simulations of orthotropic hyperelasticity.* Finite Elements in Analysis and Design, 2002. **38**(10): p. 983-998.

29. Bischoff, J.E., E.M. Arruda, and K. Grosh, *A microstructurally based orthotropic hyperelastic constitutive law.* Journal of Applied Mechanics-Transactions of the Asme, 2002. **69**(5): p. 570-579.

30. Bischoff, J.E., E.M. Arruda, and K. Grosh, *A new constitutive model for the compressibility of elastomers at finite deformations.* Rubber Chemistry and Technology, 2001. **74**(4): p. 541-559.

31. Bischoff, J.E., E.M. Arruda, and K. Grosh, *Finite element modeling of human skin using an isotropic, nonlinear elastic constitutive model.* Journal of Biomechanics, 2000. **33**(6): p. 645-652.

32. Rief, M., et al., *Single molecule force spectroscopy on polysaccharides by atomic force microscopy.* Science, 1997. **275**(5304): p. 1295-1297.

33. Arruda, E.M., M. C. Boyce, *Statistical Mechanics Models of Equilibrium Behavior*. Chapter 4, Mechanics of Elastomeric Materials, Course Notes, ME 517, University of Michigan, c. 2008.

34. Arruda, E.M. and M.C. Boyce, *A 3-dimensional constitutive model for the large stretch behavior of rubber elastic-materials.* Journal of the Mechanics and Physics of Solids, 1993. **41**(2): p. 389-412.

35. Treloar, L.R.G., *The physics of rubber elasticity*. 2nd ed. 1958, Oxford: Clarendon Press.

36. Kuhn, W. and F. Grun, *Relations between elastic constants and the strain birefringence of high-elastic substances.* Kolloid-Zeitschrift, 1942. **101**(3): p. 248-271.

37. Cohen, A., *A pade approximant to the inverse langevin function.* Rheologica Acta, 1991. **30**(3): p. 270-273.

38. Kratky, O. and G. Porod, *Diffuse small-angle scattering of X-rays in colloid systems.* Journal of colloid science, 1949. **4**(1): p. 35-70.

39. Marko, J.F. and E.D. Siggia, *Stretching DNA.* Macromolecules, 1995. **28**(26): p. 8759-8770.

40. Liphardt, J., et al., *Reversible unfolding of single RNA molecules by mechanical force.* Science, 2001. **292**(5517): p. 733-7.

41. Arruda, E.M. and M.C. Boyce, *Evolution of plastic anisotropy in amorphous polymers during finite straining.* International Journal of Plasticity, 1993. **9**(6): p. 697-720.

42. Kuhl, E., et al., *Remodeling of biological tissue: Mechanically induced reorientation of a transversely isotropic chain network.* Journal of the Mechanics and Physics of Solids, 2005. **53**(7): p. 1552-1573.

43. Zou, Y. and Y. Zhang, *An Experimental and Theoretical Study on the Anisotropy of Elastin Network.* Annals of Biomedical Engineering, 2009. **37**(8): p. 1572-1583.

44. Yang, L., et al., *Micromechanical analysis of native and cross-linked collagen type I fibrils supports the existence of microfibrils.* Journal of the Mechanical Behavior of Biomedical Materials, 2012. **6**: p. 148-158.

45. Shen, Z.L., et al., *Viscoelastic Properties of Isolated Collagen Fibrils.* Biophysical Journal, 2011. **100**(12): p. 3008-3015.

46. Mommersteeg, T.J.A., et al., *Nonuniform distribution of collagen density in human knee ligaments.* Journal of Orthopaedic Research, 1994. **12**(2): p. 238-245.

47. Duthon, V.B., et al., *Anatomy of the anterior cruciate ligament.* Knee Surgery, Sports Traumatology, Arthroscopy, 2005. **14**(3): p. 204-213.

CHAPTER 6

Computational Modeling of Native and Engineered Ligaments and Tendons II. Finite Element Modeling

The experimental data on ACL mechanics, detailed in **Chapter 4**, are limited by the intrinsic inhomogeneous geometry and functionally graded material properties of the ACL. It is generally not possible to analytically simulate the complicated physiological loading condition of an ACL experimental setup because of the complicated geometric and loading conditions. These realities are challenges to a complete understanding of the ACL mechanical responses. To understand the detailed mechanics and failure mechanisms of the native ACL in a physiological loading condition and further evaluate the graft candidates, the establishment of a finite element (FE) model of the ACL and grafts in the knee joint is imperative. In this chapter, the establishment of an anatomically accurate ACL geometry is discussed. The inhomogeneous geometry and a constitutive model that characterizes the functionally graded mechanical properties of the ACL are implemented into FE software. The FE model is used to predict the ACL biomechanical responses in a physiological loading condition. To validate the model, the predicted results from the FE model are compared with experimental data obtained from an *in vitro* anterior tibial translation test.

6.1 Current understanding

Computational biomechanics has become an important tool to provide information that is impossible to obtain experimentally. In particular, finite element analysis (FEA) has been implemented into current ACL biomechanics investigations [1-7].

Many of these FEA studies have implemented a homogeneous isotropic neo-Hookean constitutive model to simplify the computations [2, 7], Xie et al., 2009 have implemented a polynomial strain potential energy function [6]. Hirokawa and Tsuruno 2000 have implemented an anisotropic model [1]. The neo-Hookean constitutive model has the same formulation as the Gaussian model described in **section 5.2.1**. In that chapter we demonstrated in Figure 5.5 the opposing curvatures of the responses of the Gaussian and MacKintosh models. The MacKintosh model, with its concave up curvature, has previously been shown to accurately capture the stress-strain response of soft tissues [10]. With The neo-Hookean model its opposite (concave down) curvature does not capture the stress-strain response of the ACL. We seek a more accurate material model implementation into FEA to obtain more physiological relevant results.

Constructing a precise geometry of the ACL has been difficult due to its complex features and also because of its relative insensitivity to various imaging modalities (such as MRI) [8, 9]. Because of this, many studies have treated the ACL as a homogeneous cylindrical structure [2, 4, 7]. For the purpose of simplifying FE models, this treatment is acceptable. However, it is not applicable for predicting the full-field deformation. To predict deformation more accurately in FEA, a precise ACL geometry incorporating the double-bundle and twist features in the knee joint is required.

The accuracy of a FE model determines its value and prevalence. Therefore, the goal of this study is to establish an FE model that implements an accurate, i.e. predictive, material model and an anatomically relevant geometry of the ACL.

6.2 The establishment of inhomogeneous ACL bundle geometries

As described in **Section 4.5**, the native sheep ACLs were divided into two individual bundles –anterior and posterior. Though the ACLs were no longer in an anatomical position after the bundle division, the new positions provided the best

mechanical characterization due to the fact that the two bundles can be accurately reoriented along the test axis. Prior to testing, dimensions were taken from various locations of each bundle. The width and thickness were measured at five different locations from the proximal end to the distal end of each bundle. The length of each bundle was measured at 3 different locations from the medial side to the lateral side at both the anterior and posterior sides. These measurements were then used to reconstruct a mathematical geometric model for each bundle using the commercial non-uniform spline based modeling software Rhinoceros® 4.0. Multiple polylines were employed to ensure smooth geometry. Figure 6.1 shows the reconstructed geometries of the anterior (Figure 6.1**B**) and posterior (Figure 6.1**D**) bundles are similar to the two actual bundles (Figure 6.1 **A** and **C**). The geometry of the anterior bundle was numerically reoriented to match the geometry of the ACL during an anterior tibial translation (ATT) test. Only the anterior bundle was chosen for the geometry reconfiguration because the current ATT experimental setup only captured the full-field strain contours of the anterior bundle (Figure 6.2**A**). Therefore, using just the anterior bundle in an FE analysis is sufficient to compare the simulation results to the experimental results.

The anterior bundle was numerically twisted 90 degrees internally along the longitudinal axis of the anterior bundle. Then the twisted bundle was rotated 45 degrees around the center of the femoral insertion plane. The reoriented geometry (Figure 6.2**B**) qualitatively matched the geometry of an actual ACL during ATT testing(Figure 6.2**A**). Finally, the generated geometries of the anterior bundle (Figure 6.1**B**), posterior bundle (Figure 6.1**D**), and the twisted anterior bundle (Figure 6.2**B**) were imported to ABAQUS finite element analysis software.

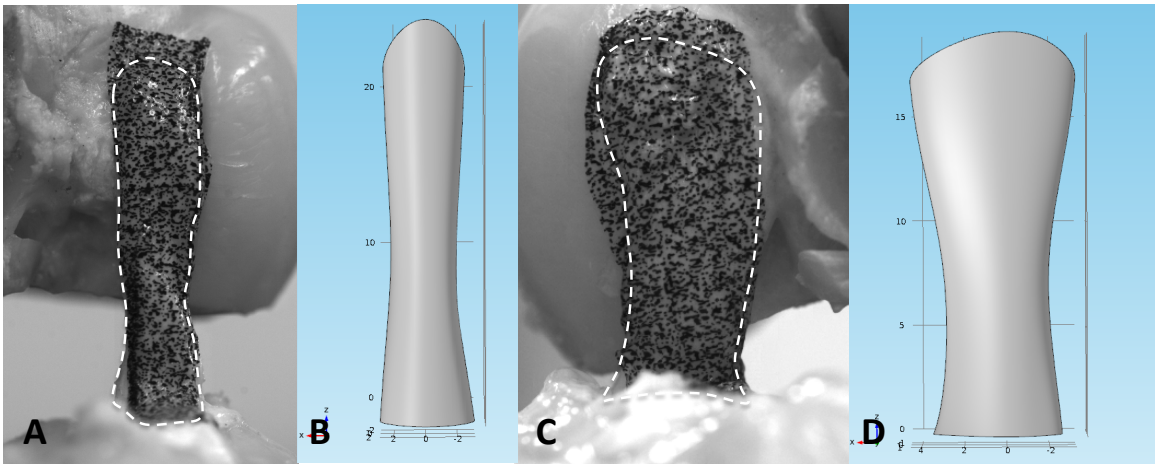

Figure 6.1 FE model establishment of the anterior bundle (A,B) and the FE posterior bundle (C, D).

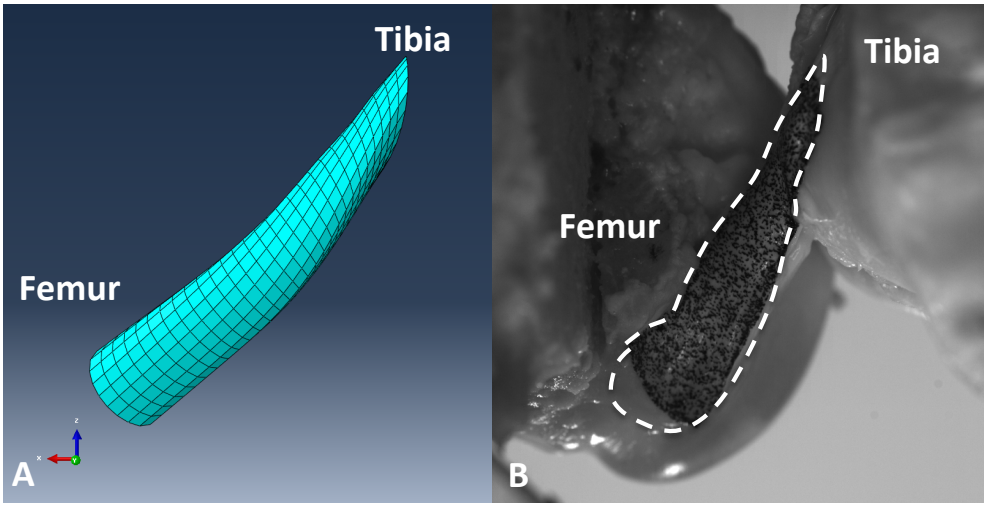

Figure 6.2 An FE model of the ACL anterior bundle in a twisted configuration (A) matched the geometry of an actual ACL anterior bundle (B).

6.3 FE model prediction of ACL strain contours during uniaxial tension testing

The anterior bundle of the ACL was modeled by applying a linear hexahedral hybrid element mesh. The distal end of each geometric model was fixed and a quasi-static displacement boundary condition was applied to the proximal end of each model. In **Chapter 5**, we have described a nonlinear viscoelastic micromechanical model that we have developed utilizing a

MacKintosh nonlinear spring, two neo-Hookean springs, and two linear dashpots. This micromechanical model predicts the mechanical responses of ligaments and tendons well. In the FE setting, it is difficult to implement the viscous effect or a highly nonlinear micromechanical model (e.g. MacKintosh semi-flexible 8-chain model). In order to decrease the computational complexity, a reduced polynomial constitutive model was used to replace the MacKintosh 8-chain model. Our ACL experimental results showed that the viscous effects during ACL load-unload and ATT testing at slow to moderate strain rates (0.005/s, 0.05/s, 0.5/s) are not significant. Therefore, we also neglected the viscous effect in our computational modeling to decrease the complexity. The strain energy density function of a two-term reduced polynomial constitutive model that replicates the mackintosh model in the small to moderate strain regime was expressed as:

$$U_{poly} = C_{10}(I_1 - 3) + C_{20}(I_1 - 3)^2$$

where C_{10} and C_{20} are the two model constants, and I_1 is the first invariant of the stretch tensor. This substitution preserves the correct nonlinear curvature of the stress-strain response of these tissues and decreases the possibilities of encountering computation problems associated with higher order strain energy functions. As shown in Figure 6.3, the two model constant reduced polynomial constitutive model captured the experimental data well. The constants used for each stress-strain response are listed in Table 6.1.

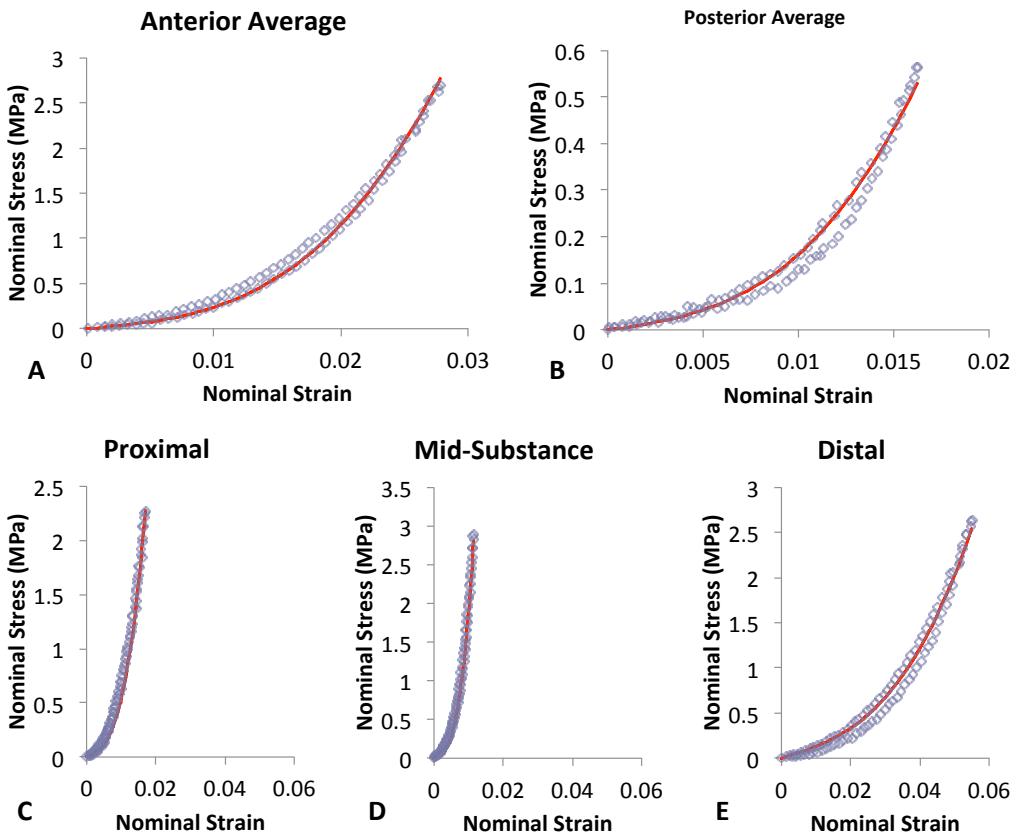

Figure 6.3 The reduced polynomial constitutive model predicts the average stress-strain responses of anterior bundle (A) and posterior bundle (B), the regional stress-strain responses of the proximal (C), mid-substance (D), and distal portions (E) of the anterior bundle.

Table 6.1 Model constants of the reduced polynomial constitutive model for all stress-strain responses.

	Anterior Bundle				Posterior Bundle
	Average	Proximal	Mid-substance	Distal	Average
C10 (MPa)	2	2	2	2	1
C20 (MPa)	3300	12000	50000	350	1000

A homogenous material has the same mechanical property at every point of the space. A non-homogenous material has mechanical properties that vary with position. As shown in Figure 6.4, a homogeneous, isotropic anterior bundle model (Figure 6.4**A**) did not capture the experimentally determined, in-plane full-

field strain contours. Strain contours of the anterior bundle (Figure 6.4**B**) demonstrated that the anterior bundle exhibits a functional gradient with the mid-substance providing the stiffest response, the distal end being the most compliant, and the proximal end being between these two responses. After the bundle was divided into these three sub-groups namely, proximal, middle or mid-substance, and distal, full-field strain contours along the testing axis predicted using an inhomogeneous isotropic FE model resembled that of the experimental data well. However, the transverse strain contours predicted from the FE model (Figure 6.5**B**) did not capture the full-field transverse strain contour (Figure 6.5**A**) obtained from the experiment. This suggests that an anisotropic model may be considered to fully capture the strain contours of the anterior bundle. The posterior bundle model with a homogenous material assumption predicted the experimental results well as shown in Figure 6.6.

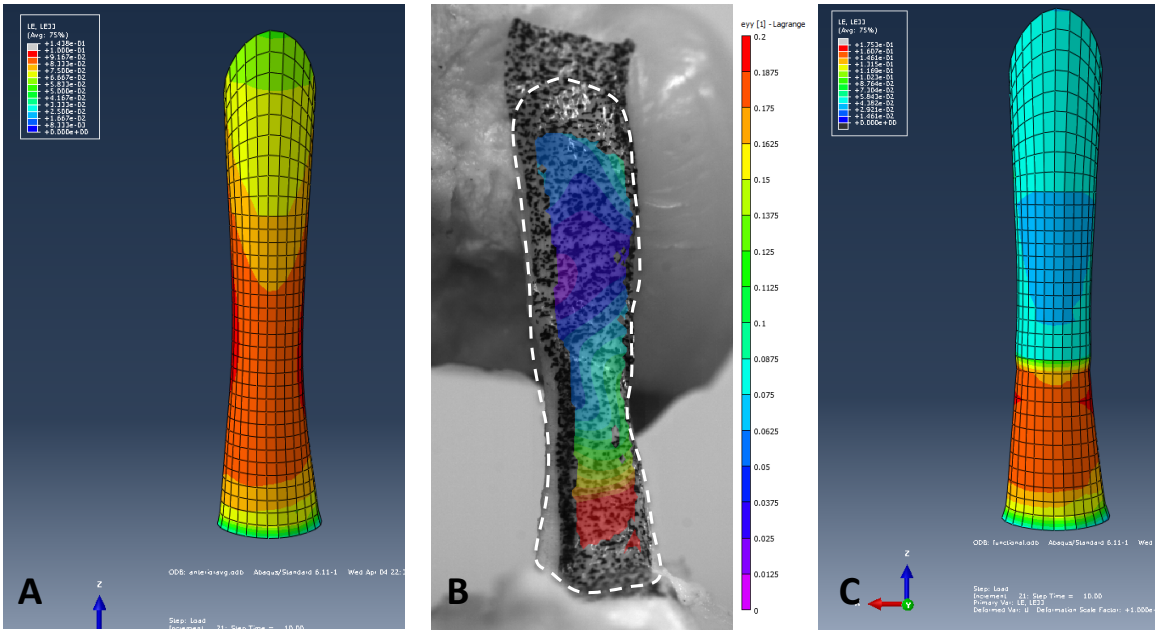

Figure 6.4 The full-field strain contour predicted from a homogeneous anterior FE model (A) does not match the experimentally obtained full-field strain contour (B). After dividing the FE model into sub-groups, the predicted full-field strain contour (C) resembles that of the experimental results.

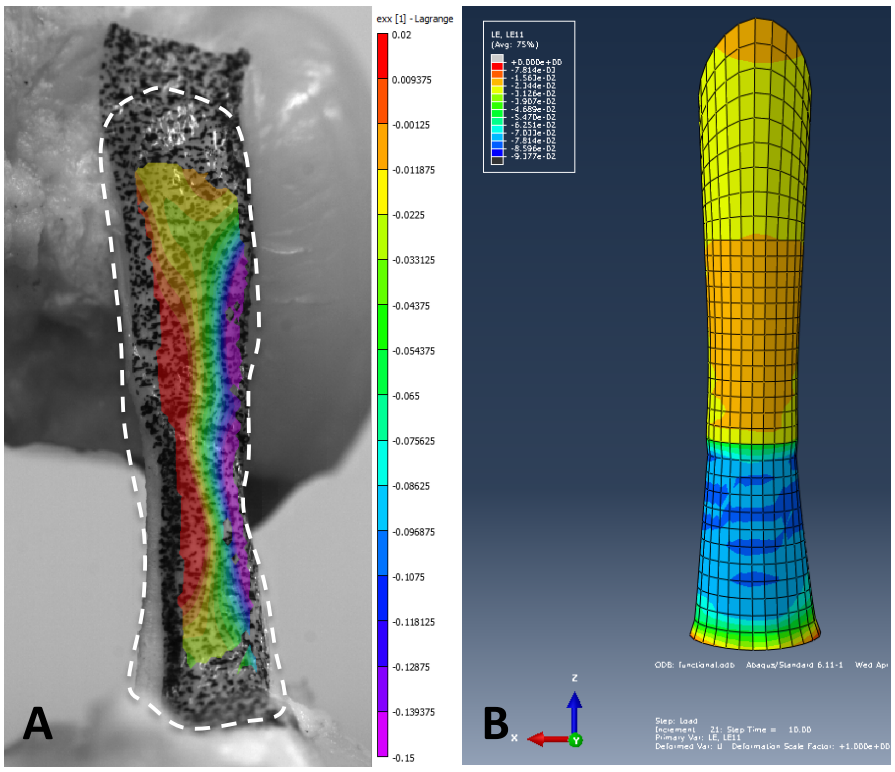

Figure 6.5 The transverse strain contour of the anterior FE model (B) did not match that of the experiments (A).

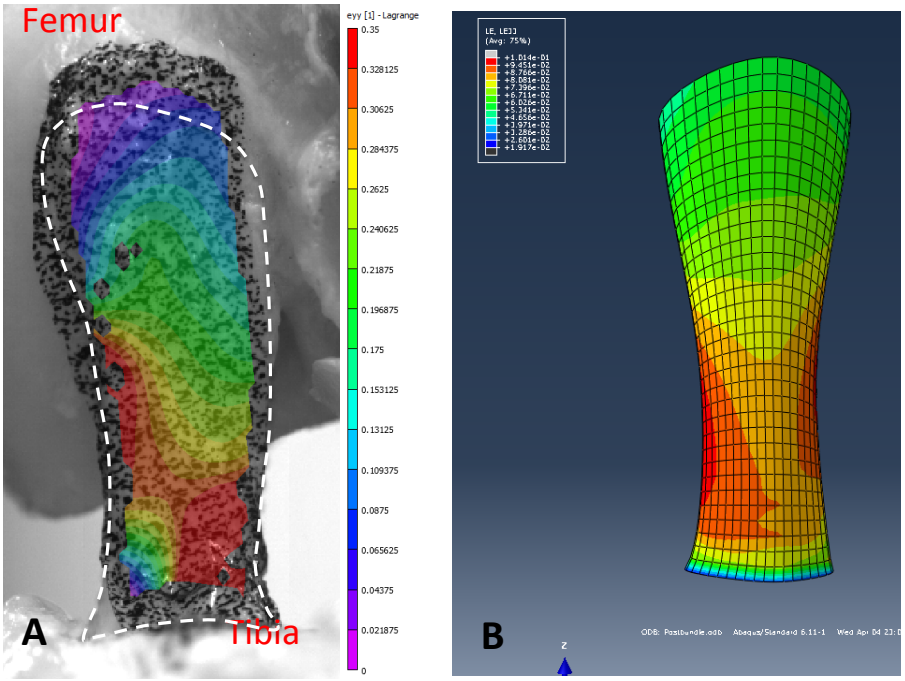

Figure 6.6 A homogeneous isotropic posterior FE model well predicts the strain contours along the testing axis (B) compared to that of the experimental full-field strain contour (A).

6.4 FE model prediction of strain contours of the ACL during ATT

The FE model was used to predict the strain contours and hence failure mechanism of the ACL during ATT to evaluate its accuracy. The geometric model of an anterior bundle presented in a previous section (Figure 6.2**B**) and this was imported into ABAQUS. With the same sub-group division, different material properties were assigned to the model to achieve inhomogeneity. The boundary condition that matched the experimental setup was applied to the FE model such that the femoral insertion was fixed in space and a quasi-static 2 mm vertical displacement control was applied to the tibial insertion. The current model assumed a zero-stress state at the beginning of an ATT simulation. Therefore, no pre-tension was added to the model. Normal strain contours along the loading direction (ε_{yy}), and perpendicular to the loading direction (ε_{xx}), and the in-plane shear strain (ε_{xy}) were computed and compared to the experimental results from **Chapter 4**. The strain contours predicted along the testing axis from the FE model (ε_{yy}) resemble the experimental data most closely with accurate strain magnitudes and peak spots located at similar positions (Figure 6.7**C** and **F**). The transverse strain contour (ε_{xx}) (Figure 6.7**D**) and the in-plane shear strain contour (ε_{xy}) (Figure 6.7**E**) from the FE model captured the overall inhomogeneous strain distributions of the experiments (Figure 6.7**A and B**). However, the numerical values of the transverse strain contour (Figure 6.7**A**) and the in-plane shear strain contour (Figure 6.7**B**) from the FE model was off from that of the experimental data. This may be due to the isotropic model assumption. The current model needs to be further validated by computing the equivalent in-plane maximum shear strain and comparing with the experimental results. The predicted results can then be quantified for validation.

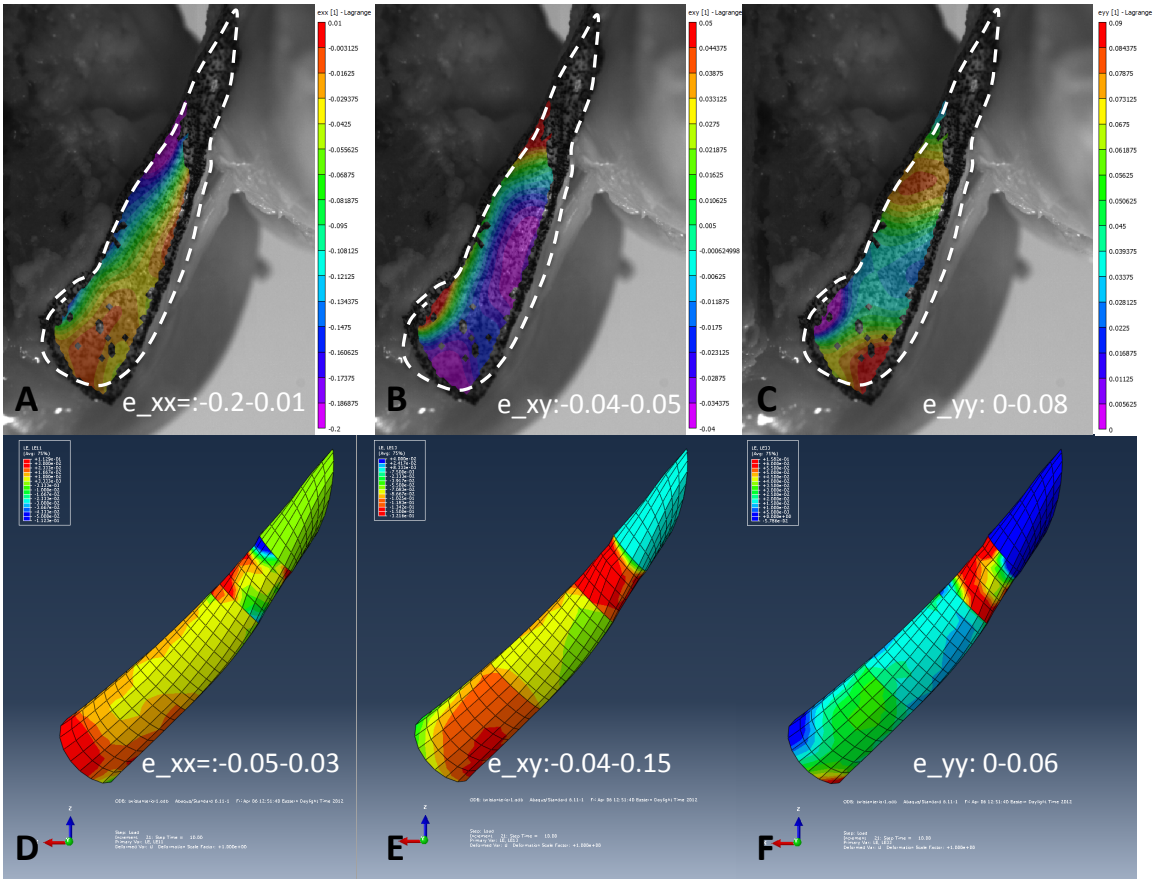

Figure 6.7 In-plane strain contours (A-C) of an actual ACL during ATT compared to the in-plane strain contours of the anterior FE model (D-F). A and D represents the transverse strain contour; B and E represents the in-plane shear strain contour; C and F represents the strain contour along the testing axis.

6.5 Summary

We have established an inhomogeneous isotropic FE model for the ACL anterior bundle. The model captured the full-field strain contour of the anterior bundle during uniaxial tension tests well. The model also qualitatively captured the in-plane strain contours of the anterior bundle during an ATT test. A homogeneous isotropic FE model for the ACL posterior bundle was able to capture the full-field strain contour of the posterior bundle during uniaxial tension tests. The unmatched ATT numerical results predicted from the FE model may be due to the anisotropy of the soft tissue. Another explanation may be that the assumption of an initial zero-stress state is not valid, as discussed in other FE studies [2,7]. During the individual bundle study, we were able to find a zero-